

鉛スペクトロメータを用いたマイナーアクチニド
核断面積の測定-Ⅲ

(動力炉・核燃料開発事業団 委託研究成果報告書)

1997年 3月

京都大学原子炉実験所

複製又はこの資料の入手については、下記にお問い合わせ下さい。

〒 311-13

茨城県東茨城郡大洗町成田町4002

動力炉・核燃料開発事業団

大洗工学センター

システム開発推進部・技術管理室

Inquiries about copyright and reproduction should be addressed to:
Technology Management Section O-arai Engineering Center. Power
Reactor and Nuclear Fuel Development Corporation, 4002 Narita-cho,
O-arai-machi, Higashi-Ibaraki, Ibaraki-Ken, 311-13, Japan

動力炉・核燃料開発事業団 (Power Reactor and Nuclear Fuel Develop-
ment Corporation) 1997

鉛スペクトロメータを用いたマイナーアクチニド
核断面積の測定-Ⅲ

(動力炉・核燃料開発事業団 委託研究成果報告書)

1997年 3月

京都大学原子炉実験所

1997年 3月

鉛スペクトロメータを用いたマイナーアクチニド 核断面積の測定－Ⅲ

小林捷平 *

要 旨

電子線型加速器と組み合わせて付設された京都大学鉛スペクトロメータKULSについて、まず、その諸特性を求めた：共鳴フィルター法により ①中性子減速時間 t (μs)とエネルギー E (keV) の関係 (ビスマス孔： $E=190/t^2$ 、鉛孔： $E=156/t^2$)、②エネルギー分解能 (ビスマス孔、鉛孔共に約40%)、飛行時間分析法により ③中性子スペクトルを測定した。MCNPコードによる計算結果は、これらの実験値と全体によい一致を示した。

次に、このKULSを用いて ~ 0.1 eVから ~ 10 keV領域におけるAm-241, Am-243, 及びAm-242mの核分裂断面積を測定した。実験には、これらの電着膜とU-235の電着膜をそれぞれ背中合わせにした核分裂電離箱を用意し、測定結果を $^{235}\text{U}(n, f)$ 反応の標準断面積に規格化した。Am-241では、Dabbs等の実験値およびENDF/B-VIの評価値は本実験値とよい一致を示したが、JENDL-3.2の評価値は10 \sim 200 eV領域において1.2 \sim 2.3倍低い値を示した。Am-243のENDF/B-VIは15 \sim 60 eV領域で低く、JENDL-3.2は100 eV以上の領域で全体に低くなっている。Am-242mに関する予備の実験では、ENDF/B-VI、JENDL-3.2の評価値に近い結果が得られた。また、Am-241, 243の熱中性子核分裂断面積についても、標準熱中性子場において測定した。

最後に、MAに関する中性子捕獲断面積測定として、Arガス入り比例計数管を用いて $^{237}\text{Np}(n, \gamma)$ 反応断面積の測定を試みた。本実験では、Np-237試料(~ 2 mg)からの中性子捕獲事象の計数率が少なく、バックグラウンドとの比較において有意な違いは得られなかった。

本報告書は、京都大学が動力炉・核燃料開発事業団の委託により実施した研究の成果である。

契約番号：080D0221

事業団担当部課室および担当者：大洗工学センター基盤技術開発部 炉心技術開発室 若林利男

* 京都大学原子炉実験所

March 1997

Measurement of Nuclear Data for Minor Actinides
with Lead Slowing-down Spectrometer - III

Katsuhei Kobayashi *

Abstract

A lead slowing-down spectrometer was installed coupled to the 46 MeV electron linac at Research Reactor Institute, Kyoto University (KURRI). Characteristics of the Kyoto University Lead Slowing-down Spectrometer (KULS) were measured for ① the relation between neutron slowing-down time $t(\mu s)$ and energy E (keV) ($E=190/t^2$ in Bi hole and $E=156/t^2$ in Pb hole), ② energy resolution ($\sim 40\%$ in Bi and Pb holes), and ③ neutron energy spectrum by the neutron TOF method. The results obtained by the MCNP code were in general agreement with these experimental ones.

The KULS has been applied to the fission cross section measurements of Am-241, Am-243 and Am-242m relative to that of U-235 from ~ 0.1 eV to ~ 10 keV, making use of the back-to-back type double fission chambers. For Am-241, Dabbs and ENDF/B-VI data are in good agreement with the present measurement. The JENDL-3.2 data are smaller by a factor of 2 between 10 and 200 eV. The ENDF/B-VI data for Am-243 are lower between 15 and 60 eV, and the JENDL-3.2 are lower in general above 100 eV. It has been found that the preliminary result for the Am-242m(n,f) reaction is close to the ENDF/B-VI and the JENDL-3.2 data. Thermal neutron cross sections for Am-241 and Am-243 have also been measured in a standard Maxwellian distribution spectrum field.

Finally, aiming at the measurement of capture cross section for MA nuclides, the experimental investigation for Np-237 sample (~ 2 mg) has been performed with the KULS. Due to the comparable background counts to the foreground ones, the capture events from the sample have scarcely been detected with an Ar-gas proportional counter.

Work performed by Research Reactor Institute, Kyoto University under contract with Power Reactor and Nuclear Fuel Development Corporation.

PNC Liaison: O-arai Engineering Center, Advanced Technology Division,
Core Physics Research Section, Dr. Toshio Wakabayashi.

* Research Reactor Institute, Kyoto University

目 次

ページ

1. 序論	1
2. MA核種の中性子核データ	4
2.1 評価済核データファイル	4
2.2 核データの現状	4
3. 京都大学 鉛スペクトロメータ	12
3.1 鉛スペクトロメータとその特徴	12
3.2 鉛スペクトロメータの原理	14
3.3 京都大学 鉛スペクトロメータ	14
3.4 鉛スペクトロメータKULS中の中性子輸送計算	15
3.5 鉛スペクトロメータKULSの特性	17
3.5.1 中性子減速時間とエネルギーの関係	17
3.5.2 KULSのエネルギー分解能	19
3.5.3 KULS内の中性子スペクトル	23
4. 鉛スペクトロメータを用いた	
マイナーアクチニド核分裂断面積の測定	25
4.1 Am-241, Am-243, Am-242m及びU-235試料と核分裂電離箱	25
4.2 核分裂断面積の測定	27
4.2.1 KULSを用いた実験	27
4.2.2 熱中性子断面積の測定	30
4.3 測定結果	31
4.3.1 $^{241}\text{Am}(n, f)$ 反応断面積	31
4.3.2 $^{243}\text{Am}(n, f)$ 反応断面積	31
4.3.3 $^{241}\text{Am}(n, f)$ 及び $^{243}\text{Am}(n, f)$ 反応の熱中性子断面積	35
4.3.4 $^{241}\text{Am}(n, f)$ 及び $^{243}\text{Am}(n, f)$ 反応断面積測定における不純物の問題	37
4.3.5 $^{242\text{m}}\text{Am}(n, f)$ 反応断面積	37

5. マイナーアクチニドの中性子捕獲断面積測定の予備実験	40
5.1 Np-237の中性子捕獲断面積	40
5.2 鉛スペクトロメータKULSを用いた中性子捕獲断面積の測定	40
5.2.1 Np-237試料	40
5.2.2 実験方法	42
5.2.3 結果及び検討	42
5. まとめ	44
参考文献	46
付 録	48

付 録

付録 A : Characteristics of the Kyoto University Lead Slowing-down Spectrometer (KULS) coupled to an Electron Linac	-----	49
付録 B : Measurement of Fission Cross Section of Np-237 in Resonance Region with Electron Linac-Driven Lead Spectrometer	-----	61
付録 C : Measurements of Thermal Neutron Cross Section and Resonance Integral for $^{237}\text{Np}(n, \gamma)^{238}\text{Np}$ Reaction	-----	68
付録 D : Fission Cross Section Measurements of Am-241 between 0.1 eV and 10 keV with Lead Slowing-down Spectrometer and Thermal Neutron Energy	-----	77
付録 E : Measurement of Fission Cross Section with Pure Am-241 Sample using Lead Slowing-down Spectrometer	-----	91
付録 F : The Influence of Impurities for Cross Section Measurement of Am-241, 243(n, f) Reactions	-----	97
付録 G : Application of BGO Scintillators to Absolute Measurement of Neutron Capture Cross Sections between 0.01 eV and 10 eV -----	-----	103

図のリスト

図 1 アクチニド核種の生成と崩壊の図

図 2 HLWの潜在的毒性指数の経年変化

図 3 $^{241}\text{Am}(n, f)$ 反応断面積の既存実験データの比較。
核データは40%のエネルギー分解能で広げている

図 4 $^{241}\text{Am}(n, \gamma)$ 反応断面積の既存実験データの比較

図 5 $^{242m}\text{Am}(n, f)$ 反応断面積の既存実験データの比較

図 6 $^{243}\text{Am}(n, f)$ 反応断面積の既存実験データの比較

図 7 $^{243}\text{Am}(n, \gamma)$ 反応断面積の既存実験データの比較

図 8 ^{241}Am の非弾性散乱断面積の評価データの比較

図 9 $^{241}\text{Am}(n, 2n)$ 反応断面積の評価データの比較

図 10 ^{241}Am の核分裂断面積の評価データの比較

図 11 ^{241}Am の核分裂断面積の評価データと実験データの比較

図 12 ^{241}Am の中性子捕獲断面積の評価データの比較

図 13 ^{241}Am の中性子捕獲断面積の評価データと実験データの比較

図 14 ^{242m}Am の非弾性散乱断面積の評価データの比較

- 図 1 5 $^{242}\text{mAm}(n, 2n)$ 反応断面積の評価データの比較
- 図 1 6 ^{242}mAm の核分裂断面積の評価データの比較
- 図 1 7 ^{242}mAm の核分裂断面積の評価データと実験データの比較
- 図 1 8 ^{242}mAm の中性子捕獲断面積の評価データの比較
- 図 1 9 ^{243}Am の非弾性散乱断面積の評価データの比較
- 図 2 0 $^{243}\text{Am}(n, 2n)$ 反応断面積の評価データの比較
- 図 2 1 ^{243}Am の核分裂断面積の評価データの比較
- 図 2 2 ^{243}Am の核分裂断面積の評価データと実験データの比較
- 図 2 3 ^{243}Am の中性子捕獲断面積の評価データの比較
- 図 2 4 ^{243}Am の中性子捕獲断面積の評価データと実験データの比較
- 図 2 5 鉛スペクトロメータ KULS の断面図
- 図 2 6 電子線型加速器室と鉛スペクトロメータ KULS の設置位置
- 図 2 7 鉛スペクトロメータ KULS の平面図（上）と垂直断面図（下）
- 図 2 8 KULS のビスマス実験孔における中性子の時間依存スペクトル
- 図 2 9 KULS 内の（定常）中性子スペクトルの計算結果
- 図 3 0 KULS のビスマス実験孔と鉛実験孔における中性子減速時間とエネルギーの関係

- 図 3 1 中性子透過法によって測定された時間スペクトルの例
- 図 3 2 共鳴捕獲 γ 線測定によるエネルギー分解能測定の例
- 図 3 3 $^{235}\text{U}(n, f)$ 反応の ENDF/B-VI 評価値と、分解能 40% で broadening した結果
- 図 3 4 $^{241}\text{Am}(n, f)$ 反応の ENDF/B-VI 評価値と、分解能 40% で broadening した結果
- 図 3 5 ^6Li ガラスシンチレータを用いて飛行時間分析法により測定した鉛スペクトロメータ内の中性子スペクトルと MCNP コードによる計算値の比較
- 図 3 6 ^{10}B -vaseline plug NaI(Tl) シンチレータを用いて飛行時間分析法により測定した鉛スペクトロメータ内の中性子スペクトルと MCNP コードによる計算値の比較
- 図 3 7 背中合わせ型の核分裂電離箱の断面図
- 図 3 8 Am-243 の α 線スペクトル
- 図 3 9 U-235 の α 線スペクトル
- 図 4 0 Am-242m の α 線スペクトル
- 図 4 1 Am-242m のガンマ線スペクトル
- 図 4 2 核分裂断面積測定の回路図
- 図 4 3 $^{243}\text{Am}(n, f)$ 反応の核分裂片パルス波高分布
- 図 4 4 $^{235}\text{U}(n, f)$ 反応の核分裂片パルス波高分布
- 図 4 5 $^{243}\text{Am}(n, f)$ 反応測定の減速時間スペクトル ($0.5 \mu\text{s}/\text{channel}$)
- 図 4 6 $^{235}\text{U}(n, f)$ 反応測定の減速時間スペクトル ($0.5 \mu\text{s}/\text{channel}$)
- 図 4 7 $^{241}\text{Am}(n, f)$ 反応断面積の測定結果と評価値の比較

図 4 8 $^{241}\text{Am}(n, f)$ 反応断面積の測定値と従来の実験値との比較

図 4 9 化学精製後の時間と $^{243}\text{Am}(n, f)$ 反応断面積測定値の変化

図 5 0 生成蓄積されてくる Pu-239 の効果を計算によって求めた $^{243}\text{Am}(n, f)$ 反応断面積 (ENDF/B-VI 評価データを使用)

図 5 1 精製後の時間と Pu-239 により上昇する 0.3eV 付近の Am-243 断面積値との関係

図 5 2 $^{243}\text{Am}(n, f)$ 反応断面積の測定結果と評価値の比較

図 5 3 市販の Am-241 試料を使った場合の $^{241}\text{Am}(n, f)$ 反応断面積の測定結果と評価値の比較 (不純物の影響で断面積が大きくなっている)

図 5 4 Pu-239 が混在する Am-243 試料を使った場合の $^{243}\text{Am}(n, f)$ 反応断面積の測定結果と評価値の比較 (0.3eV 付近は不純物の影響で断面積が大きくなっている)

図 5 5 Am-242m の核分裂断面積の評価値と本実験値との比較

図 5 6 Np-237 の核分裂断面積の評価データの比較

図 5 7 Np-237 の核分裂断面積の評価データと実験データの比較

図 5 8 Np-237 試料から得られた減速時間スペクトル
(上: Foreground run、下: Background run)

図 5 9 図 58 に示した Foreground データと Background データの比

表のリスト

表 1 マイナーアクチニド (MA) の生成量

表 2 MA核種の核分裂及び中性子捕獲反応断面積に関する実験データの現状

表 3 MA核種に対し、各反応断面積に要求される精度 (%)

表 4 中性子源としてのKULS、Linac、KURの比較

表 5 共鳴フィルターと共鳴エネルギー

表 6 ビスマス及び鉛実験孔におけるエネルギー分解能

表 7 $^{241}\text{Am}(n, f)$ 反応断面積の比較

表 8 $^{241}\text{Am}(n, f)$ 及び $^{243}\text{Am}(n, f)$ 反応断面積測定における実験誤差

表 9 $^{241}\text{Am}(n, f)$ 反応の熱中性子断面積

1. 序論

ネプツニウム(Np)、アメリシウム(Am)、キュリウム(Cm)などは、いわゆるマイナーアクチニド(MA)と称される代表的な核種であって、核燃料の燃焼と共に原子炉内で生成蓄積される。図1は、これらのMA核種の生成と変換の過程を示している。100万 kWe級の軽水炉一基あたり、MAは一年間に約20数kg生成されると言われている(表1)/1, 2/。MA核種の大部分は、超長半減期の高レベル α 放射性廃棄物(HLW)であるため、燃料再処理時の取扱い、放射性廃棄物の保管、管理において問題となる。図2は、HLWの潜在的放射性毒性指数の経年変化を示している。ここで言う毒性指数はHLW中のある核種の存在量(Bq単位)を経口年摂取限度(Bq単位)として定義している。この図を見ると、MAには半減期の長い核種が多く、200年以上経つとMAが占めるようになる。核分裂生成物(FP)は最初の100年間で占めているが、Tc-99やI-129など半減期の長いものは殆んど減少しない。こうしたMAやFPなどを負の遺産として、またそのリスクを次の世代に残さないためにも、これらの高レベル放射性廃棄物をどの様に処理処分するかが、今日の我々に課せられた大きな課題となっている/1, 2/。

現在、放射性廃棄物の処理処分法の中で最も有力視されている方法に地層処分が挙げられる。核種の半減期が短く、人が直接管理できる低レベル放射性廃棄物の場合には、比較的浅い地層中で保管管理することも考えられるが、半減期の長いFPやMA核種のように長半減期の高レベル放射性廃棄物の場合には、人が住む環境に影響を及ぼさない地下約1000mの岩盤中に隔離貯蔵する深地層処分の方法が考えられている。このような場合でも、廃棄物の量をできるだけ減量しておくことが望まれる。

MAは単なる放射性廃棄物ではなく、中性子と反応させれば核分裂を起こしてエネルギー源にもなり、中性子を吸収させれば核変換する点が注目される。消滅処理とは、MAやFPを原子炉や加速器で核分裂消滅させたり、核変換によって半減期の短い核種や毒性の少ない核種に変換させることをいう。消滅処理が実用化できれば、放射性廃棄物の減量化と共に数100年以降の毒性も下がり、次世代の人々へのリスクを低減した地層処分ができるようになる。最近では、MAの燃焼・消滅処理のみならず、核兵器解体から出てきた余剰Puの扱いについても世界的に強い関心事となっている。原子炉を用いた消滅処理法では、Pu、MAの核的性質から高速炉による燃焼・消滅が有力視されている。しかし、高速炉の実用化には今少し時間を要することと、高速炉にこれらの核種を装荷した場合、ボイド係数が正側に移行するなどの問題が存在すると言われている。最近ではPuの場合同様、MAを現有の軽水炉で燃焼させる考え(プルサーマル方式)が検討されている/3, 4/。さらに、強力中性子源によるMAの燃焼特性を論じた研究も幾つか発表されている/3, 4/。

MAに関連した核データは、原子炉の安全性・経済性評価のみならず、核燃料の燃焼特性や使用済燃料中に生成蓄積されるMA量の予測、MA消滅処理における有効性評価にと

っても極めて重要な基礎データである。今日までに、MAに関する核データの実験研究は、主として1960年頃から1980年代中頃にかけてかなり行われてきたものの、測定値間の差異が著しく、評価済核データにおいてもまだ不十分である/5/。その主な理由として、MAは強いアルファ放射体で自発核分裂性核種も含んでおり、実験上その取扱いが難しくなること、バックグランドが高くなること、純度の高い試料が得にくいこと等が考えられる。Wagemans は、試料中の不純物が核データの測定値を大きく乱す（断面積を見かけ上大きくする）ことについて忠告している/6/。特に、MA核種は同位体元素も多く、不純物として混入し易いため、試料純度の問題は一層重要である。また、純度の高い試料であっても、試料自身の核変換/崩壊によって不純物となる核種が徐々に生成蓄積する場合もある/6/。一方、実験を行う中性子源の状況からは、熱中性子から高速中性子までの広いエネルギー領域をカバーできる一連の実験が実施できる強力中性子源は得難いため、多数の実験者による測定結果をつなぎ合わせて断面積評価が行われていることが評価済核データの結果に食い違いが生じている原因ともなっている。さらに、一般的には、エネルギー依存の中性子断面積の絶対値測定は必ずしも容易なことではないと言う問題もある。

本研究では、まず、MA核データの実験値、評価値の現状について紹介した後、京都大学原子炉実験所の46MeV電子線型加速器と組み合わせて付設された鉛（減速）スペクトロメータ(KULS)について、その特性など明らかにされた結果について述べる。次に、これを用いて行われた $^{241}\text{Am}(n, f)$ 、 $^{243}\text{Am}(n, f)$ 反応断面積の測定とこれに引続き行われた $^{242m}\text{Am}(n, f)$ 反応断面積の予備的な測定結果を示し、評価核データファイルや既存の実験データとの比較を行う。最後に、鉛スペクトロメータを用いた中性子捕獲断面積実験に関連する課題として、数mgのNp-237試料を用いた予備実験についても述べる。

表1 マイナーアクチニド(MA)の生成量

冷却期間 核種	3410MWt-PWR		2500MWt-FBR
	3年	10年	3年
^{237}Np	57.9%	41.3%	9.45%
^{241}Am	27.4	48.8	54.9
^{242m}Am	0.06	0.04	1.38
^{243}Am	11.9	8.33	25.4
^{243}Cm	0.03	0.02	0.29
^{244}Cm	2.67	1.44	7.73
^{245}Cm	0.15	0.10	0.89
全重量	23.8kg	33.9kg	24.0kg

計算 : データ JENDL-2, 計算コード SRAC-FPGS
 燃焼度 : 33GWd/MT(PWR) 150GWd/MT(FBR)
 再処理から群分離までの冷却期間 : 5年
 U,Puの回収率 : 100 %

2. MA核種の中性子核データ

2.1 評価済核データファイル

核分裂で生まれた高速中性子は、核燃料及び原子炉構造材と相互作用を繰り返しながら、減速・拡散し、その間には周辺物質による吸収、炉心からの漏洩など複雑な振る舞いをする。こうした中性子の挙動は原子炉の核的特性として、多群のエネルギー構造を持つ輸送計算^{/7/}や連続エネルギー減速モンテカルロ計算^{/8/}などによって求められる。これらの計算では、熱中性子から20MeV近辺までの中性子エネルギー領域における散乱、吸収、捕獲及び核分裂の断面積など、全てをカバーする一貫した核データが必要とされる。ところが、個々の実験データはある特定のエネルギーや反応に限られたものであるため、これらを取りまとめて評価し、作成されたところの「評価済核データファイル」が必要となる。

日本において作成された評価済核データファイルは、JENDL (Japanese Evaluated Nuclear Data Library: 最新バージョンは JENDL-3.2) ^{/9/}と呼ばれ、水素元素からフェルミウムまでの殆んど全核種に対して中性子全断面積、中性子吸収断面積、中性子捕獲断面積、核分裂断面積、散乱断面積などが収納されている。米国、ヨーロッパ、ロシア及び中国においても、同種の評価済核データファイルとして、それぞれ ENDF/B-VI、JEF-2、BROND-2、CENDL-2 が独自に作成されている。これらは熱中性子から20MeV領域の実験データをベースにして評価され、データの欠けている領域、反応では理論計算で補う形で用意されている。しかし、実験データの不十分さ、評価法の違いなどによって評価済核データ間にも著しい差異が見受けられる場合がある。これらは、後の実験により検証、修正され、より信頼度の高い評価済核データファイルへとバージョンアップされて行くことになる。

最近では、研究の進展と共に、核データに対する要請も具体的になり、上に挙げた一般的な評価済核データファイルの他に、ある特定の利用目的のために、Dosimetry File、Fusion File、Actinide File(半減期が1日以上核種で、Th(Z=90)からEs(Z=99)までの89核種が予定される)などが用意されている。

2.2 核データの現状

MA核種に関連した核データの実測値は、U-235、U-238、Pu-239 等のメジャーアクチノイド核種の場合に比べて少なく、また、データ間の差異も依然大きいものがある^{/5, 10/}。今までに世界各国において測定された実験データは、殆んど全て NEA Data Bank に登録され、NESTOR-2 として収納されているが、MAの実験データとなると一般的に数少ない。表2には、MAに対する核分裂及び中性子捕獲反応断面積の現状がまとめられている。また、表3は、これらの核種、反応断面積に対し要求されている精度を示している^{/10/}。これらを

見ると、中性子捕獲断面積の実験データは、核分裂断面積に比べて質、量ともに乏しく、共鳴領域以上になるとさらにデータは不十分であることが分かる。本研究では、 $^{241}\text{Am}(n, f)$ 、 $^{243}\text{Am}(n, f)$ および $^{242\text{m}}\text{Am}(n, f)$ 反応断面積の測定を取り上げることもあって、Am-241、Am-243、Am-242m核種に対する主な中性子核反応の実験データと評価データの現状について調査した。その結果を図3～図24にまとめる/10/。これらの図から分かることは、高エネルギー領域の評価値データ間において、特に、非弾性散乱、 $(n, 2n)$ 反応断面積に著しい差異が存在していることである。これは、評価の対象として引用された実験データの不十分さ、評価に用いられた理論計算パラメータの選び方の難しさ等によるものと思われる。また、実験データには、互いに大きく相違しているもの、あるエネルギー領域では未だデータが測定されていないものもある。実験データの乏しい場合、データ間の差異が著しい場合にはその検証のためにも新たな核データの測定が望まれる。また、MA核種に対する核変換／消滅処理を検討評価する観点からも、現状の核分裂および中性子捕獲断面積は質、量において必ずしも十分とはいえない。

表2 MA核種の核分裂及び中性子捕獲
反応断面積に関する実験データの現状

	thermal~resonance			keV~MeV	
	fiss	capt	res	fiss	capt
	max. energy (eV)				
^{232}U	○	○	200	○	×
^{234}U	max	○	1500	○	×
^{236}U	○	○	4000	○	○
^{237}U	max	○	200	○	×
^{237}Np	○	○	600	○	○
^{238}Np	○	×	×	×	×
^{239}Np	×	○	×	×	×
^{236}Pu	○	×	×	○	×
^{238}Pu	○	○	500	○	○
^{242}Pu	max	○	3800	○	○
^{241}Am	○	○	150	○	○
^{242}Am	○	×	×	×	×
$^{242\text{m}}\text{Am}$	○	○	20	○	×
^{243}Am	○	○	250	○	○
^{242}Cm	max	○	265	○	×
^{243}Cm	○	○	66	○	×
^{244}Cm	○	○	970	○	○
^{245}Cm	○	○	60	○	×
^{246}Cm	○	○	300	○	×

○:yes, ×: no, max: maximum value only

表3 MA核種に対し、各反応断面積
に要求される精度(%)

	σ_{fis}	σ_{cap}	σ_{inel}	σ_{2n}	ν
^{237}Np	5	5	10	20	5
^{238}Pu	5	5	20	20	5
^{242}Pu	10	10			20
^{241}Am	5	5	20	20	10
^{242}Am	20	20			30
$^{242\text{m}}\text{Am}$	10	10			15
^{243}Am	5	5	20	20	10
^{242}Cm	10	10			20
^{243}Cm	10	20			30
^{244}Cm	10	10			20
^{245}Cm	10	10			30
^{246}Cm	10	20			30

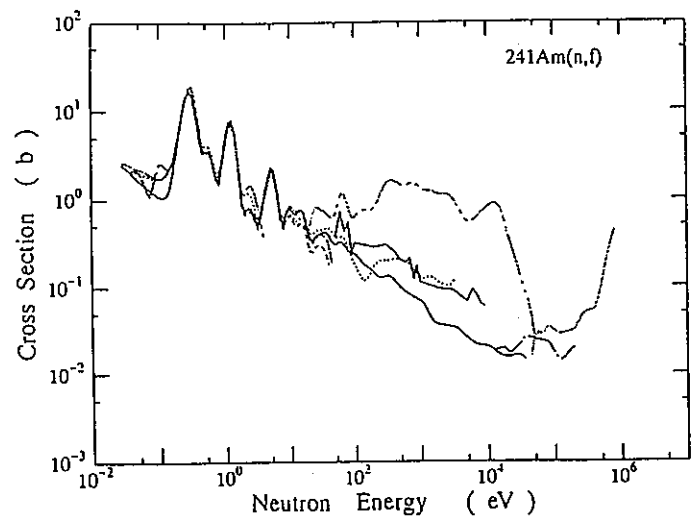


図 3 $^{241}\text{Am}(n, f)$ 反応断面積の既存実験データの比較。
核データは40%のエネルギー分解能で広げている

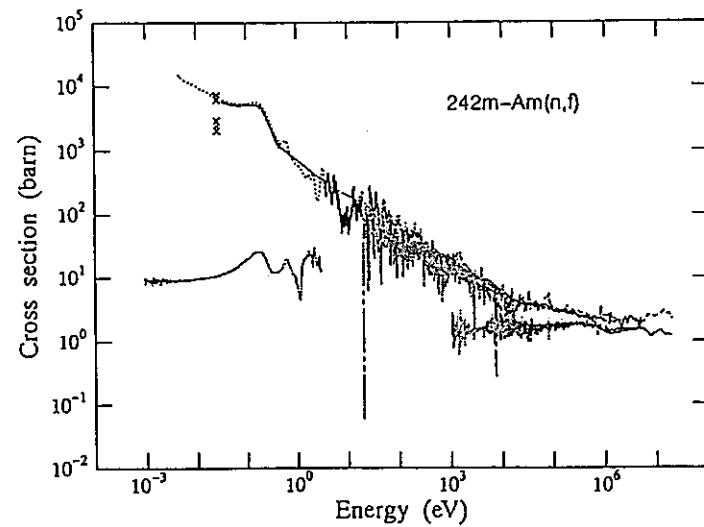


図 5 $^{242m}\text{Am}(n, f)$ 反応断面積の既存実験データの比較

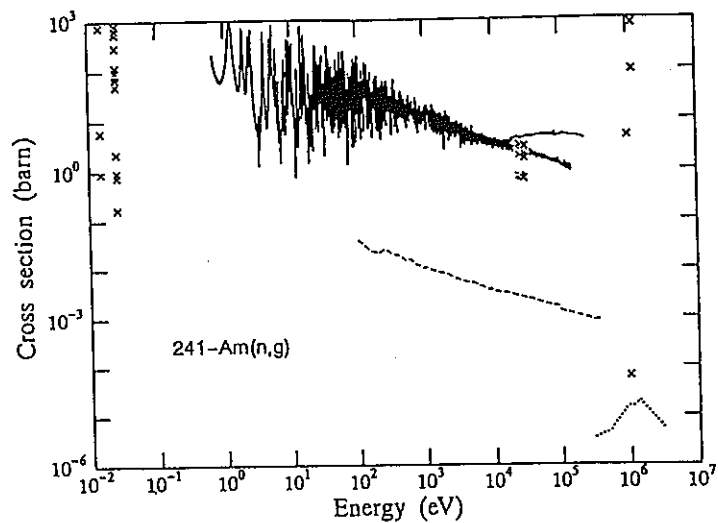


図 4 $^{241}\text{Am}(n, \gamma)$ 反応断面積の既存実験データの比較

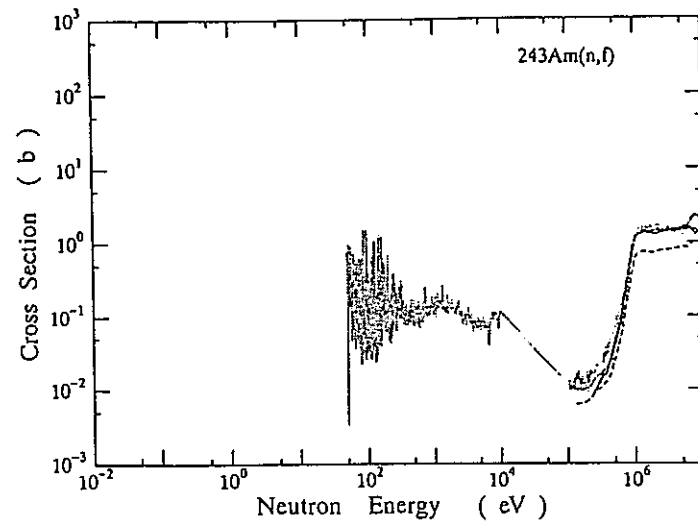


図 6 $^{243}\text{Am}(n, f)$ 反応断面積の既存実験データの比較

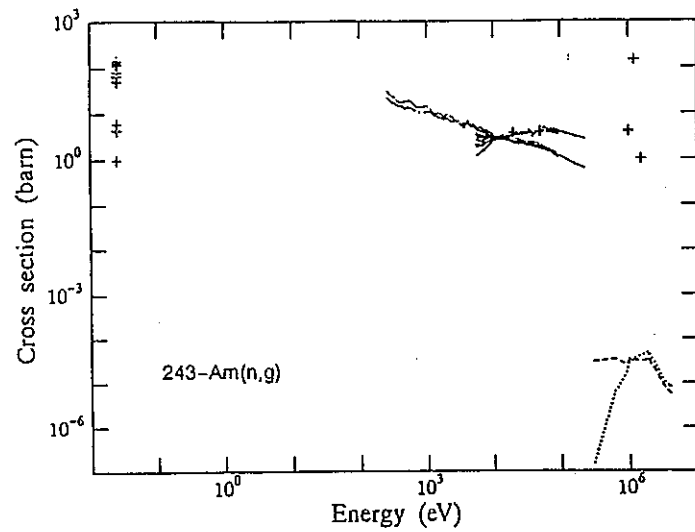


図 7 $^{243}\text{Am}(n, \gamma)$ 反応断面積の既存実験データの比較

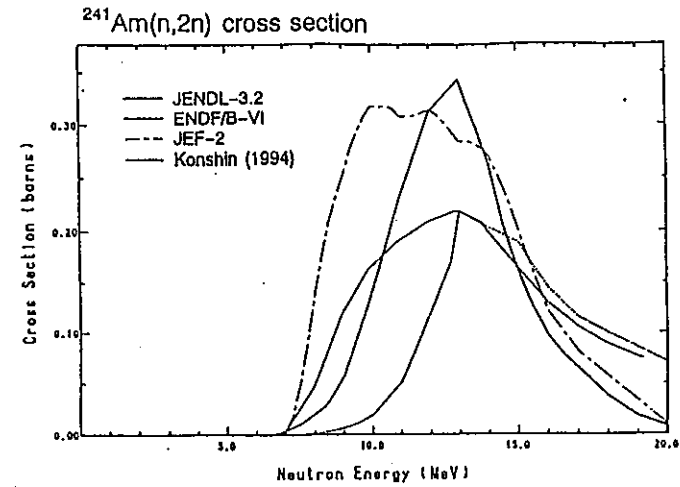


図 9 $^{241}\text{Am}(n, 2n)$ 反応断面積の評価データの比較

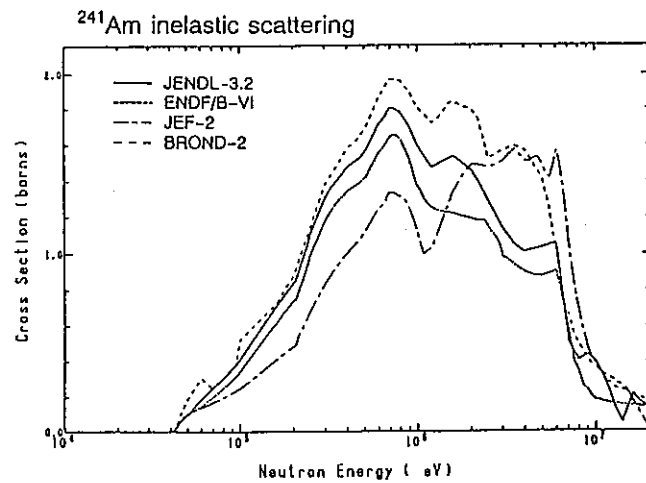


図 8 ^{241}Am の非弾性散乱断面積の評価データの比較

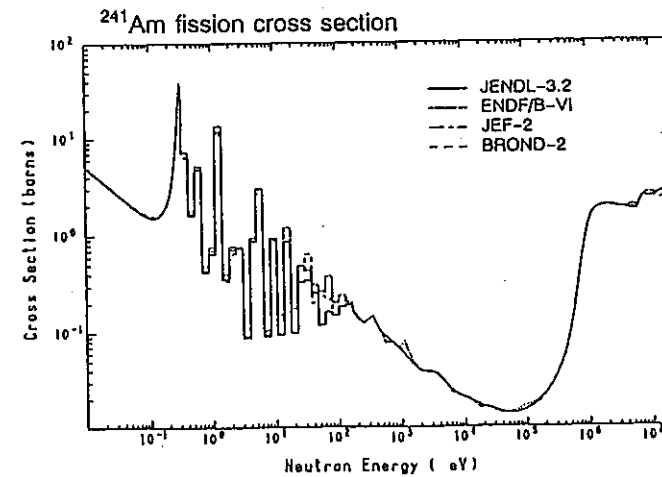


図 10 ^{241}Am の核分裂断面積の評価データの比較

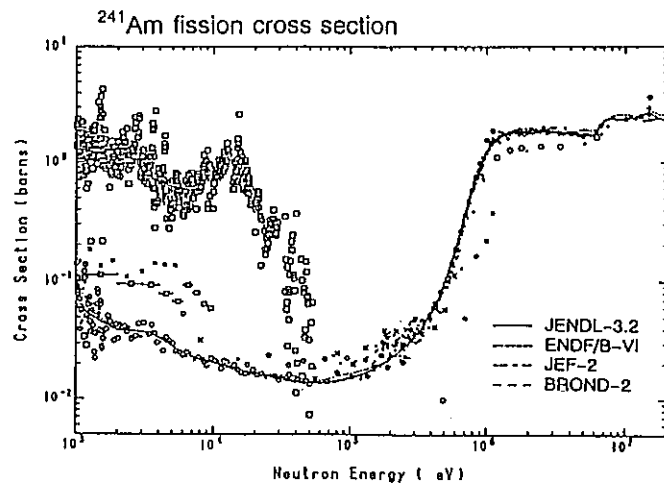


図 1.1 ^{241}Am の核分裂断面積の評価データと実験データの比較

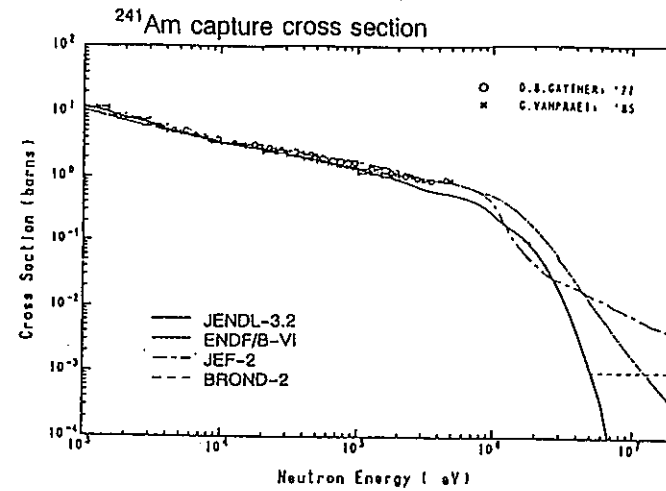


図 1.3 ^{241}Am の中性子捕獲断面積の評価データと実験データの比較

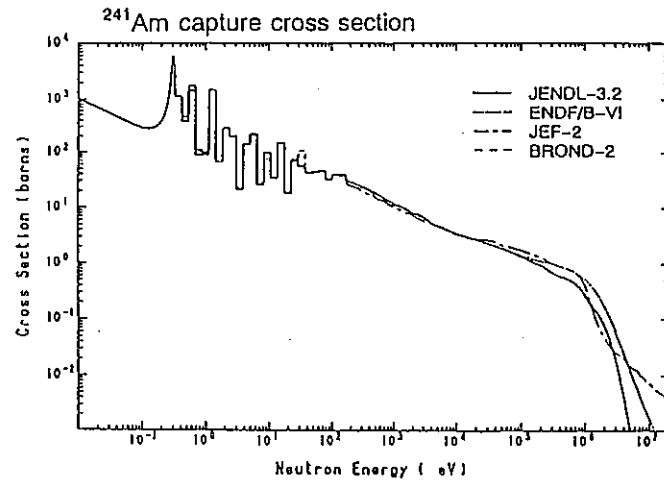


図 1.2 ^{241}Am の中性子捕獲断面積の評価データの比較

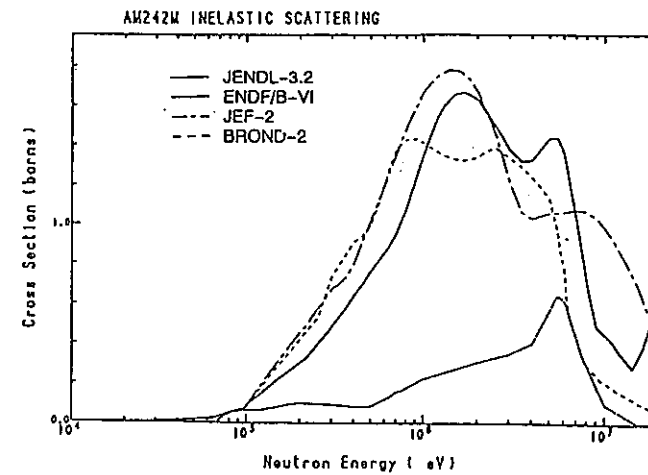


図 1.4 $^{242\text{m}}\text{Am}$ の非弾性散乱断面積の評価データの比較

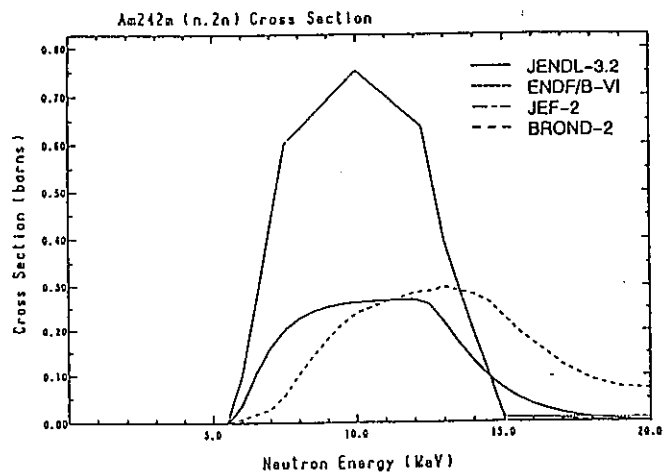


図 1 5 $^{242m}\text{Am}(n, 2n)$ 反応断面積の評価データの比較

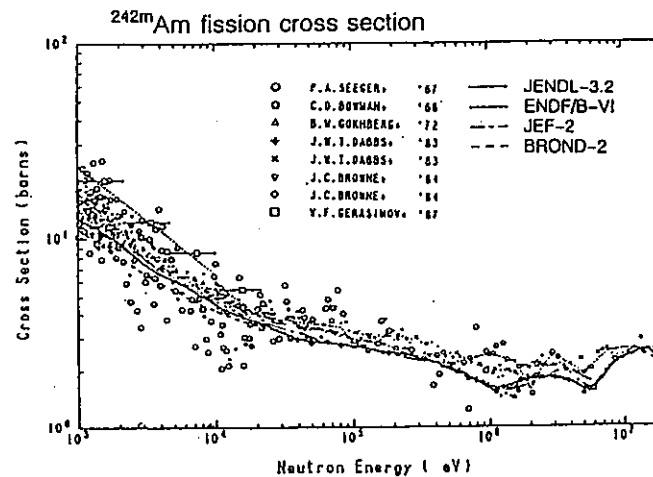


図 1 7 ^{242m}Am の核分裂断面積の評価データと実験データの比較

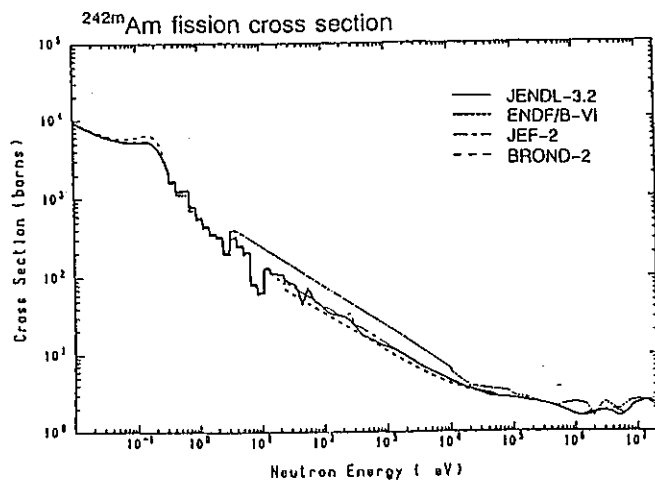


図 1 6 ^{242m}Am の核分裂断面積の評価データの比較

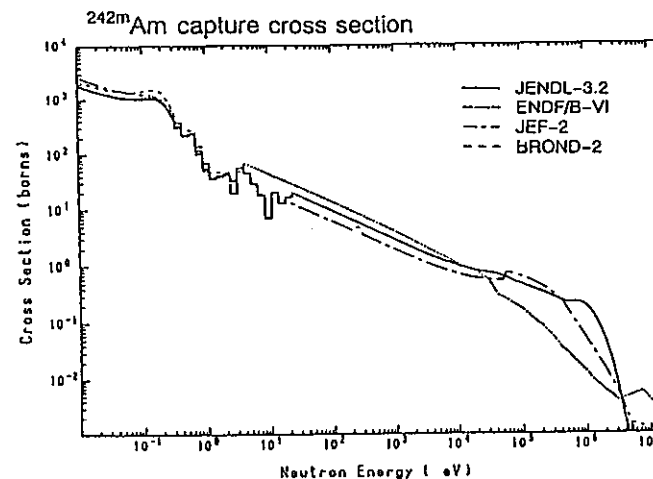


図 1 8 ^{242m}Am の中性子捕獲断面積の評価データの比較

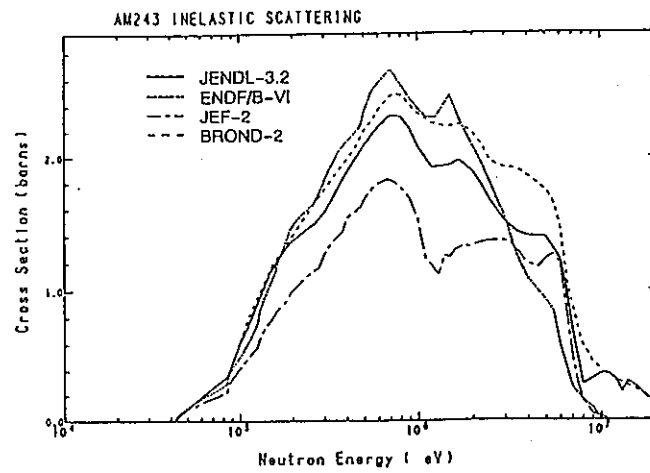


図 1 9 ^{243}Am の非弾性散乱断面積の評価データの比較

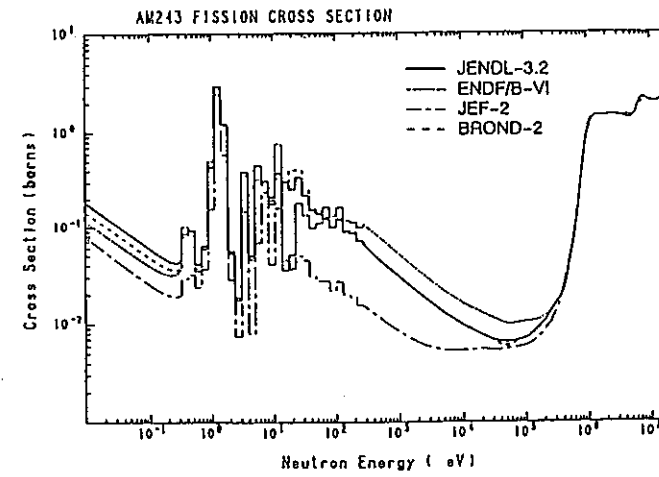


図 2 1 ^{243}Am の核分裂断面積の評価データの比較

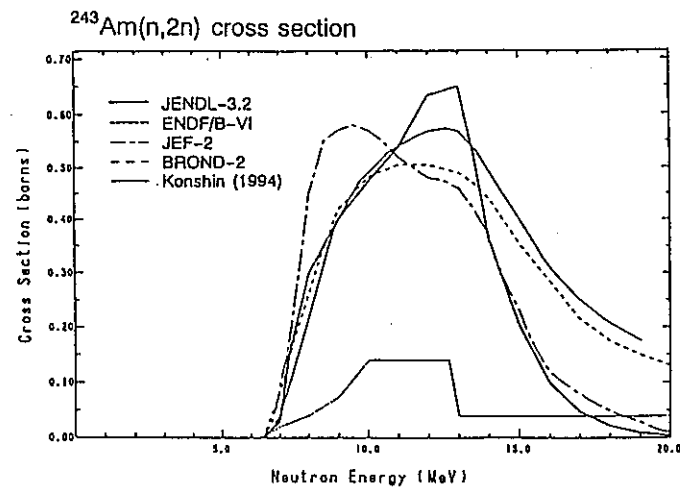


図 2 0 $^{243}\text{Am}(n, 2n)$ 反応断面積の評価データの比較

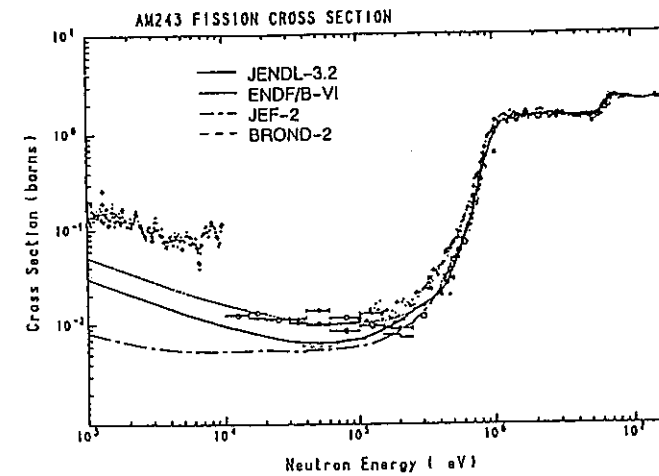


図 2 2 ^{243}Am の核分裂断面積の評価データと実験データの比較

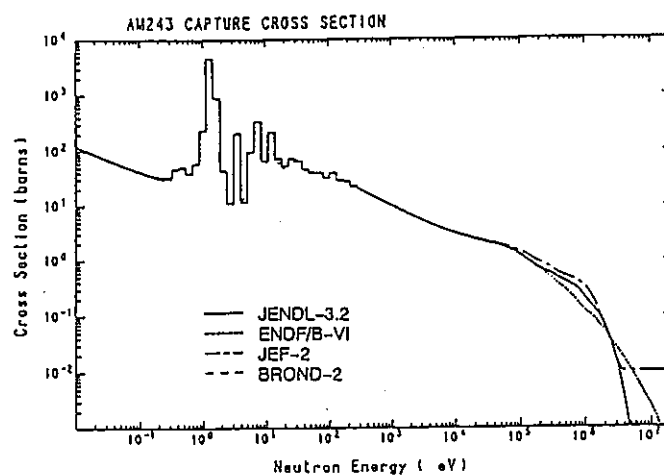


図 2 3 ^{243}Am の中性子捕獲断面積の評価データの比較

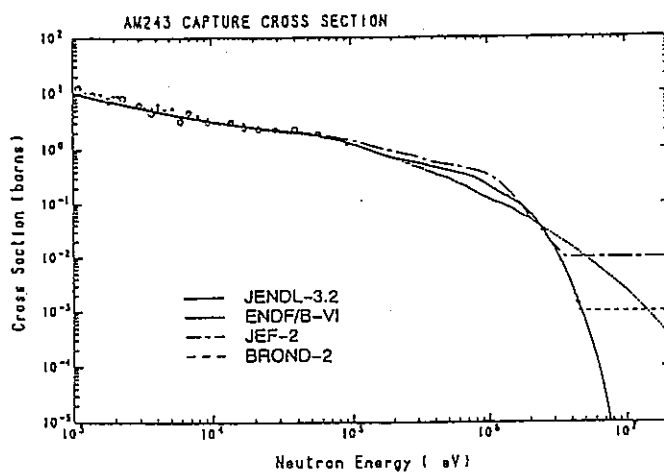


図 2 4 ^{243}Am の中性子捕獲断面積の評価データと実験データの比較

3. 京都大学 鉛スペクトロメータ

3.1 鉛スペクトロメータとその特徴

重い核であって、その中性子吸収断面積が小さい物質から成る大きな体系（一辺が 1.5 ~ 2m）にパルス状中性子を打ち込むと、中性子は体系から殆んど漏れ出ることなく、弾性散乱を繰り返しながら減速していく。この場合、散乱当たりに減速される割合が小さいため、多数回の散乱を繰り返す中で、比較的狭い velocity group に集まる傾向を示しながら、中性子打ち込み後の減速時間と共にエネルギーが下がっていく。1950年頃、Lazarev & Feinberg は、こうした現象に着目し、これをスペクトロメータとして応用できないかと考えた/11/。Bergmanらは、1955年の第1回ジュネーブ原子力平和利用国際会議において、初めて鉛減速スペクトロメータ（または単に「鉛スペクトロメータ」とも言う）の原理と実験結果について報告している/11/。それ以後、世界各国で幾つかの鉛スペクトロメータが設置されたが、今日稼動状態にあるものは、米国のレンスラー工科大学(RPI)に付設されているRINS/12/を含め、数基程度かと思われる。

大きな鉛集合体のほぼ中央部にパルス状高速中性子が打ち込まれると、鉛は中性子吸収断面積が小さいため、中性子は弾性散乱（0.57 MeV以上では非弾性散乱も起こり得るが）を繰り返し減速して行く。高エネルギー側の中性子はそれだけ速くエネルギーを失うため、エネルギーの focus 現象が起こり、50~100keV 以下の中性子になると、減速時間に対応してほぼガウス分布に近いエネルギー分布を持つようになる。その平均中性子エネルギーは減速時間の自乗に反比例する関数として導かれる/11,13/。減速途中の中性子 velocity group が持つエネルギー分解能（半値幅）は、鉛スペクトロメータ固有の核的な特性により30~40%と広がっている。この点が鉛スペクトロメータ最大の短所と言える。しかし、鉛スペクトロメータの最大の特徴は、中性子源より僅か数10cmの場所で実験が行えることもあって、強力な中性子束が得られることである。例えば、通常の飛行時間分析実験に比べ、中性子強度が数千倍から1万倍（飛行路が5mの場合）にもなると言われている/12/。この点に注目して、RPI では鉛スペクトロメータを用いて、keV 領域における U-238 の sub-threshold 核分裂断面積の測定/12/、100 keV以下でのトリウム、キュリウム、アインシュタニウム等に対する核分裂反応断面積の測定/14-17/が行われている。これらの実験においては、反応断面積が μ b オーダと小さいか、実験試料の入手量が極めて制限される等の実験上不利な条件下にあっても測定が可能であった。Block等は、鉛スペクトロメータを用いて核分裂断面積を測定する場合、測定可能となる最低条件として「 1μ g b」と言う表現を使っている/12/。即ち、 1μ g 以上の試料があれば1 bの核分裂断面積の測定が可能であり、1 g 以上の試料があれば 1μ bの核分裂断面積測定が可能となる一つの目安を示している。 α 崩壊、 β 崩壊を伴い、実験上のバックグラウンドが高くなるアクチナイド核

種、試料量を十分入手できないF P核種、断面積の小さい核種等の核データ測定、物質の assay 等の基礎的な研究に対しても、鉛スペクトロメータは、その特徴を生かして活用されている/12, 14-19/。

中性子源としてのK U L Sについて、飛行時間分析実験に使われる京都大学原子炉実験所の電子線型加速器 (Linac : 最高電子エネルギー=46MeV) /20, 21/、及び5 MWの研究炉 (K U R) /22/と比較し、それらの特徴を表4にまとめた。K U L Sはエネルギー分解能の点でLinac飛行時間分析法に比べ遥かに及ばないが、実験場の中性子束は数千倍の強さがある。しかし、中性子束の高さから言うと、K U RはK U L Sの場合より一段と高いが、定常中性子源であるため時間的にもエネルギー的にも得られる情報は積分量である。これらの中性子源には、それぞれ特徴があつて、これを生かした相補的使い方により一層充実した研究の遂行が期待できる。

表4 中性子源としてのK U L S、L i n a c、K U Rの比較

項 目	K U L S	L i n a c	K U R
中性子発生 の原理	Linacのパルス 中性子源を使用	電子を加速し重 金属を標的に照射 光中性子を発生	ウランを核分 裂させる
中性子発生 の制御方法	Linacパワーを 調整する	電子の加速状態 を制御	制御棒で連鎖 反応量を制御
中性子発生 部位の体積	スペクトロメータ内 全域(実験孔)	小さい: 約10cmx10cmx 10cm程度	容積は大きい 約50cmx50cmx 50cm程度
中性子発生 の時間的様相	Linacパルスの 発生に同じ	間欠的、パルス状 毎秒数百回程度	連続的に発生 定常中性子源
中性子エネルギー スペクトル	0.1eV~100keV 共鳴領域	熱中性子から MeV領域まで	熱中性子から MeV領域まで
中性子束強度	Linac条件と 実験場による $10^5 \sim 10^8 \text{ n/cm}^2/\text{s}$	平均 $\sim 10^{12} \text{ n/s}$ パルス当 $\sim 10^{18} \text{ n}$	$\sim 10^{14} \text{ n/cm}^2/\text{s}$
利用できる 放射線	共鳴中性子が主	中性子の他、 電子、陽子、 γ	中性子が 支配的
中性子利用 方法、形態	核データ、 即発 γ 線分析 assay	TOF実験、核 データ、照射、 放射光、物性・ 陽電子研究、 RI製造	中性子を多量 に、ビーム実 験、照射、RI 製造

3.2 鉛スペクトロメータの原理

鉛は、原子番号が 82、質量数が 207.2 と大きい物質であるため、中性子が鉛との衝突によって低エネルギーまで減速するためには（1 衝突当たりのレサジーの平均増加量： $\xi = 0.0096$ ）、多数回の衝突を繰り返すことになる（例えば、1 MeV の中性子が 0.1 eV になるまで：1680 回）。また、鉛の中性子断面積は殆んどが散乱断面積（熱中性子で 11.2 b）であり、中性子吸収断面積が小さいため（熱中性子で 0.17 b）、パルス状の高速中性子が大きな鉛の体系に打ち込まれると、鉛による中性子の吸収は殆んど無く、また体系からの漏れが少ないため、中性子は体系内に長く留まって、その中性子束群は減速時間と 1 対 1 の対応関係を保ちながら、低エネルギーまで減速されていく。

鉛体系内に打ち込まれた高速中性子の時間的な振る舞いは、次のような時間依存減速方程式によって与えられる/13/：

$$\frac{dn(v, t)}{dt} = -v \Sigma_s n(v, t) + \frac{2v}{1 - \alpha} \Sigma_s n(v', t) \frac{dv'}{v'} \quad (1)$$

重核の均質媒質の内部では、弾性散乱によって減速して行く中性子の平均速さを v とすると、中性子の減速時間 t は、次のように導かれる/13/：

$$t = A \lambda \times \left(\frac{1}{v} - \frac{1}{v_0} \right) = \frac{A \lambda}{v} = \frac{A}{v \Sigma_s} \quad (2)$$

ここで、 v_0 は中性子の初期速さ、 A は散乱媒質の質量数、 λ は散乱の平均自由行程、 Σ_s は散乱断面積である。

$$E = \frac{1}{2} m v^2 = \frac{1}{2} m \left(\frac{A}{t \Sigma_s} \right)^2 = \frac{K}{t^2} \quad (3)$$

となって、中性子の平均エネルギー E (keV) は、減速時間 t (μs) の自乗に反比例することが分かる。 K は減速時間定数である。実際の測定においては、減速時間のゼロ時間補正項 t_0 が入るため、(3) 式において一般的には t に代わって $t + t_0$ が用いられる。エネルギー分解能は中性子速度の広がり（分散）によって決まり、

$$\left(\frac{\Delta E}{E} \right)^2 = \frac{\langle E^2 \rangle - \langle E \rangle^2}{\langle E \rangle^2} = \frac{8}{3A} \quad (4)$$

で与えられる/13/。半値幅は標準偏差 $\Delta E / E$ の 2.35 倍であるから、鉛スペクトロメータにおける理想的な条件下でのエネルギー分解能（半値幅）は 27% と導ける。

3.3 京都大学 鉛スペクトロメータ

京都大学原子炉実験所に付設されている鉛スペクトロメータは、当初、東京大学工学部に設置され（昭和 43 年）、その後、同大学原子力総合研究センターに移管された「鉛減速

時間スペクトロメータ (LESP)」/23/を、平成3年になって京都大学原子炉実験所の方に譲り受けたもので、46 MeV 電子線型加速器と組み合わせた京都大学 鉛 (減速) スペクトロメータ (K U L S) として実験に使用されることとなった/24/ (付録A)。

本鉛スペクトロメータは、 $10 \times 10 \times 20 \text{ cm}^3$ の大きさを持つ高純度鉛 (99.9%) ブロックを約1600個積み重ね、1辺が1.5mからなる立方体で総重量は約40トンである。図25に鉛スペクトロメータの断面図を示す。鉛ブロックを積み上げるとき、表面の酸化膜や油分、水分を除去するため、サンドペーパーやワイヤブラシで1個ずつ丁寧に研磨し、エタノールで十分洗浄を行っている。

本鉛スペクトロメータKULSの設置に当たり、幾つかの工夫が加えられた/24/。

- ①京大原子炉実験所電子線型加速器のターゲット室に鉛スペクトロメータを設置 (図26) するとき、従来から進めてきた実験も支障なく行えるよう、ターゲット室の床面の補強工事を行い、鉛体系全体を頑丈な台車の上に乗せて移動できるようにした。
- ②LESPには、中心付近に貫通孔、その後方と上部にも実験孔があったが、図27に示すように、今回はさらに8ヶ所に角柱型 (断面 $10 \times 10 \text{ cm}^2$) 実験孔 (奥行き50cm~60cm) を新設した。
- ③新設実験孔の内、1ヶ所はその周辺を厚さ10~15 cmのビスマス層で覆う構造とした。鉛からの中性子捕獲 γ 線は6~7 MeVと高いのに比べ、ビスマスのそれは約4 MeVと低い。鉛から受ける中性子捕獲 γ 線により、実験試料に誘発核分裂 (光核分裂) が起こることを避けるための低 γ 線量場としてビスマス実験孔を設けた。
- ④KULSのほぼ中央部に金属タンタルターゲットを置いて、パルス状高速中性子を発生させるが、電子線型加速器のドリフトチューブはスペクトロメータ入り口までとし、加速器側の真空系が実験系によって乱される恐れがないよう、加速器側と光中性子源用タンタルターゲットシステムとは独立させている。

加速器の運転条件によっては、ターゲットに打ち込まれるパワーは500W前後にもなるが、圧縮空気を流す冷却方式によりターゲットケースの表面温度を250℃前後までに抑えて実験を行うことが可能である。タンタルターゲットより得られる光中性子は、平均エネルギー約1 MeV前後のものが多く、U-235の核分裂スペクトルを低エネルギー側に約1 MeVシフトさせたような分布、広がりを持つスペクトル形状を示している/20, 24/。

3.4 鉛スペクトロメータKULS中の中性子輸送計算

京大原子炉実験所に付設された46MeV電子線型加速器からパルス状高速中性子が鉛スペクトロメータKULSに打ち込まれた後、鉛体系内で徐々に減速されていく中性子の時間的振舞いは、連続エネルギー減速モンテカルロコードMCNP/8/を用いた計算により求められた/24/。MCNPは中性子と γ 線の輸送計算が行える計算コードとして知られているが、これに加えてパルス状中性子に対する固定中性子源問題では、中性子の時間的変化を 10^{-8} 秒間の間隔

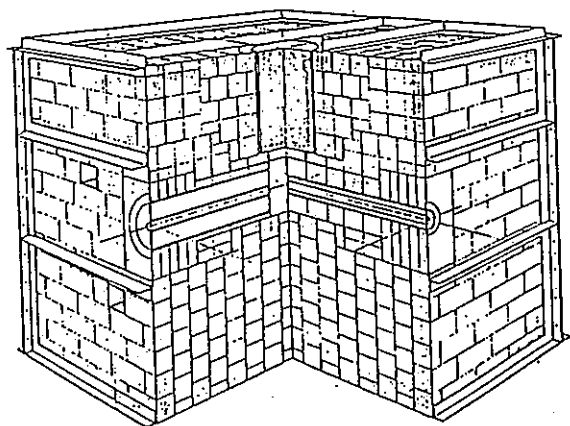


図 2 5 鉛スペクトロメータKULSの断面図

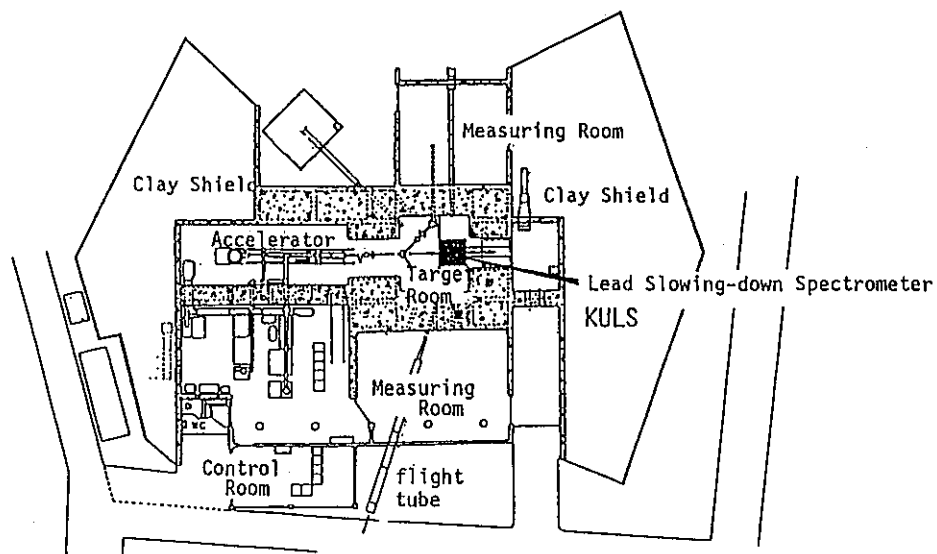


図 2 6 電子線型加速器室と鉛スペクトロメータKULSの設置位置

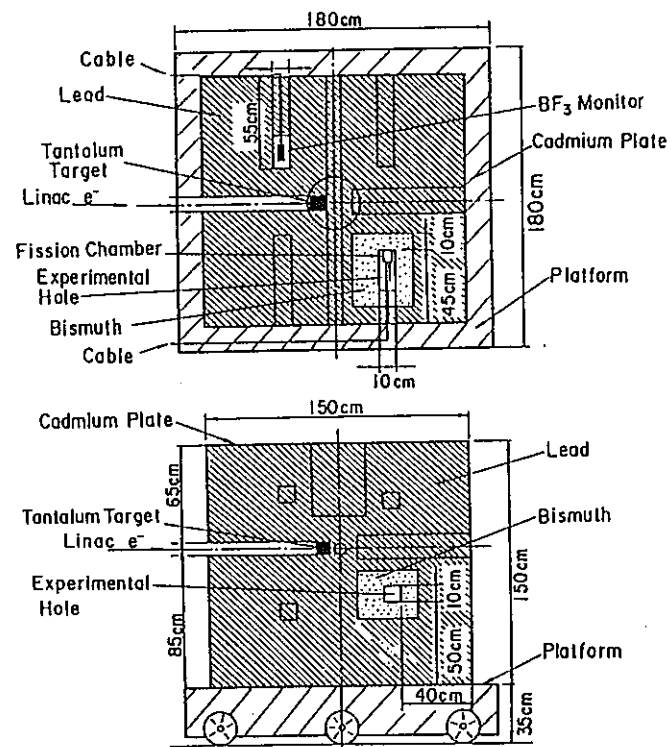


図 2 7 鉛スペクトロメータKULSの
平面図 (上) と垂直断面図 (下)

毎に追跡することが可能である。MCNPは鉛スペクトロメータ中での中性子の時間的な挙動を計算によって求めるコードとして適していると言える。米国のRPIの研究グループにおいても、鉛スペクトロメータ中での中性子挙動（時間スペクトル、エネルギー分解能など）を求める計算に、本コードを使用している/25/。

本計算では、KULSを設置した台車を含めた3次元計算を行っている。さらに、KULS内部に設けたビスマス実験孔部についても考慮し、中性子源の位置、KULSを覆ったカドミウム板など、実際に即した計算配置を取っている。図28は、KULSのビスマス実験孔における時間依存スペクトルの計算結果で、加速器からパルス状中性子源が打ち込まれた後、 $4\mu s$ 、 $9\mu s$ 、 $50\mu s$ 、 $100\mu s$ 、 $310\mu s$ における結果を示す。高速中性子のエネルギー領域では、入射中性子源スペクトルの広がりそのまま広いエネルギー幅となっているが、やがてガウス分布に近い漸近形を保ちながら中性子が減速していく様子が分かる。本計算の結果、ビスマス実験孔における減速時間とエネルギーの関係($E = K/t^2$)を示す定数Kとして、 $191 \pm 3 (\text{keV} \cdot \mu s^2)$ が得られた。鉛の実験孔においても、ほぼ同様の時間依存スペクトルが観測され、Kとして $157 \pm 4 (\text{keV} \cdot \mu s^2)$ が得られた。本MCNP計算に依る減速時間とエネルギーの関係をみると、ビスマス実験孔の方が鉛実験孔の場合に比べ中性子の減速が約18%程度遅いことが分かる。また、エネルギー分解能は何れの実験孔においても40~45%程度の値を示した。

本KULSにおける中性子挙動・特性の1つとして、先にMCNPコードを用いて時間依存スペクトルを計算したが、これを時間積分すると定常中性子源としての減速中性子スペクトルが得られる。計算には、MCNPコード用にENDF/B-IVより作成された核データファイルを使用した。他にJENDL-3、ENDL-85データファイルによる計算も比較のために実施した。これらの核データファイルによる計算結果を図29に示す。KULS内では、 $1/E$ より硬い中性子スペクトルが得られ、熱中性子は少ないことが分かる。3つのデータファイルによる計算結果は全般的に一致しているが、10keV以下のエネルギー領域では、ENDF/B-IVによる計算値が他のものより大き目となっている。

3.5 鉛スペクトロメータKULSの特性

3.5.1 中性子減速時間とエネルギーの関係

鉛スペクトロメータKULSのエネルギー較正は、表5に示した共鳴フィルターの透過中性子スペクトル測定及び共鳴中性子の捕獲 γ 線測定の方法に依った/24/。まず、中性子透過率測定では、BF₃カウンター（直径12mm、有効長50mm、内圧1気圧）を用意し、これを共鳴フィルターで巻き、中性子の減速時間の関数として中性子計数を行った。測定された時間スペクトルには、フィルターの共鳴エネルギーに対応した時間位置（即ちエネルギー点）に凹みが見れる。共鳴フィルターを交換しながら、中性子の透過率測定を繰り返し、共鳴エネルギー毎に減速時間との関係を求めた。また、共鳴捕獲 γ 線はArガスカウンター（直

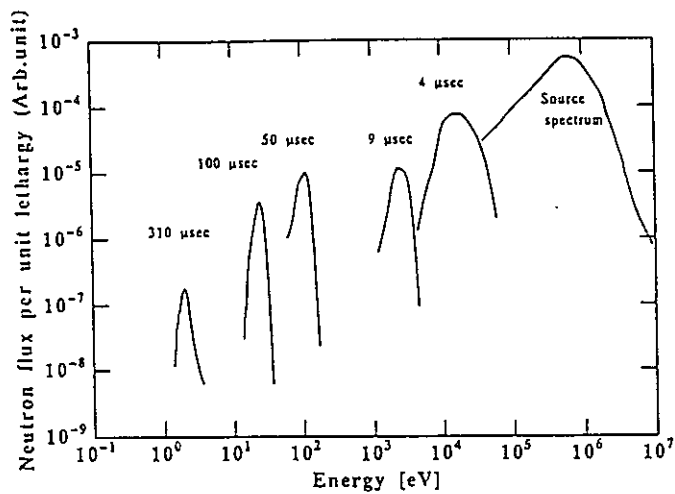
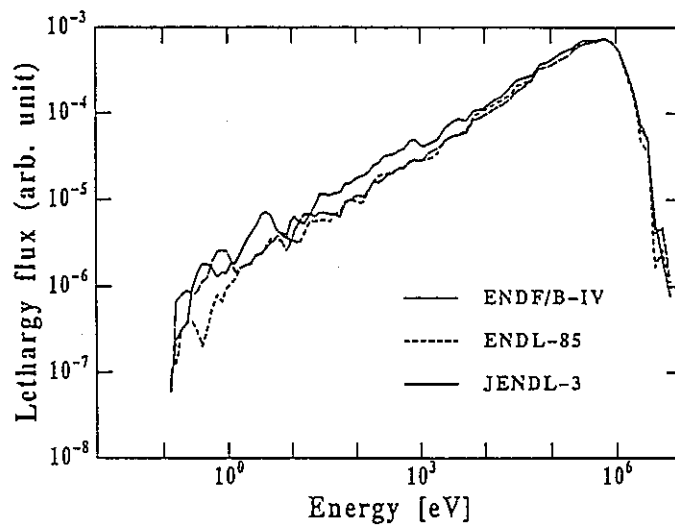


図 2 8 KULSのビスマス
実験孔における
中性子の時間
依存スペクトル

図 2 9 KULS内の (定常)
中性子スペクトルの
計算結果



Material	Energy (eV)	Thickness (mm)	Form
In	1.46	0.2	foil
Te	2.33	7.0	powder
Ta	4.28	0.2	foil
Ta	10.4		
Au	4.91	0.05	cylinder
Ag	5.19	0.5	cylinder
Ag	16.3		
Cd	27.5	0.3	cylinder
Mo	44.9	7.0	powder
Co	132	0.3	cylinder
Cu	230	1.0	cylinder
Cu	579		
Mn	336	7.0	powder

表 5 共鳴フィルターと
共鳴エネルギー

径0.5"、有効長2.5"、内圧1気圧：Ar:97%、CO₂:3%）を用いて測定したが、その時間スペクトルには共鳴エネルギーに対応して凸みが現れる。これを用いて共鳴エネルギーと減速時間の関係を求めた。図30は、Arガスカウンターと共鳴フィルターを用いて求めたビスマス及び鉛実験孔における中性子減速時間とエネルギーの較正曲線を示す。これらの結果を最小自乗フィットすることにより減速時間定数Kを求めると、ビスマス及び鉛実験孔のそれぞれについて 190 ± 2 および $156 \pm 2 (\text{keV} \cdot \mu\text{s}^2)$ が得られ、BF₃カウンターによる測定結果 $191 \pm 3 (\text{keV} \cdot \mu\text{s}^2)$ ともよい一致を示した。これらの測定値は、先のMCNPコードによる計算から求めた定数 ($191 \pm 3 (\text{keV} \cdot \mu\text{s}^2)$) ともよい一致を示している。また、鉛実験孔における定数は、以前に東京大学のLEPS時代に測定された値 $155 (\text{keV} \cdot \mu\text{s}^2)/23/$ ともよい一致を示した。

3.5.2 KULSのエネルギー分解能

鉛スペクトロメータKULSにとって、エネルギー分解能も重要な特性の1つである。エネルギー分解能測定には、次の条件を備えた物質（フィルター）の使用が望まれる：①共鳴ピークが大きく、その幅が狭いこと、②共鳴エネルギーが既知で、隣の共鳴ピークから十分離れていること、③共鳴物質（フィルター）の厚さが薄いこと、などである。

本研究におけるエネルギー分解能測定も、先の表5に示したように、大きくて鋭いピークを持つ共鳴フィルターを使い、BF₃カウンターを用いた中性子透過率測定法と、Arガスカウンターによる共鳴捕獲 γ 線測定の方法に依った/24/。まず、BF₃カウンターでは、中性子透過率測定において求めた時間スペクトルを凹型のガウス分布関数にフィットして求め、その半値幅からKULSのエネルギー分解能を算出した。中性子の透過時間スペクトルの測定例を図31に示す。Arガスカウンターを用いたエネルギー分解能測定では、BF₃カウンターによる測定に用いた大きな共鳴のフィルターより、むしろカドミウムや銅試料に見られる δ 関数状の極めて狭く鋭い共鳴ピークに注目した。図32は、銅フィルターによる579eVと230eVの共鳴捕獲ピークについて測定した時間スペクトルの例である。KULSの持つエネルギー分解能の広がりを見ると、 δ 関数状の鋭い共鳴ピークを中性子透過率法によって測定することは困難である。また、透過率測定法では使用したフィルターの共鳴断面積にもある程度の幅があるため、これらに対する補正が必要となる。しかし、共鳴捕獲 γ 線測定法では鋭い共鳴ピークの場合でも測定が可能であり、むしろ共鳴ピーク幅を考慮せずに分解能測定が行える長所がある。KULSのビスマス及び鉛実験孔において、我々が求めたエネルギー分解能測定の結果を表6にまとめる。これには、MCNPコードによる計算値も示したが、それらは何れも誤差内でよい一致を示している。数eVからkeV付近までのエネルギー分解能の実測値は約40%となり、このエネルギー領域より高いエネルギー側、低いエネルギー側では、共に分解能は大きくなっている。

U-235やAm-241に関するENDF/B-VI、JENDL-3.2等の評価データによると、いわゆる共鳴領域のeV～200eVにおいてはエネルギー幅が極めて狭く、鋭いピークを示す多数の共鳴が存在

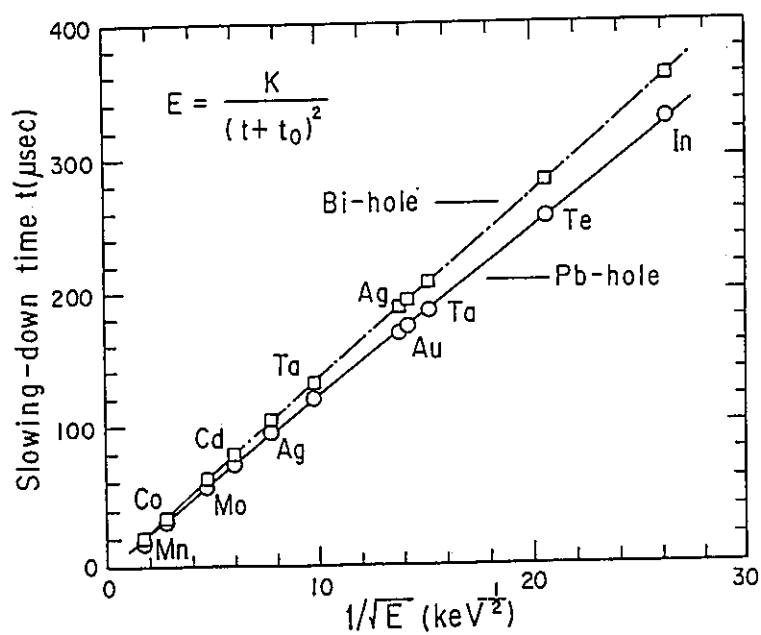


図 30 KULSのビスマス実験孔と鉛実験孔における中性子減速時間とエネルギーの関係

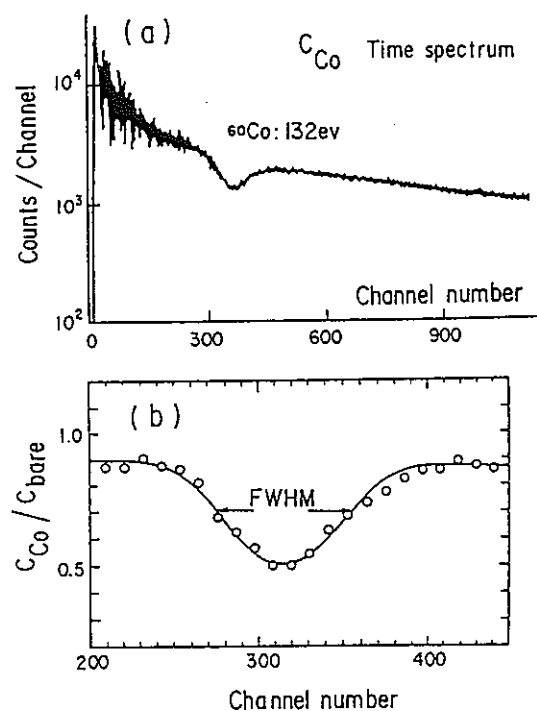


図 31 中性子透過法によって測定された時間スペクトルの例

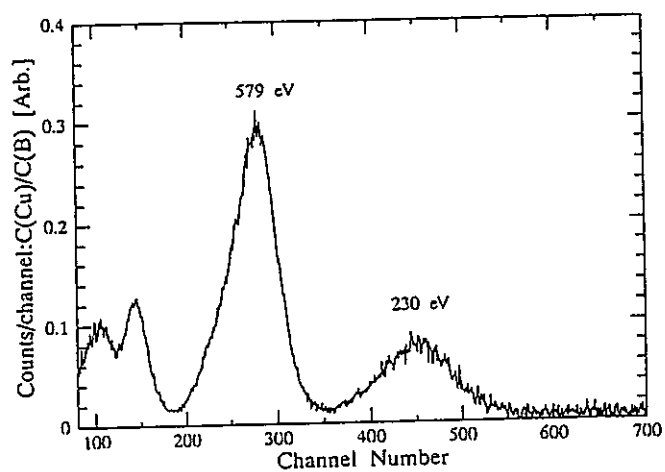


図 3 2 共鳴捕獲 γ 線測定によるエネルギー分解能測定例

表 6 ビスマス及び鉛実験孔におけるエネルギー分解能

Measurements				Calculations		
Energy (eV)	BF3 counter Bi hole	Ar gas counter Bi hole Pb hole		Energy (eV)	MCNP code Bi hole Pb hole	
1.46	51 \pm 3			3.02		35.7
4.9	40 \pm 2			3.56	37.4	
10.4	38 \pm 1			10.0		28.5
27.5		38 \pm 2	37 \pm 2	11.6	31.6	
44.9	38 \pm 1			29.8		28.2
132	39 \pm 2			33.8	35.7	
230		38 \pm 3	40 \pm 3	99.1		29.8
336	40 \pm 3			113	34.5	
579		42 \pm 3	42 \pm 4	298		33.7
2370	53 \pm 3			339	38.3	
				990		38.1
				1091	43.2	
				2988		50.3
				3208	51.8	

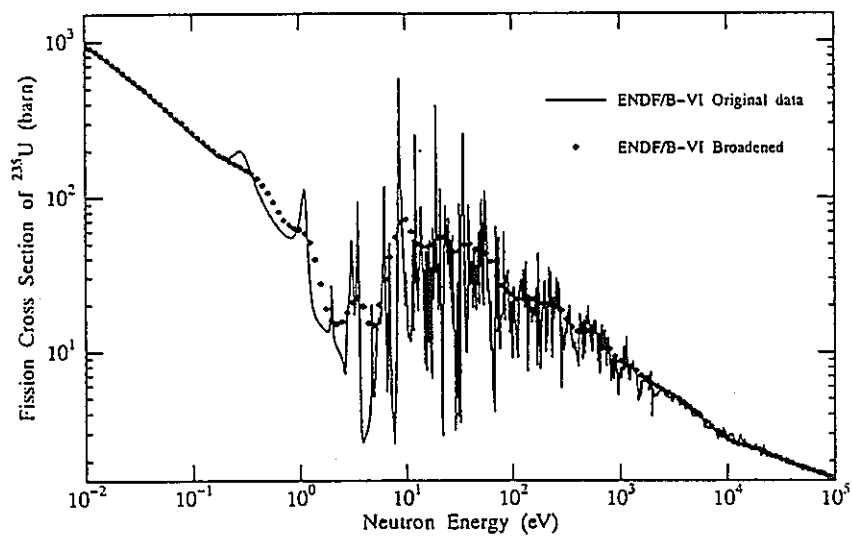


図 3 3 $^{235}\text{U}(n, f)$ 反応の ENDF/B-VI 評価値と、
分解能40%でbroadeningした結果

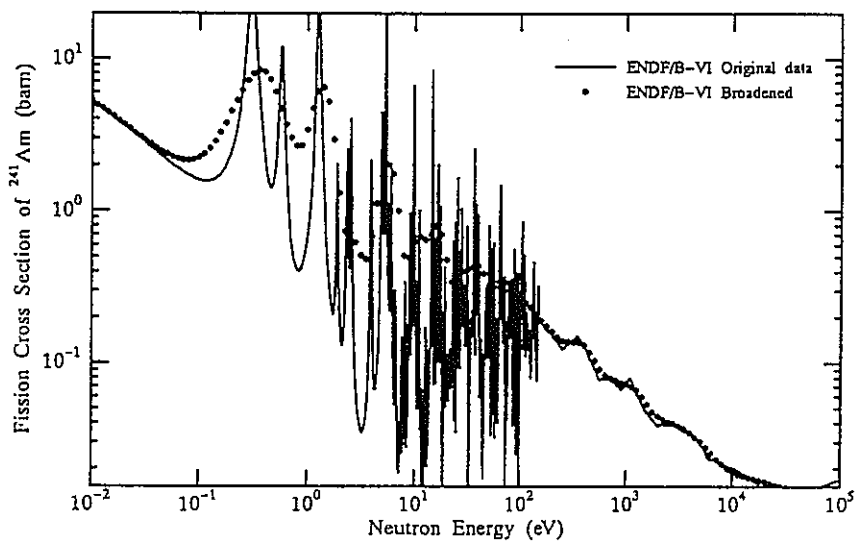


図 3 4 $^{241}\text{Am}(n, f)$ 反応の ENDF/B-VI 評価値と、
分解能40%でbroadeningした結果

している。KULSによる実験では、エネルギー分解能が $\sim 40\%$ にも及ぶため、後述の実験値と評価値の比較においては、ガウス型の分解能関数を使って評価データのbroadeningを行っている。図33、図34は、それぞれの評価データに対し、KULSの分解能でbroadening操作を行う前とその後のデータの例を示している。

3.5.3 KULS内の中性子スペクトル

本研究では、KULSの特性実験の一環として、22m飛行路を用いた中性子飛行時間分析法により、鉛スペクトロメータ中の中性子スペクトルを測定した²⁴⁾。KULSのほぼ中央部にセットされたタンタルターゲット製の光中性子源の後方約15cmの位置に、直径8cmの貫通孔が設けられている(図27)。その中央部まで飛行路側の鉛プラグを抜き取り、設けられた実験孔(リエントラントホール)の底部から、ターゲット位置に対し90度方向に取り出された中性子を測定した。本実験には、我々が従来より使用してきている⁶Liガラスシンチレータ及び¹⁰B-vaseline plug NaI(Tl)検出器²⁶⁾を用いた。図35、図36は、それぞれの検出器を用いて測定したKULSの中性子スペクトルを示す。また、これらの図では、ENDF/B-IV、JENDL-3、ENDL-85ファイルから作成された断面積セットを用いて計算した結果とそれぞれの実験値を比較している。計算値は実験値と全般的によい一致を示しているが、10keV近辺より下のエネルギー領域では、ENDF/B-IVによる計算値が他の定数による計算及び実験結果より高目になっていることが分かる。このことはENDF/B-IVの鉛の評価データについて再評価の必要性を示唆している。また、KULS内では低エネルギー、特に熱中性子は殆んど存在していないことが分かる。ここで図35、図36を見ると、KULS内の中性子場は大型の高速炉における炉心スペクトルの形状に近くなっている。このことから、KULS内の中性子場は標準的な中速中性子スペクトル場としても今後の利用が期待できよう。

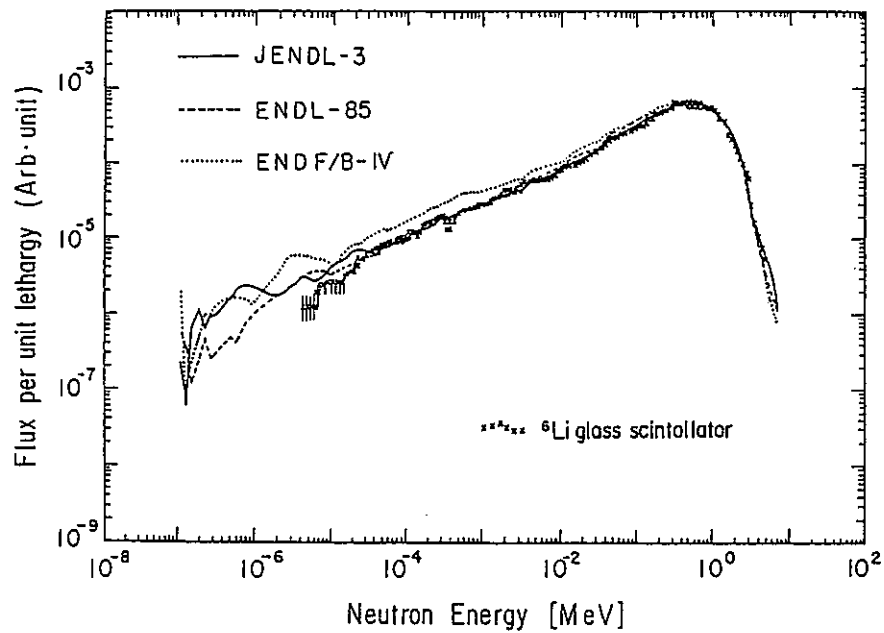


図 3.5 ^6Li ガラスシンチレータを用いて飛行時間分析法により測定した鉛スペクトロメータ内の中性子スペクトルとMCNPコードによる計算値の比較

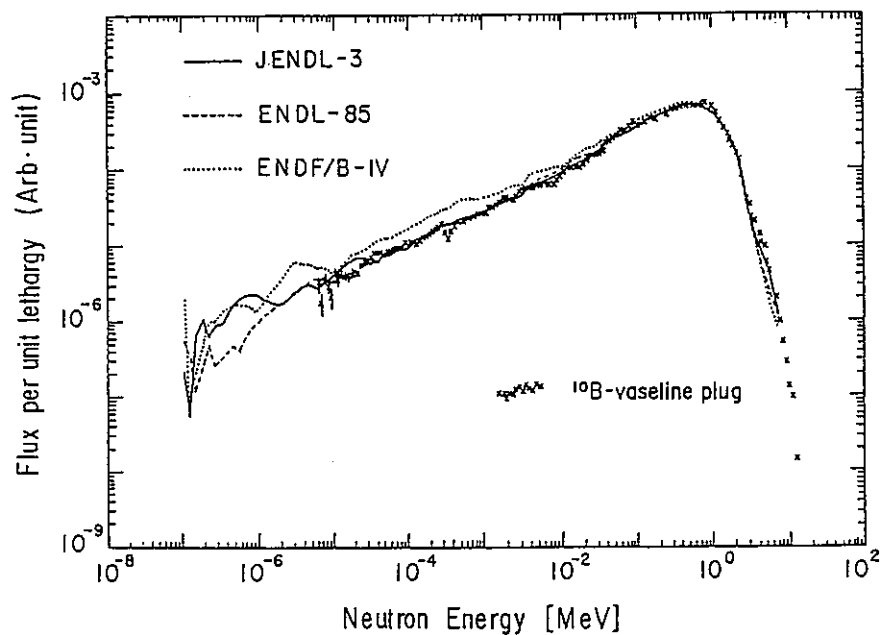


図 3.6 ^{10}B -vaseline plug NaI(Tl) シンチレータを用いて飛行時間分析法により測定した鉛スペクトロメータ内の中性子スペクトルとMCNPコードによる計算値の比較

4. 鉛スペクトロメータを用いた マイナーアクチニド核分裂断面積の測定

4.1 Am-241、Am-243、Am-242m 及び U-235 試料と核分裂電離箱

Am-241、Am-243 試料は、何れも、これらに含まれる不純物を除去するために、まず、イオン交換樹脂によって化学的に分離精製された/27/。これを電着膜とした後、核分裂電離箱として本実験に使用した。Am-241試料の場合、第一回目の化学精製操作で U、Np、Pu を取り除き、第二回目で Cm 等の不純物核種を除去した。元々、質量分析器を使って分析した試料をAm-241はIAEAから、Am-243はORNLから購入したものである。これらの α 線スペクトルを表面障壁型シリコン検出器を用いて測定した結果、殆んど不純物らしいものは観測されていない。Am-243の場合もAm-241と同様の化学精製を行った後、その α 線スペクトルを測定した結果、 α 放射能比（不純物核種：主としてCm-243/Am-243）にして0.8から0.00004（原子数の比 $=1.5 \times 10^{-7}$ ）へと純度が上がった。また、Am-241/Am-243 の α 計数比では0.007（原子数の比 $=4 \times 10^{-4}$ ）得られた。

Am-243試料については、これを化学精製しても時間と共に α 崩壊によってAm-243からPu-239が生成蓄積されてくるので、このPu-239の存在は $^{243}\text{Am}(n, f)$ 反応断面積測定における不純物として大きな影響を与えることになる。今回使用したAm-243試料は化学精製後約4週間、5ヶ月、13ヶ月経ったところで実験を行っているが、この間にAm-243から生成蓄積されたPu-239不純物の影響については、データ解析時においてその効果を補正している/28/。

化学精製されたAm-241、Am-243試料は、何れも厚さ0.2mm、直径28mmのステンレス板の中央部に、酸化物として直径20mmの円板形状に電着された。その後、電着膜がはく離しないようバーナで軽く焼固めている。

U-235試料は濃縮度が99.91%の硝酸ウラニールを溶解して精製した後、Am-241、243試料同様、厚さ0.2mm、直径28mmのステンレス円板に電着されている。これらを、図37に示すように、Am-241またはAm-243とU-235の電着膜を背中合わせにした、いわゆるback-to-back (B T B) 型の核分裂電離箱/29/として封じ込め、 $^{241}\text{Am}(n, f)$ 、 $^{243}\text{Am}(n, f)$ 反応断面積の測定に使用した。核分裂電離箱の中には、電離ガスとしてアルゴン97%、窒素3%の混合ガスが1気圧封入されている。U-235の核分裂断面積は精度よく求められている標準的な断面積の1つであり、これを用いてAm-241、Am-243試料に入射する中性子束を測定した。しかし、U-235及びAm-241の共鳴エネルギー領域では、これらの核分裂断面積の共鳴が互いに干渉して測定値に影響が出るのを避けるため、1 keV以下のエネルギー領域における $^{241}\text{Am}(n, f)$ 反応断面積測定においては、BF₃カウンターを用いた $^{10}\text{B}(n, \alpha)$ 反応によって中性子束をモニターしている。

Am-241、Am-243及びU-235試料の原子数は、表面障壁型シリコン検出器を用いた α 線スペクトルの測定によって求められた。Am-243及びU-235電着試料からの α 線スペクトル測定の

- ①真空引き・ガス導入管
- ②コネクター
- ③容器 (アルミニウム)
- ④電極板 (陽極)
- ⑤電着板支持棒
- ⑥オーリング (ゴム)
- ⑦電極板支持材 (テフロン)

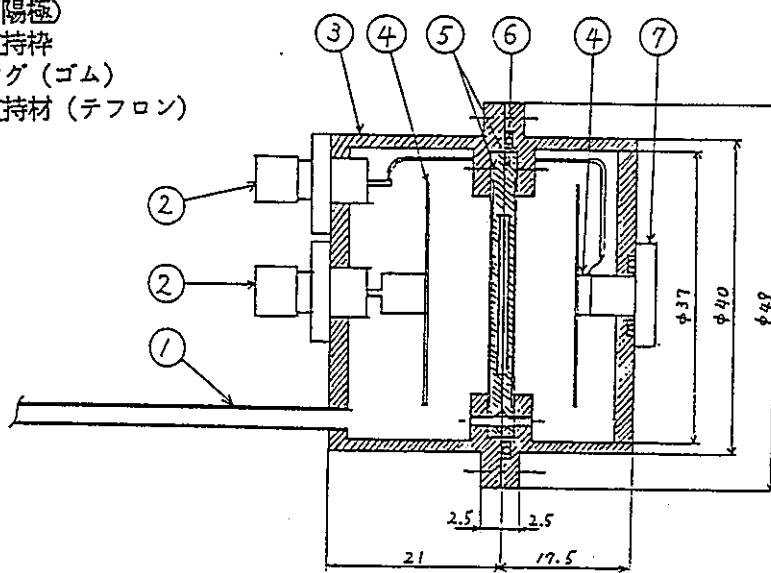


図 3 7 背中合わせ型の核分裂電離箱の断面図

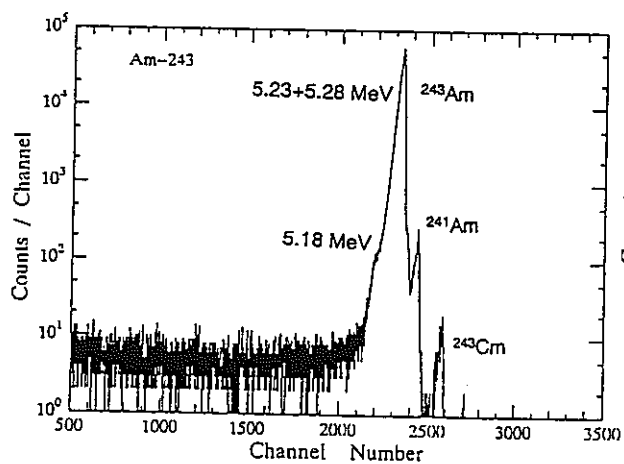


図 3 8 Am-243の α 線スペクトル

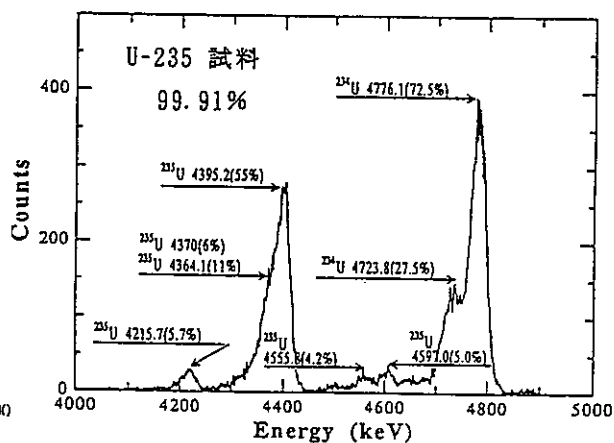


図 3 9 U-235の α 線スペクトル

例が図 3 8、図 3 9 である。図 3 8 には、Am-243 試料中に僅かに含まれる Am-241 からの α ピークが観測される。さらに、高エネルギー側の 5.8 MeV 近辺には Cm-243 からと思われる α 線のピークが僅かに見られる。これらは、化学精製直後の α 線スペクトル測定において既に観測されていたもので、半減期の違いも考慮に入れると本実験においては問題となる不純物量ではない。また、これら以外の不純物核種は観測されなかった。得られた α 線の計数データ、電着試料が α 線検出器に張る立体角、及び崩壊定数から、Am-241、Am-243、U-235 それぞれの原子数を算出した。また、高純度 Ge 検出器 (HPGe) を用いて γ 線測定も行ったが、その結果から求めた各試料の原子数は何れも 3 % 以内で α 線測定の結果と一致した。

Am-242m は、なかなか入手が困難な試料の 1 つである。欧米の RI 線源を供給、販売している施設でも、現在は取扱っていないようであったが、幸いロシアから入手することができた。その Am-242m 試料の特性は；化学形：AmO₂、化学組成：Am-242m:85.25% のほかに Am-241 及び Am-243 が含まれる。図 4 0、図 4 1 は、それぞれ Am-242m 試料の α 線及びガンマ線のパルス波高分布測定の一例である。Am-242m の α 線及びガンマ線の放出強度はいずれも低い、僅かではあるが Am-242m のピークが観測されている。これらのデータから Am-242m の原子数を算出するためのデータ解析を現在進めているところである。この Am-242m 試料も先の Am-241, 243 の場合と同様、厚さ 0.2 mm、直径 28 mm のステンレス円板に電着 (直径 20 mm) されている。これを U-235 電着膜と共に、BTB 型の核分裂電離箱に封入し、使用した。

4.2 核分裂断面積の測定

4.2.1 KULS を用いた実験

鉛スペクトロメータ KULS を用いた $^{241}\text{Am}(n, f)$ 、 $^{243}\text{Am}(n, f)$ 及び $^{242m}\text{Am}(n, f)$ 反応断面積の測定法は、先に我々が行った $^{237}\text{Np}(n, f)$ 反応断面積測定の場合と基本的には同じである /30/ (付録 B)。back-to-back 型核分裂電離箱を用いた実験の回路系 (Am-241 と U-235 の電着膜試料を用いた場合) を図 4 2 に示す。二種類の電離箱に対し測定系も独立に 2 系統を用意している。各時間分析器のチャンネル幅として 62.5 ns 及び 0.5 μ s を選び、そのチャンネル数は 4096 とした。図 4 3、図 4 4 は、Am-243 および U-235 の核分裂測定のパルス波高分布の例を示す。Am-243、U-235 何れの測定においても、数百チャンネル付近で凹型に波高分布が低くなっている箇所に核分裂信号と雑音信号の弁別値をセットした。また、これらの減速時間分析測定の結果を図 4 5、図 4 6 に示す。

$^{241}\text{Am}(n, f)$ 反応断面積測定における電子線型加速器の運転条件は、パルス幅 10~22 ns、パルスの繰り返し数 150~200 Hz、ピーク電流値 500~800 mA、加速電子エネルギー 30~32 MeV で、約 250 時間の実験の中程で、核分裂電離箱内の Am-241 と U-235 電着試料の位置を入れ換えた。

$^{241}\text{Am}(n, f)$ 反応断面積は、次式によって導かれる：

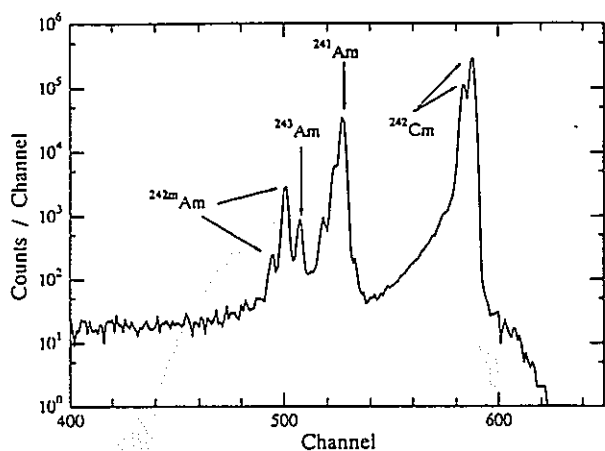


図 4 0 Am-242mの α 線スペクトル

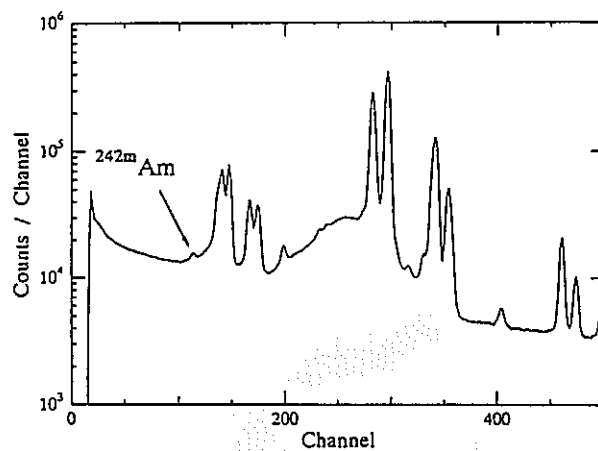


図 4 1 Am-242mのガンマ線スペクトル

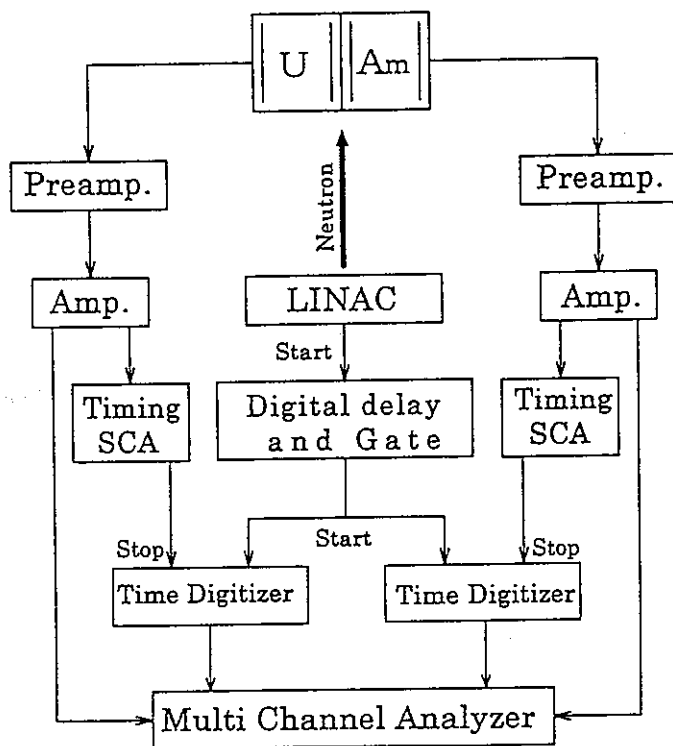


図 4 2 核分裂断面積測定回路図

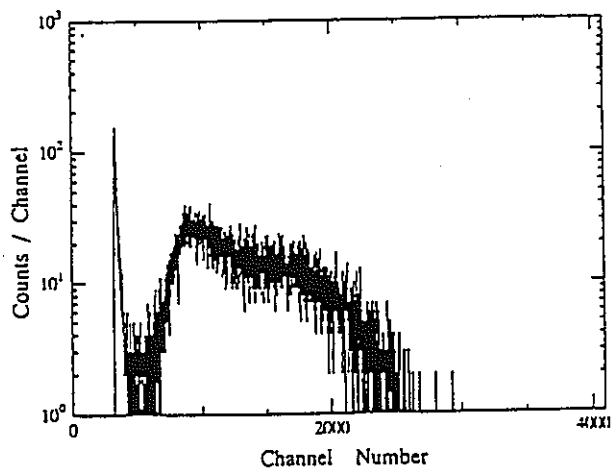


図 4 3 $^{243}\text{Am}(n, f)$ 反応の核分裂片
パルス波高分布

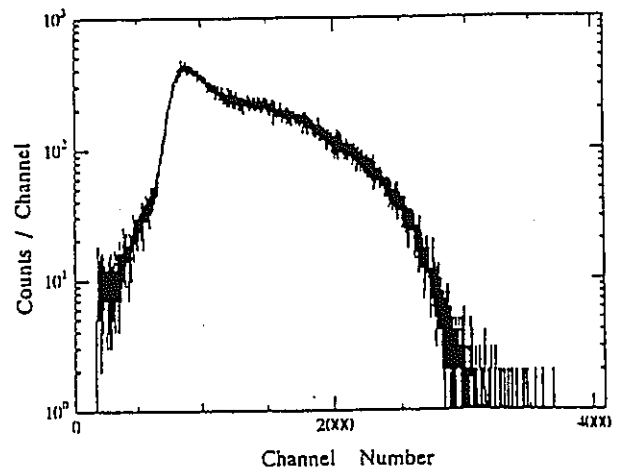


図 4 4 $^{235}\text{U}(n, f)$ 反応の核分裂片
パルス波高分布

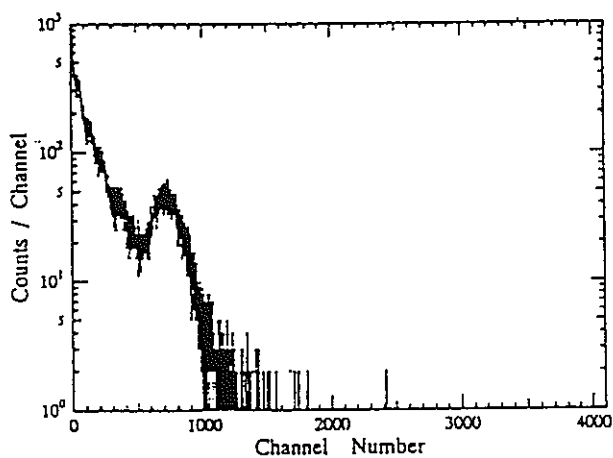


図 4 5 $^{243}\text{Am}(n, f)$ 反応測定 of 減速
時間スペクトル
($0.5 \mu\text{s}/\text{channel}$)

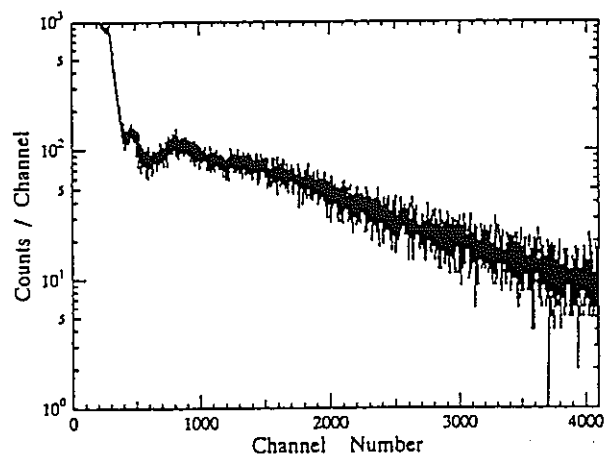


図 4 6 $^{235}\text{U}(n, f)$ 反応測定 of 減速
時間スペクトル
($0.5 \mu\text{s}/\text{channel}$)

$$\sigma_{Am}(E) = \frac{\text{Am-241の核分裂率}}{\text{U-235の核分裂率}} \times \frac{N_U}{N_{Am}} \times \sigma_U(E) \quad (5)$$

ここで、 N_{Am} 、 N_U : Am-241 及び U-235の原子数、

$\sigma_U(E)$: $^{235}\text{U}(n, f)$ 反応断面積。

本実験に用いた $^{235}\text{U}(n, f)$ 反応標準断面積は、評価済核データファイルENDF/B-VIに収納されているデータから引用し、KULSのエネルギー分解能でbroadeningして使用した。U-235の核分裂電離箱に代わるBF₃カウンターによる相対測定の場合には (U-235の核分裂率/ N_U) を $^{10}\text{B}(n, \alpha)$ 反応の計数率、 $\sigma_U(E)$ を $^{10}\text{B}(n, \alpha)$ 反応断面積に置き換えるものとする。この断面積は、本実験のエネルギー領域では標準的な1/v型形状を示している。また、 $^{243}\text{Am}(n, f)$ 反応断面積測定の場合も加速器の運転条件、測定時間などは $^{241}\text{Am}(n, f)$ 反応測定の場合とほぼ同様であったが、 $^{242}\text{Am}(n, f)$ 反応の場合には、その断面積が大きいこともあって実験時間はAm-241の場合の1/3から1/2程度であった。なお、 $^{243}\text{Am}(n, f)$ 及び $^{242}\text{Am}(n, f)$ 反応断面積の測定では、(5)式に示された241を243または242mと置き換えるものとする。

4.2.2 熱中性子断面積の測定

本研究においては、KULSを用いて0.1eV～10keV領域の $^{241}\text{Am}(n, f)$ 反応および $^{243}\text{Am}(n, f)$ 反応断面積を測定したのみならず、京都大学原子炉実験所の研究炉 (KUR) に付設されている重水熱中性子設備/31/ (付録C) においても、これらの熱中性子核分裂断面積を測定した。この場合の実験も、先のKULSにおける実験と同様、back-to-back型の核分裂電離箱を用いる方法によった。

マックスウェル分布型の標準熱中性子スペクトル平均断面積は、次式で定義される/13, 31/。

$$\sigma_{th} = \frac{\sigma_{th}(v_0)}{1.128} g(T_n) \sqrt{\frac{T_0}{T_n}}$$

ここで、 $v_0=2,200$ m/s、 $T_0=293.6$ K、 T_n は中性子温度、 $g(T_n)$ は g-factor と呼ばれる。そこで、2,200 m/sに当たる0.0253eVでの $^{241}\text{Am}(n, f)$ 反応断面積は、 $^{235}\text{U}(n, f)$ 反応の標準熱中性子断面積を使って、次のように与えられる。

$$\sigma_{th} = \frac{C_{Am}}{C_U} \frac{N_U}{N_{Am}} \frac{g_U(T_n)}{g_{Am}(T_n)} \sigma_U(0)$$

ここで、 C_{Am} 、 C_U : Am-241、U-235の核分裂計数率、

$g_{Am}(T_n)=0.996$ 、 $g_U(T_n)=0.976$: Am-241、U-235の g-factor、

$\sigma_U(0)$: 0.0253eVでの $^{235}\text{U}(n, f)$ 反応の標準断面積。

本実験では、 $^{235}\text{U}(n, f)$ 反応の標準熱中性子断面積値としてENDF/B-VIに与えられた586 bを引用した。

$^{243}\text{Am}(n, f)$ 反応の熱中性子断面積も、 $^{241}\text{Am}(n, f)$ 反応断面積の場合とほぼ同様の実験条件、実験方法によって測定した。

4.3 測定結果

4.3.1 $^{241}\text{Am}(n, f)$ 反応断面積

KULSを用いて測定された $^{241}\text{Am}(n, f)$ 反応断面積の結果、及びJENDL-3.2、ENDF/B-VIの評価済核データの結果を表7、図47に示す。ここに示した評価データは、KULSの持つエネルギー分解能（半値幅）～40%により broadening された結果である。 $^{241}\text{Am}(n, f)$ 反応断面積の絶対値は、U-235とAm-241の電着膜を背中合わせに封じ込んだ核分裂電離箱による測定結果から求めた。しかし、U-235やAm-241に共鳴ピークが存在する200eV以下の領域では、BF₃カウンターを用いた $^{10}\text{B}(n, \alpha)$ 反応によって、まず、 $^{241}\text{Am}(n, f)$ 反応断面積の相対値を求め、これを $^{235}\text{U}(n, f)$ 反応によって測定された200eV～1 keV領域の絶対値に規格化する方法によった。本実験における実験誤差を表8に示す。

全般的に見て、ENDF/B-VIとJENDL-3.2の評価値同志、及びこれらの評価値と本実験値とはよく一致している。しかし、よく見ると両評価値間にも22～140eV領域で違いが見られ、本実験値と比較するとJENDL-3.2は1.2～2.3倍小さくなっている。2～4 eV領域では両評価値とも低くなっているが、この場合はKULSの持つエネルギー分解能の問題が影響していることも考えられる。表7に関しては、高エネルギー領域を除いてENDF/B-VIの評価値は実験値と全体によく一致しているが、JENDL-3.2では0.89eV～200eV領域で低くなっている。Dabbsら/32/のデータは低エネルギー領域で高目の傾向を示している。

次に、図48では従来の実験データと本実験の結果を比較している。Dabbsら/32/の実験値は低エネルギー側を除き全般的に見て、本実験データとよい一致を示しているが、他の実験者らによるデータと本実験値とは必ずしもよい一致は見られない。Gaytherら/33/の測定値は本実験値と比べて55eV以上の領域で50～100%高く、Bowmanら/34/の測定値も200eV以上で倍の大きさを示している。数10eV以下では、Bowman、Gerasimov/35/、Derrien/36/らの測定結果は本実験値に近くなっている。Leonardら/37/のデータは2～5 eV領域で高い。Seegerら/38/の測定は20eV以上で著しく大きいことが分かる/39/（付録D）。

4.3.2 $^{243}\text{Am}(n, f)$ 反応断面積

実験に使用した試料を化学精製した後、4週間、5ヶ月、13ヶ月経った時点で測定を行った $^{243}\text{Am}(n, f)$ 反応断面積の結果を図49に示す。これを見ると、Am-243が α 崩壊して生成蓄積されたPu-239の主共鳴である0.3eV前後の断面積に影響が現れ、約0.6eV以下の領域で測定値が徐々に上昇していることが分かる/28/。図50は、 $^{243}\text{Am}(n, f)$ 反応断面積が、主として0.3eV近辺において、化学精製後どのように上昇してくるかをENDF/B-VIデータを使った計算により求めた結果である。図51は、化学精製後の時間と共にPu-239が精製蓄積され、0.3eV近辺のAm-243断面積値が見かけ上どのように上昇するかを計算に

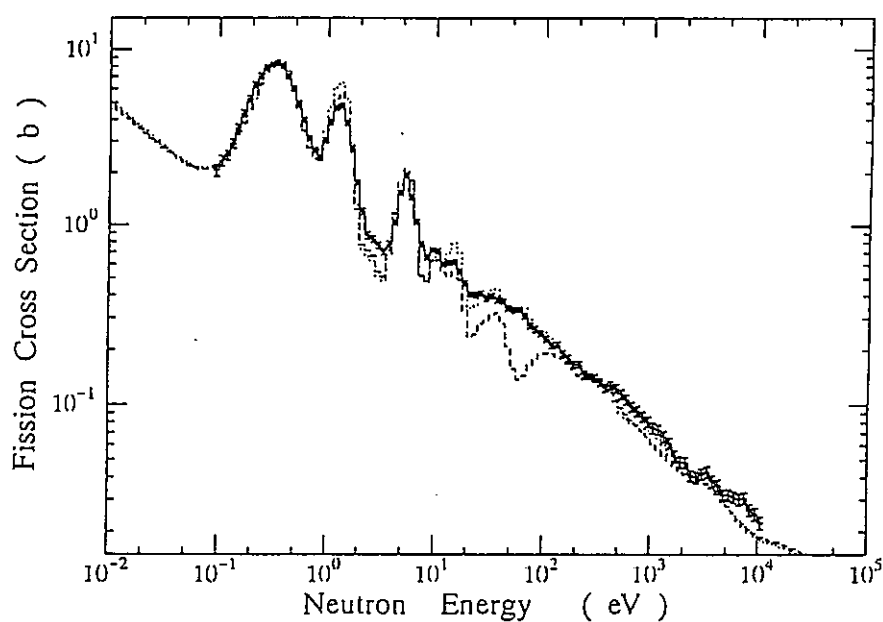


図 4 7 $^{241}\text{Am}(n, f)$ 反応断面積の測定結果と評価値の比較


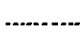

 Present
 ENDF/B-VI
 JENDL-3.2

表 7 $^{241}\text{Am}(n, f)$ 反応断面積の比較

Energy range (eV)	ENDF/B-VI	JENDL-3.2	Dabbs et al.	Present
0.1 - 0.89	4.753+0*	4.724+0	5.133+0	4.897+0
0.89 - 3.55	2.046+0	1.853+0	2.182+0	1.914+0
3.55 - 20.0	7.982-1	7.106-1	8.438-1	7.636-1
20.0 - 200	2.558-1	1.893-1	2.524-1	2.514-1
200 - 1000	9.701-2	9.708-2	10.224-2	10.965-2
1000 - 10000	3.031-2	3.009-2	3.110-2	3.570-2

* read as 4.753×10^{-0}

表 8 $^{241}\text{Am}(n, f)$ 及び $^{243}\text{Am}(n, f)$ 反応断面積測定における実験誤差

Uncertainties due to	Error in %	
	Am-241	Am-243
Statistical error for ^{241}Am for ^{235}U	0.08 - 6.2 0.06 - 1.1	0.09 - 7.3 0.08 - 1.5
Assignment error of fission counts for ^{241}Am for ^{235}U	< 1.9 < 0.65	< 2.0 < 0.65
Number of atoms for ^{241}Am for ^{235}U	1.3 1.2	1.5 1.2
Reference cross section for the $^{235}\text{U}(n, f)$ reaction	2 - 4	2 - 4
Reference cross section for the $^{10}\text{B}(n, \alpha)$ reaction	2	—
Correction for setting position of ^{241}Am and ^{235}U deposits in the BTB chambers	0.3	0.3
Correction to in-scattered neutrons by the chambers	0.2	0.2
Correction to background subtraction	< 0.2 - 0.4	< 0.2 - 0.5

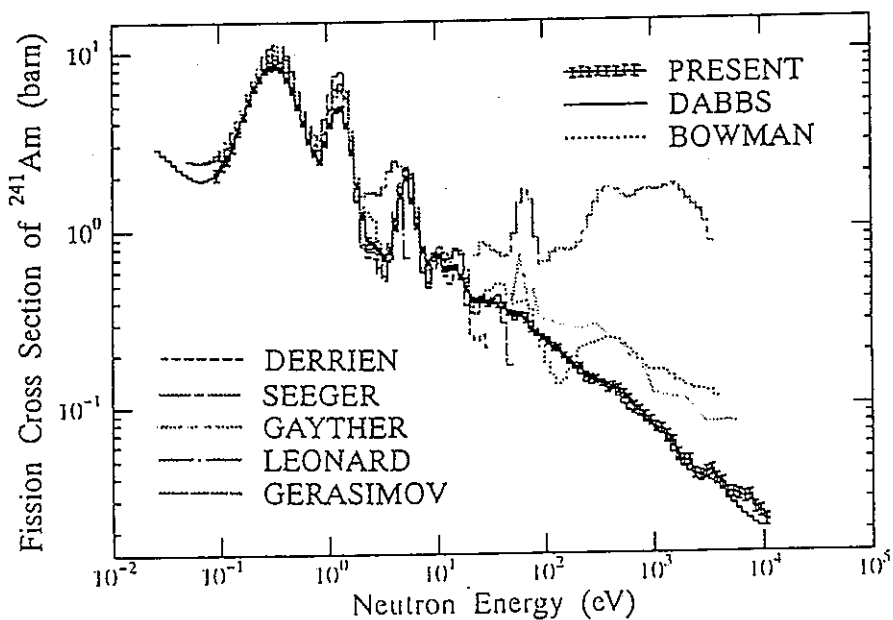


図 4 8 $^{241}\text{Am}(n, f)$ 反応断面積の測定値と従来の実験値との比較

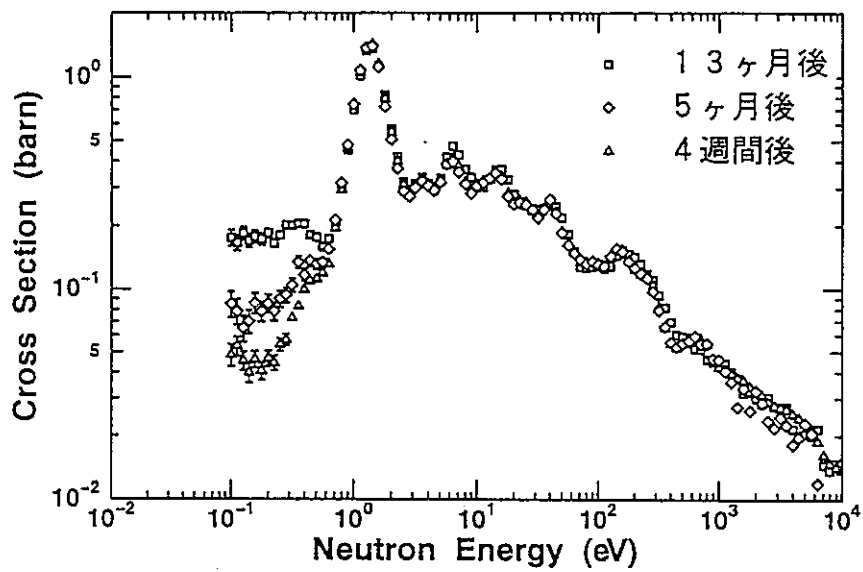


図 4 9 化学精製後の時間と $^{243}\text{Am}(n, f)$ 反応断面積測定値の変化

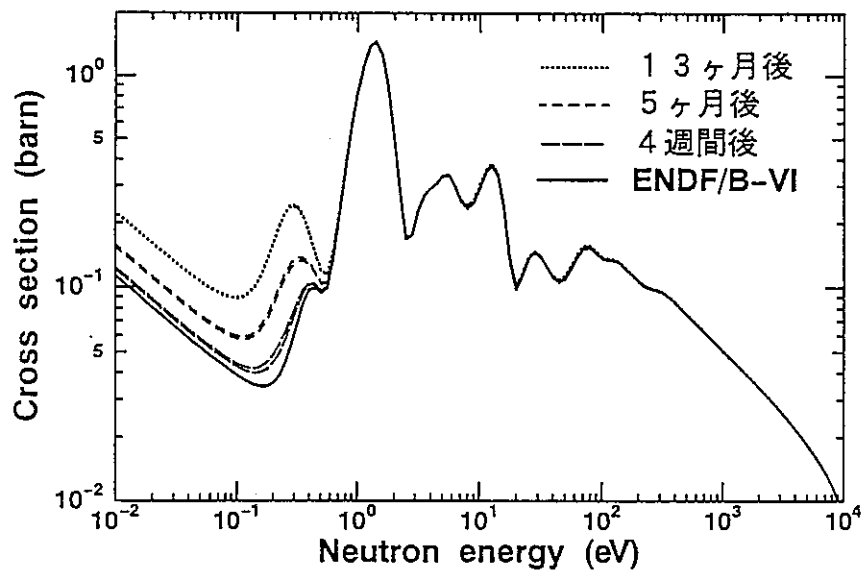


図 5 0 生成蓄積されてくるPu-239の効果を計算によって求めた $^{243}\text{Am}(n, f)$ 反応断面積(ENDF/B-VI評価データを使用)

よって求めた結果である(図49と図50の結果から)。不純物(Pu-239)生成による断面積上昇の計算値が我々の実測値とよい一致を示していることが分かる。以上の結果を基に、化学精製後の時間に対するPu-239の効果を補正して求めた $^{243}\text{Am}(n, f)$ 反応断面積の測定結果が図52である。この図には、本実験の結果とKULSの持つエネルギー分解能(半値幅)~40%によりbroadeningしたJENDL-3.2/7/、ENDF/B-VI/8/の評価済核データを比較して示している。本実験における誤差も表8にまとめられており、全体で4~8%程度になる。

ENDF/B-VIとJENDL-3.2の評価値間では0.3eV以下と15eV以上の領域で差異が見られる。前者は概して本実験値と一致の傾向にあるが、15~60eV間では低すぎる。JENDL-3.2データは100eV以上のエネルギー領域で全体に低目の傾向にある。3eV付近の凹み領域には両評価値と実験データとの間に差異が見られるが、これは鉛スペクトロメータのエネルギー分解能による問題とも考えられる。

$^{243}\text{Am}(n, f)$ 反応断面積の実測データは、図22にも見られるように、50eV以下では熱中性子での測定値を除き殆んど存在していない。今回の実験データは、この領域のデータを新たに提供している/40/(付録E)。

4.3.3 $^{241}\text{Am}(n, f)$ 及び $^{243}\text{Am}(n, f)$ 反応の熱中性子断面積

熱中性子に対する $^{241}\text{Am}(n, f)$ および $^{243}\text{Am}(n, f)$ 反応断面積も、KURの重水熱中性子設備におけるマックスウェル分布型の標準熱中性子スペクトル場/31/を用いて測定された。この場合も、先のU-235電着膜と組み合わせた背中合わせ型の核分裂電離箱が用いられ、 $^{235}\text{U}(n, f)$ 反応断面積を標準として熱中性子束がモニターされた。その結果、 $3.15 \pm 0.14 \text{ b}$ の $^{241}\text{Am}(n, f)$ 反応断面積を得た。表9では、 $^{241}\text{Am}(n, f)$ 反応断面積を従来のもものと比較している/39/。JENDL-3.2の評価値は、本実験値より約4.2%低い、他の評価データ(Mughab

表9 $^{241}\text{Am}(n, f)$ 反応の熱中性子断面積

Cross Section (b)	Reference
3.15 ± 0.14	Present
3.153	ENDF/B-VI
3.019	JENDL-3.2
3.177	JEF-2.2
3.20 ± 0.09	Mughabghab
3.13 ± 0.15	Hulet
3.20 ± 0.15	Zhuravlev
2.8 ± 0.25	Gavrilov
3.0	Hanna
3.8 ± 0.2	Hyakutake

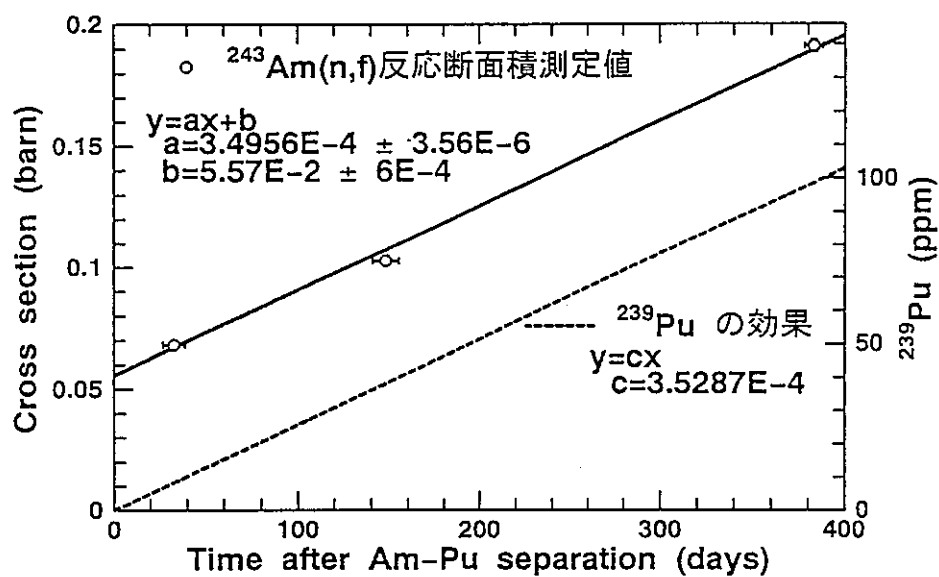


図 5 1 精製後の時間と Pu-239 により上昇する 0.3eV 付近の Am-243 断面積値との関係

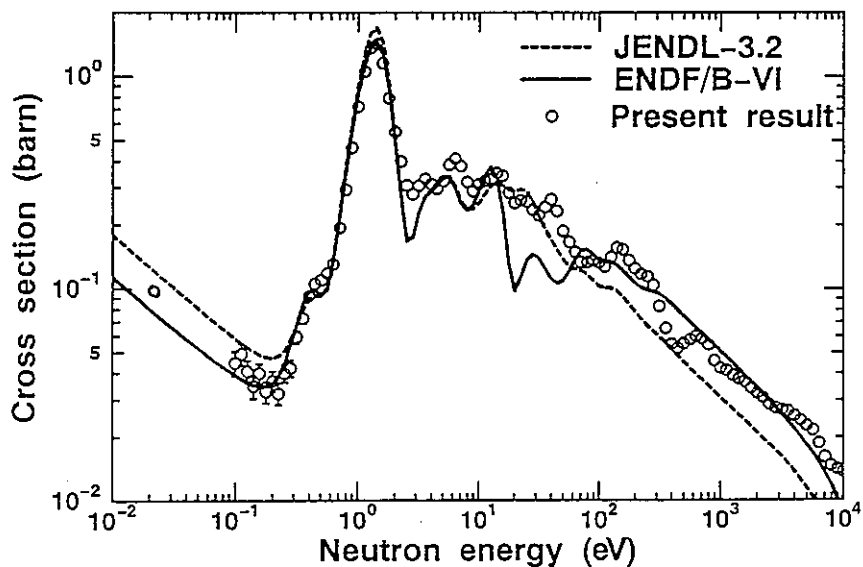


図 5 2 $^{243}\text{Am}(n,f)$ 反応断面積の測定結果と評価値の比較

ghabより上のデータ)は我々の値に近い。実験データ(Huletより下のデータ)には古いものも含まれるが、Gavrilov等のデータは今回の実験値に比べ約11%低く、Hyakutake等のデータは20%程大きくなっている/39/ (付録D)。

$^{243}\text{Am}(n, f)$ 反応の熱中性子断面積は、図5-2のように、ENDF/B-VIとJENDL-3.2の評価データの中に位置している/40/。従来の熱中性子断面積データも含めた詳細な比較、検討は今後の課題である。

4.3.4 $^{241}\text{Am}(n, f)$ 及び $^{243}\text{Am}(n, f)$ 反応断面積測定における不純物の問題

本実験においては、高純度のAm-241、Am-243試料を用いることが出来たが、かつて我々は市販の試料を用いてこれらの核分裂断面積測定を試みたことがある。この場合、存在していないはずのPu-239等の不純物によって $^{241}\text{Am}(n, f)$ 反応断面積の測定値が3倍近くも大きくなった/41/。その結果を参考までに図5-3に示す。Wagemansの指摘どおり/6/、 $^{241}\text{Am}(n, f)$ 反応断面積は、図4-7、図4-8に示した測定値に比べ全体に持ち上がった状態で大きくなっていることが分かる。この時使用したAm-241試料にはPu-239他の不純物が混入していたことが、その後の注意深い α 線測定の結果判明した/42/。また、Am-243の場合は、その試料自身の α 崩壊によってAm-243試料中にPu-239が徐々に生成蓄積されるので、一般に入手できるAm-243試料は必ずPu-239が放射平衡状態で存在していることになる。図5-4に示した $^{243}\text{Am}(n, f)$ 反応断面積を先の測定結果(図5-2)と比較すると、断面積曲線は0.3eV近傍で大きな凸型形状を示している。これは明らかに0.3eVに大きな共鳴を持つPu-239がAm-243試料中に不純物として混在しているために生じたものと思われる。そのため、我々は $^{243}\text{Am}(n, f)$ 反応断面積の測定実験を開始する前に、先に述べた化学精製を実施し、その後数ヶ月以内に実験を完了している/28/ (付録F)。

4.3.5 $^{242m}\text{Am}(n, f)$ 反応断面積

アメリカウムに関する一連の実験として、Am-241、Am-243に続き、KULSを用いてAm-242mの核分裂断面積測定を行った/43/。現在のところ、実験結果はまだ予備的な段階であるが、得られた成果を次にまとめる。

KULSにおいて約7時間の実験を行い、0.1eVから10keV領域の $^{242m}\text{Am}(n, f)$ 反応断面積を測定した。本実験により得られた結果を図5-5に示す。統計誤差は、数パーセント以下で、実験点(○印)の大きさ内に収まる程度である。ここでは、JENDL-3.2とENDF/B-VIの評価値を鉛スペクトロメータのエネルギー分解能(約40%)でbroadeningした結果と実験値を比較している。Am-242mの原子数を算出するため、その α 線、 γ 線測定を行い。現在データ解析を行っているところである。今回は、JENDL-3.2とENDF/B-VIの評価値がよい一致を示す0.1eV～1eV領域において、本実験値をJENDL-3.2の積分値と一致するように規格化している。これを見ると、両評価値と本実験値のエネルギー依存性は全体により一致を示している。約4eV以上の領域でENDF/B-VIとJENDL-3.2のデータ間に差異が見られるが、本実験値

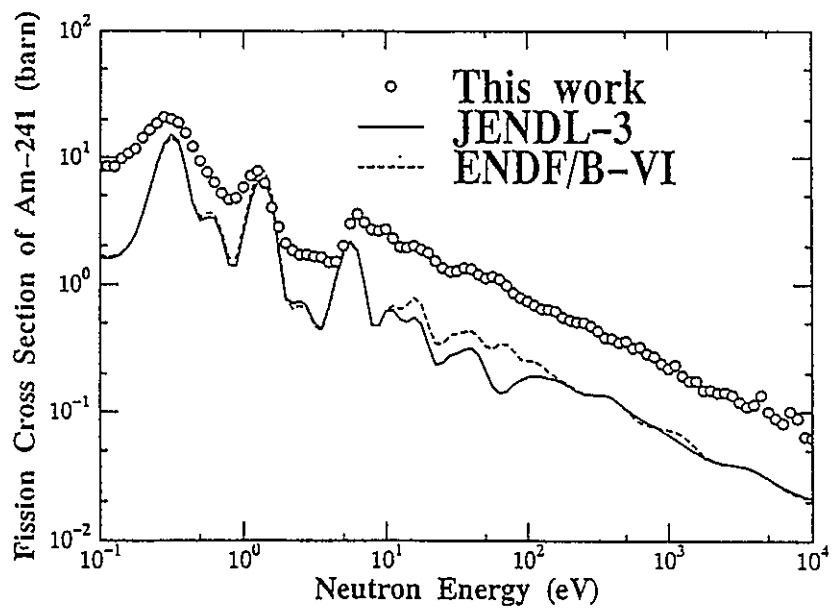


図 5 3 市販のAm-241試料を使った場合の $^{241}\text{Am}(n, f)$ 反応断面積の測定結果と評価値の比較（不純物の影響で断面積が大きくなっている）

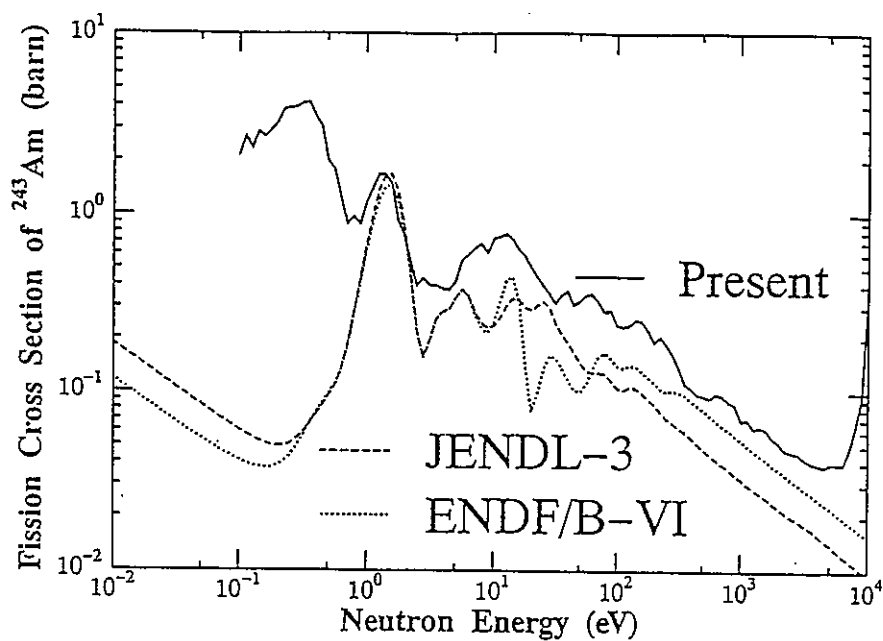


図 5 4 Pu-239が混在するAm-243試料を使った場合の $^{243}\text{Am}(n, f)$ 反応断面積の測定結果と評価値の比較（0.3eV付近は不純物の影響で断面積が大きくなっている）

はそれらのほぼ中間領域にあることが分かる。今後はAm-242mの原子数を実験的に求めて、断面積を絶対値で与えるようにしたい。

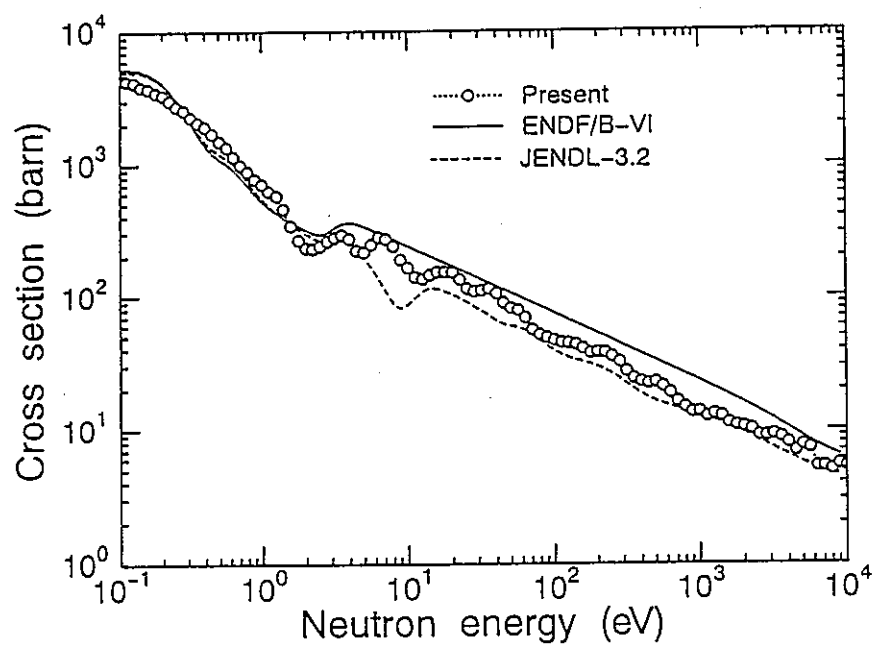


図 5 5 Am-242mの核分裂断面積の評価値と本実験値との比較

5. マイナーアクチニドの中性子捕獲断面積測定の予備実験

原子炉及び加速器などの中性子源を用いたMA核種の消滅処理法として、核分裂あるいは核変換法を利用することが考えられる。核変換法では、対象とする核種やエネルギー領域によっては、核分裂断面積よりむしろ中性子捕獲断面積の方が大きく、MA消滅処理の観点からより有効と考えられる核種が存在している。MAに関する中性子捕獲断面積としては、我々は先に原子炉の標準熱中性子場において $^{237}\text{Np}(n, \gamma)$ 反応の熱中性子断面積、標準的な $1/E$ 中性子場を用いてその共鳴積分を実験的に求めている/31/。ここでは、まず、 $^{237}\text{Np}(n, \gamma)$ 反応断面積データの現状を概観した後、鉛スペクトロメータを用いて共鳴領域における $^{237}\text{Np}(n, \gamma)$ 反応断面積の測定を試みたので、その実験結果について紹介する。

5.1 Np-237の中性子捕獲断面積

Np-237は、MAの中でも消滅処理の観点から最も注目される核種の1つである。表2、表3はMAに関する核分裂及び中性子捕獲に対する実測データの現状と、これらの核データに対する要求精度を示している/10/。 $^{237}\text{Np}(n, \gamma)$ 反応断面積の評価データを図56、図57に示す。図56を見る限り、評価データ間に大きな差異は見られないが、多くの実験グループが測定を行っている訳ではない/44/。図57では、200keV以下で評価値と実験値のグループ間に大きな違いが存在している。そこで、表3に示された $^{237}\text{Np}(n, \gamma)$ 反応断面積の要求精度に応えるためにも新たな実験が期待されるところである。

5.2 鉛スペクトロメータKULSを用いた $^{237}\text{Np}(n, \gamma)$ 反応断面積の測定

5.2.1 Np-237試料

我々は、既にKULSを用いて $^{237}\text{Np}(n, f)$ 反応断面積の測定を実施しているが、その時使用したNp-237試料の原子数は 1.99×10^{17} 個($78 \mu\text{g}$)であった/30/。核分裂断面積測定の場合は、 $1 \mu\text{g}$ 以上の条件があれば、鉛スペクトロメータを用いて測定可能となる条件を備えていると言われている/12/。実際、我々の $^{237}\text{Np}(n, f)$ 反応断面積測定の場合、断面積を10~100 mbと仮定すると、この条件を満たしている。しかし、中性子捕獲反応断面積の測定においては、断面積を10~100 b/44/、鉛スペクトロメータ実験孔内の中性子束を約 $10^7 \text{ n/cm}^2/\text{s}$ と仮定すると/24/、 $^{237}\text{Np}(n, \gamma)$ 反応の割合は毎秒20~200程度になる。検出器の即発ガンマ線の測定効率を~1%以下とすれば（核分裂電離箱と違って、試料は検出器の横にセットされる）、先のNp-237試料による捕獲反応断面積の測定は極めて困難である。

極最近になって、東北大学工学部量子エネルギー工学科の岩崎智彦氏のご厚意により、約1 mgのNp-237試料(原子数: 2.5×10^{18})を2枚お借りできる機会があった。この試料は、厚さ0.5 mm、直径5 cmの白金板に約1 mg/枚のNp-237が電着されている。これは、先のNp-237原

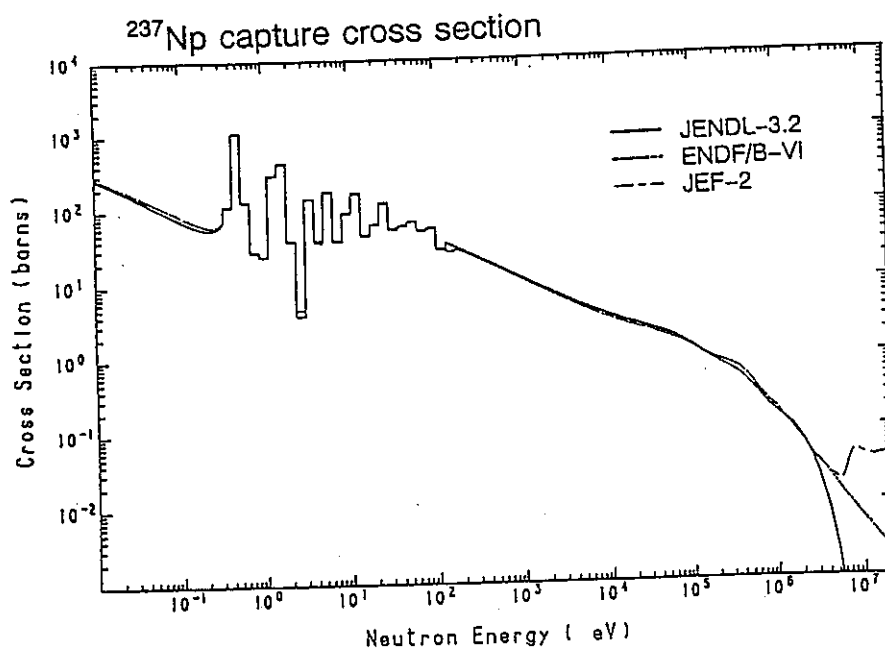


図 5 6 Np-237 の核分裂断面積の評価データの比較

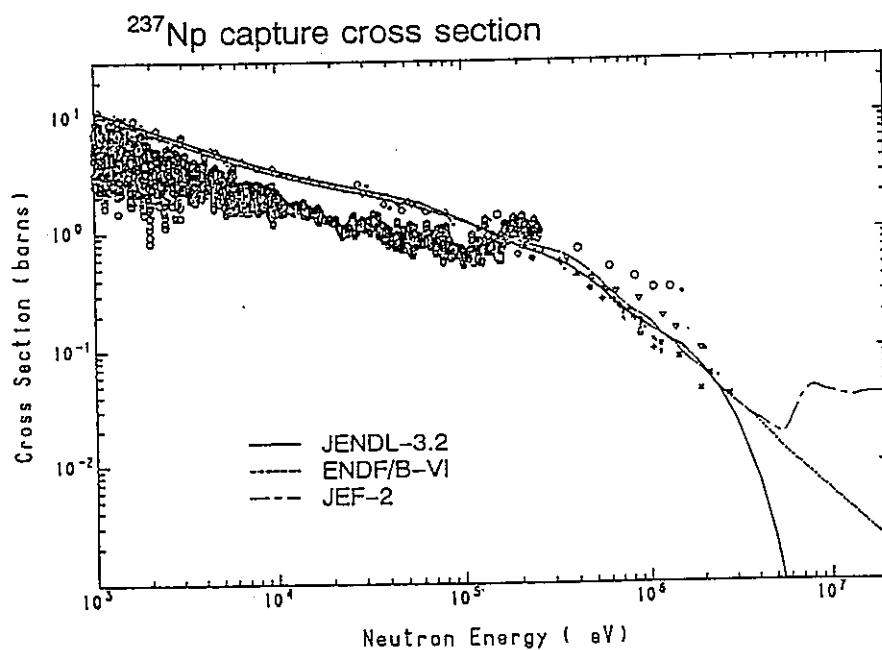


図 5 7 Np-237 の核分裂断面積の評価データと実験データの比較

子数の25倍 x 2に相当しているので、これを用いて $^{237}\text{Np}(n, \gamma)$ 反応断面積測定を試みることにした。

5.2.2 実験方法

本実験に使用する即発ガンマ線測定用検出器は、中性子に対し殆ど応答を示さないArガス入りの比例計数管（直径:1.27cm、有効長:6.35cm、内圧1気圧）である。これを2枚のNp-237試料板で挟みKULSの実験孔に挿入した。前置増幅器以外は図42に示された電子回路系とほぼ同じものを1系統用いた。測定系のチャンネル幅、チャンネル数、電子線型加速器の運転条件なども先の実験とほぼ同様である。

中性子捕獲断面積の相対測定値は、先の核分裂断面積測定の場合とほぼ同様に、次式で求められる。

$$\sigma_c(E) = \frac{\text{各試料に対する中性子捕獲事象の計数率}}{\text{マイクロBF}_3\text{カウンターの計数率}} \times \sigma_B(E)$$

ここで、マイクロBF₃カウンターは、入射中性子束のモニターとして使用されている。 $^{10}\text{B}(n, \alpha)$ 反応断面積 $\sigma_B(E)$ は、いわゆる1/v型曲線を示し、標準断面積としてもよく知られている。また、Arガスカウンターの即発 γ 線測定に対する検出効率は、入射中性子エネルギーに依存しないものと仮定した。

5.2.3 結果及び検討

約2mgのNp-237試料とArガス入り比例計数管を用いて得られた減速時間スペクトルを図58に示す。この図に示した上のデータは、いわゆるForeground runのデータであり、下はNp-237が付着していない白金板からなるBackground runのデータである（両者は測定時間で規格化している）。両データとも400~500チャンネルおよび700~800チャンネル付近にピークが見られるが、前者は電着の基板である白金からの捕獲ガンマ線によるものであり、後者は鉛スペクトロメータ内のビスマス遮蔽体中に存在する銀と思われる不純物からの捕獲ガンマ線によるものであることが分かった。

図58の結果について、Background runに対するForeground runの比を求め、これを図59に示す。この図を見ると、両データの比スペクトルは全チャンネルにわたってほぼ1に近くなっている上に、比のスペクトル形状に凹凸が見られないことから、ForegroundカウントはBackgroundの場合と変わらず、 $^{237}\text{Np}(n, \gamma)$ 反応断面積測定にとって有意な情報が得られていないことが分かる。

当初の目的が達成できなかった原因は、(i)Np-237の原子数が、なお十分でなかったものと思われる、(ii)信号に比べ、白金板やビスマス中の不純物によるバックグラウンドが高過ぎた、(iii)即発ガンマ線の検出効率が低いこと等が考えられる。今後は、さらに多量の実験試料を用いることの必要性が感じられると共に、即発ガンマ線検出器の選び方、その研究開発・試作も含めた検討、実験手法の改善が必要であろう。

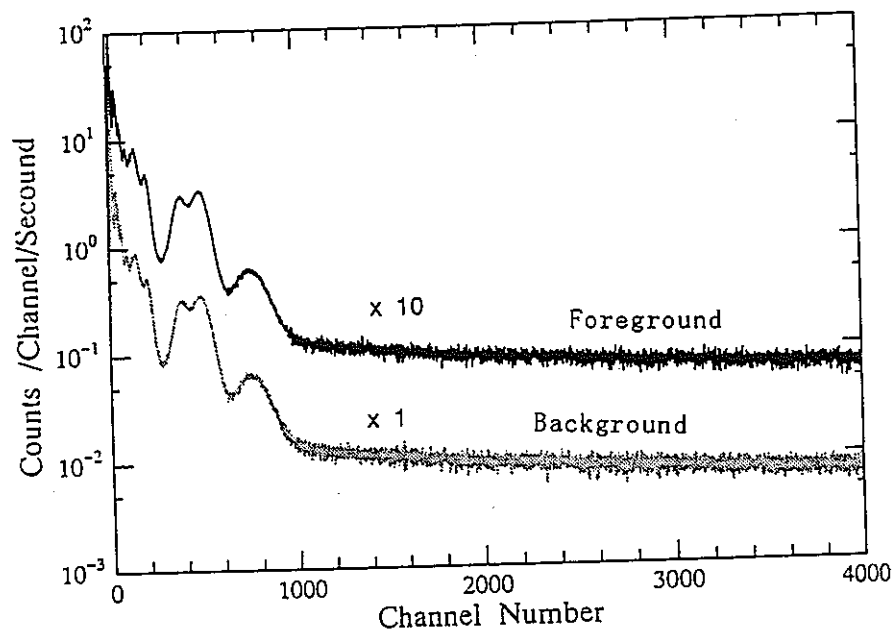


図 5 8 Np-237試料から得られた減速時間スペクトル
(上:Foreground run、下:Background run)

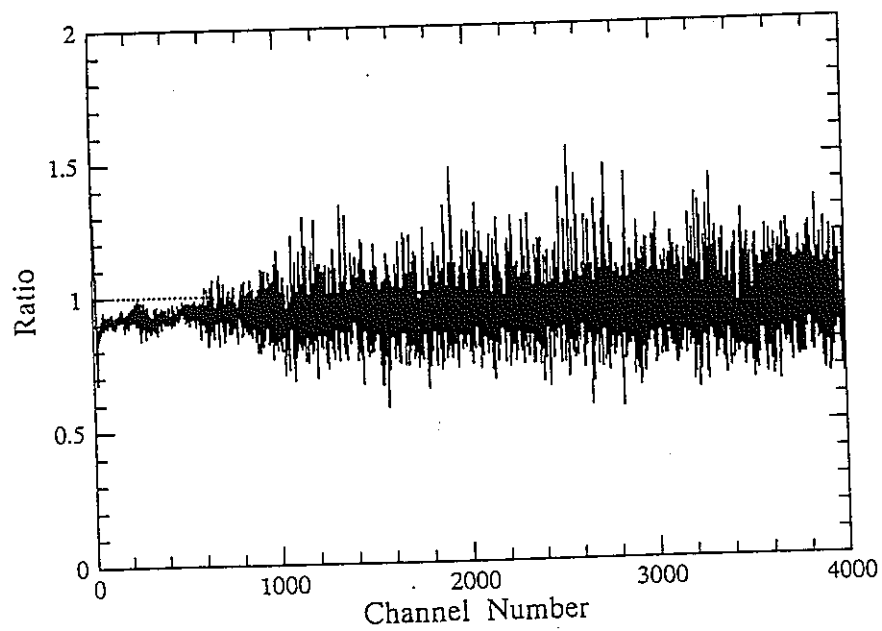


図 5 9 図58に示したForegroundデータとBackground
データの比

6. まとめ

アクチノイド核種の消滅を目指した中性子核反応断面積に関する実験的研究において、まず、京都大学原子炉実験所に付設された鉛スペクトロメータKULSについて、その諸特性を実験と計算の両面より明らかにした。その後、この鉛スペクトロメータを用いて、先の $^{237}\text{Np}(n, f)$ 反応断面積測定に続き、本年度はMAとして代表的な核種であるAm-241、Am-243及びAm-242mについて、それらの核分裂断面積を測定した。本実験で求めた測定値と従来の実験データ及び評価データを比較し、得られた結果について検討を行った。最後に、MAの中性子捕獲断面積測定として、 $^{237}\text{Np}(n, \gamma)$ 反応断面積測定に関する予備的な実験を試みた。

本研究において明らかとなったことを、以下にまとめる。

1. まず、KULSの諸特性を実験と計算の両面から求めることができた：共鳴フィルターを用いた実験により、①中性子の減速時間とエネルギーの関係 $E = K/t^2$ を示す定数Kとして、ビスマス実験孔では $K=190 \pm 2 (\text{keV} \cdot \mu\text{s}^2)$ 、鉛実験孔では $K=156 \pm 2 (\text{keV} \cdot \mu\text{s}^2)$ を得た。②エネルギー分解能は何れの実験孔においてもほぼ40%となり、約1 eV以下と5 keV以上の領域では40%を超える半値幅を示した。③飛行時間分析法によってKULS内の中性子スペクトルを測定したが、MCNPコードによる計算結果もこれらの実験値とよい一致を示した。
2. 次に、KULSを用いて $^{241}\text{Am}(n, f)$ 反応断面積を $\sim 0.1\text{eV}$ から数10keV領域において測定した。本実験においては、Am-241とU-235の電着膜を背中合わせとする核分裂電離箱を試作、使用し、入射中性子束を $^{235}\text{U}(n, f)$ 反応の標準断面積によってモニターした。本実験の結果、Dabbs等の実験値、及びENDF/B-VIの評価値は本実験値に近いことが分かった。JENDL-3.2の評価データも全般的に本実験値と一致したが、10 \sim 200eV領域では、本実験値やENDF/B-VIデータと比べて明らかに(約2倍程度)低い値を示した。これらの評価値を本実験値と比較する場合、何れもKULSのエネルギー分解能でbroadeningしている。
3. 続いて、 $^{243}\text{Am}(n, f)$ 反応断面積を測定したが、その方法は先の $^{241}\text{Am}(n, f)$ 反応断面積測定の場合とほぼ同様である。ENDF/B-VIデータはKULSによる実験値と一致しているが、15 \sim 60eV領域では低すぎる。JENDL-3.2データは、KULSの実験値に比べ100eV以上で全体に低目の傾向にある。
4. さらに、熱中性子に対する $^{241}\text{Am}(n, f)$ 、 $^{243}\text{Am}(n, f)$ 反応断面積を標準的なMaxwell分布を示す熱中性子場において測定した。この場合も、 $^{235}\text{U}(n, f)$ 反応断面積を標準とした背中合わせ型の核分裂電離箱を用いた。 $^{241}\text{Am}(n, f)$ 反応の評価データは、何れも今回の測定値 $3.15 \pm 0.14\text{b}$ に近い値を示している。実験データは一般的に初期の頃のものが多いが、2 \sim 3のものを除けば概ね今回の測定値と一致している。 $^{243}\text{Am}(n, f)$ 反応断面積に関する今回の測定結果は、ENDF/B-VIとJENDL-3.2の評価データのほぼ中間の値を示したが、今後は従来の実験値なども含めた比較検討を行う。

5. 一連のアメリシウムに関する核分裂断面積実験の第3番目として、KULSを用いて ^{242}Am (n, f) 反応断面積の測定を行った。本実験の方法も先の2つの測定の場合と同様である。本実験は、極最近開始したばかりで、現在のところ、実験結果はまだ予備的な段階である。 Am-242m 試料の定量が未だ終了していないため、相対値として断面積曲線のエネルギー依存性についてENDF/B-VIやJENDL-3.2の評価データと比較した。両評価データがよく一致している0.1～1 eV領域に本実験値を規格化すると、両評価値に違いが現れる～4 eV以上の領域で実験値が両者の中間領域に位置している。今後は、 Am-242m の原子数を実験的に求めて、断面積として絶対値で与えるようにしたい。

6. 最後に、MA核種の中性子捕獲断面積の測定を念頭において、KULSによる $^{237}\text{Np}(n, \gamma)$ 反応断面積の測定を試みた。しかし、 Np-237 試料(～2 mg)から得られた中性子捕獲事象の計数率は極めて少なく、バックグラウンドの中に埋もれてしまって有意な信号の計数値が得られなかった。本実験の目的を達成するためには、今後、信号／雑音比を改善する方向で、試料の増量、バックグラウンドの低減を図ると共に、本実験に適した即発ガンマ線検出器の研究開発も含めた実験手法の改善が望まれる。鉛スペクトロメータを用いた捕獲反応断面積の測定は、今後に残された大きな研究課題と言える。

【参考文献】

- /1/ 「消滅処理研究の現状」、日本原子力学会 消滅処理研究専門委員会 1994。
- /2/ 「高レベル廃棄物の消滅処理研究開発」、日本原子力学会誌、Vol.37, No.3, p.159 (1995)。
- /3/ 例えば、向山武彦：私信 (1993)、1993 Future Nuclear System: Emerging Fuel Cycles and Waste Disposal Options を中心に。
- /4/ 例えば、平川直弘：私信 (1996)、1995 Future Nuclear System: Emerging Fuel Cycles and Waste Disposal Options を中心に。
- /5/ 菊池康之、中川庸雄、高野秀機、向山武彦、「アクチノイド核データの信頼性—微分データとその積分的検証」、日本原子力学会誌、Vol.36、No. 3、211 (1994)。
- /6/ C. Wagemans, Nucl. Instr. Methods in Phys. Res., A236, 429 (1985)。
- /7/ 例えば、K. Tsuchihashi, et al., "SRAC; JAERI Thermal Reactor Standard Code System for Reactor Design and Analysis", JAERI 1285 (1983), and "Revised SRAC Code System", JAERI 1302 (1986)。
- /8/ 例えば、「MCNP - A General Monte Carlo Code for Neutron and Photon Transport, Version 3A", LA-7396-M, Rev.2, Los Alamos National Laboratory (1986)。
- /9/ T. Nakagawa, et al., J. Nucl. Sci. Technol., Vol.32, No.12, p.1259 (1995)。
- /10/ 中川庸雄、日本原子力研究所 核データセンター発行「核データニュース」、No.50、p.13 (1995)、及び 中川庸雄氏私信(1995)。
- /11/ A. A. Bergman, et al.: Proc. 1st Int. Conf. on Peaceful Uses At. Energy, United Nations, 4, 135 (1955)。
- /12/ R. E. Slovacek, et al.: Nucl. Sci. Eng., 62, 455 (1977)。
- /13/ K. H. Beckurts & K. Wirtz: "Neutron Physics", Springer-Verlag, New York, p. 167 (1964)。
- /14/ Y. Nakagome, et al.: Phys. Rev., C43, 1824 (1991)。
- /15/ H. T. Maguire, Jr. et al.: Nucl. Sci. Eng., 89, 293 (1985)。
- /16/ B. Alam, et al.: Nucl. Sci. Eng., 99, 267 (1988)。
- /17/ Y. Danon, et al., Nucl. Sci. Eng., 109, 341 (1991)。
- /18/ E. C. Vanterpool, et al.: Nucl. Sci. Eng., 110, 186 (1992)。
- /19/ N. M. Abdurrahman, et al.: Nucl. Sci. Eng., 115, 279 (1993)。
- /20/ K. Kobayashi, et al., Annu. Rep. Res. Reactor Inst. Kyoto Univ., Vol.22, p. 142 (1989)。
- /21/ K. Kobayashi and Y. Fujita, Annu. Rep. Res. Reactor Inst. Kyoto Univ., Vol. 26, p.92 (1993)。

- /22/ K. Kobayashi, et al., Annu. Rep. Res. Reactor Inst. Kyoto Univ., Vol.20, p. 1 (1987).
- /23/ H. Wakabayashi, et al.: J. Nucl. Sci. Technol., 6, 487 (1970).
- /24/ K. Kobayashi, et al., Nucl. Instr. Methods in Nucl. Phys. Res. A, 385, 145-156 (1997).
- /25/ R. C. Little, et al.: Trans. Am. Nucl. Soc., 43, 119 (1982).
- /26/ I. Kimura, et al., Nucl. Instr. Meth., 137, 85 (1976).
- /27/ S. Usuda and N. Kohno, Separation Science and Technology, 23 1119 (1988).
- /28/ T. Kai, K. Kobayashi, et al., Proc. of the 1996 Symp. on Nucl. Data, JAERI, to be published.
- /29/ 大部 誠、 JAERI-M 9757 (1981).
- /30/ A. Yamanaka, et al., J. Nucl. Sci. Technol., Vol.30, No.9, 863 (1993).
- /31/ K. Kobayashi, et al., J. Nucl. Sci. Technol., Vol.31, No.12, p.1239 (1994).
- /32/ J. W. T. Dabbs, et al.: Nucl. Sci. Eng., 83, 22 (1983).
- /33/ D. B. Gayther, et al.: 4-th All Union Conf. on Neutron Physics, at Kiev, on 18-22 April 1977.
- /34/ C. D. Bowman, et al.: Phys. Rev. B, 137, 326 (1965).
- /35/ V. F. Gerasimov, Yaderno-Fizicheskie Issledovaniya, 2, 16 (1966).
- /36/ H. Derrien, et al., Proc. Int'l Conf. on Nucl. Cross Sections and Technol., Washington D. C. (1975).
- /37/ B. R. Leonard Jr., Bull. of Am. Phys. Soc., 4, 31(K1) (1959).
- /38/ P. A. Seeger, et al.: Nucl. Phys., A96, 605 (1967).
- /39/ S. Yamamoto, K. Kobayashi, et al., Nucl. Sci. Eng., to be published in June 1997.
- /40/ K. Kobayashi, et al., Proc. of the 1996 Symp. on Nucl. Data, JAERI, to be published, 及び 小林捷平ほか、日本原子力学会、春の大会、B20、1996年3月。
- /41/ K. Kobayashi, et al., "Fission Cross Section Measurement of Am-241 between 0.1 eV and 10 keV with Lead Slowing-down Spectrometer", Gatlinburg, Tenn., May 1994, J. K. Dickens(Ed.), ORNL, Vol.1, p.242 (1994).
- /42/ 三好光晴、「241Amの中性子エネルギー依存核分裂断面積の測定」、修士学位論文、京都大学大学院工学研究科 (1995年3月)。
- /43/ 小林捷平、甲斐哲也ほか、日本原子力学会、春の大会、1997年3月、発表予定。
- /44/ V. McLane, et al., "Neutron Cross Sections", Vol.2, Neutron Cross Section Curves, Academic Press, Inc. (1988).

付 録

付録 A : Characteristics of the Kyoto University Lead Slowing-down Spectrometer (KULS) coupled to an Electron Linac	- - - - -	49
付録 B : Measurement of Fission Cross Section of Np-237 in Resonance Region with Electron Linac-Driven Lead Spectrometer	- - - - -	61
付録 C : Measurements of Thermal Neutron Cross Section and Resonance Integral for $^{237}\text{Np}(n, \gamma)^{238}\text{Np}$ Reaction	- -	68
付録 D : Fission Cross Section Measurements of Am-241 between 0.1 eV and 10 keV with Lead Slowing-down Spectrometer and Thermal Neutron Energy	- - - - -	77
付録 E : Measurement of Fission Cross Section with Pure Am-243 Sample using Lead Slowing-down Spectrometer	- - - - -	91
付録 F : The Influence of Impurities for Cross Section Measurement of Am-241, 243(n, f) Reactions	- - - - -	97
付録 G : Application of BGO Scintillators to Absolute Measurement of Neutron Capture Cross Sections between 0.01 eV and 10 eV	- - - - -	103



ELSEVIER

付録 A

Characteristics of the Kyoto University Lead Slowing-down Spectrometer (KULS) coupled to an electron linac

Katsuhei Kobayashi^{a,*}, Shuji Yamamoto^a, Akihiro Yamanaka^{b,1}, Yoshihiro Nakagome^a, Yoshiaki Fujita^a, Satoshi Kanazawa^b, Itsuro Kimura^b

^aResearch Reactor Institute, Kyoto University, Kumatori-cho, Sennan-gun, Osaka 590-04, Japan

^bDepartment of Nuclear Engineering, Kyoto University, Yoshidahonmachi, Sakyo-ku, Kyoto 606-01, Japan

Received 20 September 1995; revised form received 17 September 1996

Abstract

A lead slowing-down spectrometer coupled to a 46 MeV electron linear accelerator (linac) was installed at Research Reactor Institute, Kyoto University (KURRI). The size of this Kyoto University Lead Slowing-down Spectrometer (KULS) is $1.5 \times 1.5 \times 1.5 \text{ m}^3$, and it is covered with Cd sheets 0.5 mm thick. One of the eleven experimental holes in the KULS is covered with 10 to 15 cm thick bismuth layers to suppress high energy capture gamma-rays from lead.

The characteristics of this KULS have been experimentally obtained and the results are compared with the predicted values by Monte Carlo calculations using the MCNP code. 1) The slowing-down constant K in the relation $E = K/t^2$ between the neutron slowing-down time t and energy E is $190 \pm 2 \text{ (keV } \mu\text{s}^2)$ for the bismuth hole and $156 \pm 2 \text{ (keV } \mu\text{s}^2)$ for an ordinary lead hole, respectively. The K values agree with the calculated ones. 2) The measured energy resolution $\Delta E/E$ at full-width-at-half-maximum (FWHM) was about 40% for both holes, while the calculated values were lower by about 10% than the measured ones in the relevant energy region. 3) The neutron energy spectrum from 0.01 eV to 20 MeV and the spatial distribution of neutrons in the KULS were measured by the foil activation method. The angular neutron spectrum perpendicular to the linac electron beam was also obtained experimentally in the energy range from a few eV to about 10 MeV by the neutron time-of-flight (TOF) method. The measured results are compared with the calculated ones in which we have used the three evaluated nuclear data JENDL-3, ENDL-85 and ENDF/B-IV for lead. Through the comparison a check on the nuclear data has been performed.

1. Introduction

Lead is one of the heavy mass elements and it has no inelastic scattering cross section below about 600 keV, where the neutron total cross section mainly consists of elastic scattering cross section, since the absorption cross section is very small. Therefore, when pulsed fast neutrons are put into the central region of a large lead assembly, the neutrons are slowed down by repeating many elastic scattering processes, because of little leakage of neutrons. The slowing-down neutrons present focusing behaviour and keep an asymptotic form at each energy corresponding to the slowing-down time [1]. There exists a relation $E = K/t^2$ between the mean energy E in keV of the slowing-down neutrons and the mean slowing-down time t

in μs [1], where K is the slowing-down constant. The energy resolution of the slowing-down neutrons is theoretically given at full-width-at-half-maximum (FWHM) by [1]

$$\begin{aligned} (\Delta E/E)_{\text{FWHM}} &= 2.35 \times (\Delta\sigma/\sigma)_{\text{Gaussian}} \\ &= 2.35 \times (8/3A)^{1/2} = 27\%, \end{aligned}$$

where, $(\Delta\sigma/\sigma)_{\text{Gaussian}}$ is the standard deviation in a Gaussian function and A is the atomic mass (207.2) of lead.

Hence a large lead assembly was proposed to be applicable as a neutron spectrometer and practically used by Bergman et al. [2] for the first time. Since that, in some laboratories or universities, lead slowing-down spectrometers coupled to a D-T pulsed neutron source by a Cockcroft-Walton accelerator have been installed and widely applied to measurements of neutron capture and fission cross sections in the intermediate and/or resonance neutron energy region [1–7].

* Corresponding author.

¹ Present address: Hitachi Works, Hitachi Ltd., Saiwai-cho, Hitachi-shi, Ibaraki 317, Japan.

Most of electron linear accelerators have been developed in 1960s as an intense neutron source and neutron time-of-flight (TOF) method has often been used for neutron cross section measurements [8]. The usage of a lead slowing-down spectrometer coupled to an electron linear accelerator (linac) was proposed for the measurement of small amount of samples with low cross sections and for the cross section measurement of radioactive materials to give high background level. The first spectrometer was installed at the Rensselaer Polytechnic Institute (RPI) as an intense neutron spectrometer [9]. Since neutrons can be detected at the distance of tens of centimeters from the pulsed neutron source in the lead slowing-down spectrometer, higher neutron intensities by more than thousands times than those at the measuring station of 5 m flight path for the conventional neutron TOF method can be obtained [9]. Making use of the spectrometer, the RPI groups have made measurements of sub-threshold fission cross sections [9,10] of ^{238}U and ^{232}Th and measured fission cross sections of trans-uranium nuclides [11–13] in the energy range from about 1 eV to several tens of keV. Recently, the spectrometer was also applied to the nondestructive assay of spent fuels [14,15].

In the present work, we have experimentally investigated characteristic behaviour of neutrons in the lead slowing-down spectrometer coupled to a 46 MeV electron linear accelerator (linac) at the Research Reactor Institute, Kyoto University (KURRI). The spectrometer was originally installed at University of Tokyo [5] and transferred to KURRI in 1991. With this Kyoto University Lead Slowing-down Spectrometer (KULS), we first obtained the relation between neutron slowing-down time and energy and the neutron energy resolution by the experiments with resonance filters and by the calculations using the continuous energy Monte Carlo code MCNP [16]. Secondly, making use of the NEUPAC and the SAND-II codes [17,18], the neutron flux spectrum in the KULS has been analyzed by the adjustment method with activation foil data. Radial flux distributions of neutrons have also been measured by Au foils and Ni wires. In addition, neutron TOF method has been employed to measure the angular neutron flux spectrum in the KULS, as we have done before [19,20]. These experimental results have been compared with calculations performed by the MCNP code using the evaluated nuclear data files of ENDF/B-IV [21], ENDL-85 [22] and JENDL-3 [23]. The nuclear data for lead is useful to understand the characteristics of a lead slowing-down spectrometer.

2. Lead slowing-down spectrometer

The lead slowing-down spectrometer was recently installed by coupling to the 46 MeV linac at KURRI. Specific features of the Kyoto University Lead Slowing-down Spectrometer (KULS) are as follows.

1) The KULS is a cube of $1.5 \times 1.5 \times 1.5 \text{ m}^3$ and about 40 tons in weight, and is set on a platform car in the linac target room so that it can be removed when the conventional neutron TOF measurement is made, as shown in Fig. 1.

2) The number of the lead blocks used was about 1600 (each size: $10 \times 10 \times 20 \text{ cm}^3$, and purity: 99.9%). Each block was carefully cleaned with alcohol or acetone and piled up to make the cube without any structural steel. All sides of the KULS were covered with cadmium sheet of 0.5 mm in thickness to shield low energy neutrons scattered from the surroundings.

3) Two types of photoneutron targets were employed: one was a cylindrical lead block (8 cm in diameter and 5 cm thick) casted with an aluminum pipe for air cooling, and the other was a tantalum target assembly (8 cm in diameter and 6 cm in effective thickness), which was made to set 12 sheets of tantalum plates in all (1 to 5 mm in each thickness) in a cylindrical titanium case. The tantalum target assembly was also cooled by compressed air flow. The photoneutron target is separated from the linac vacuum system to prevent troubles by which the linac machine is disturbed. The temperature on the target case was monitored with thermocouples and the linac operating conditions were controlled so that the temperature was kept less than 300°C . During the KULS experiments, the linac beam power on the target was about 200 to 500 W.

4) For the multi-purpose and/or parallel measurements, as seen in Fig. 1, we added eight experimental/irradiation

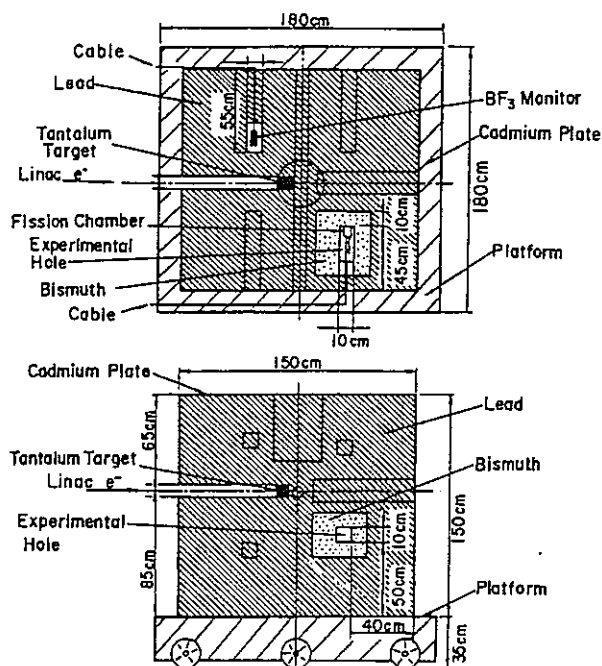


Fig. 1. Cross sectional view of Kyoto University Lead Slowing-down Spectrometer, KULS.

holes (10×10 cm², 55 or 45 cm in depth) to the spectrometer which were originally designed at University of Tokyo [5]. One of the good points of the KULS is that one of the lead holes was covered by a bismuth layer of 10 to 15 cm (neutron source side of the hole) in thickness to shield high energy gamma-rays (6 to 7 MeV) by the Pb(n, γ) reaction in the spectrometer. The bismuth layers are useful to reduce background counts due to photofissions in the fission event measurement [10].

5) An advantageous point of the KULS is the design to be able to measure the neutron energy spectrum in the KULS by the conventional TOF method. At a distance of 12.5 cm behind the photoneutron target, a through hole of 8 cm in diameter is provided at a right angle to the incident electron beam, as shown in Fig. 1. Moreover, in the forward and the upper directions there are large experimental plugs of lead, each of which has an axial irradiation hole of 3 mm in diameter along the central axis. Activation foils or wires can be set to measure the flux distribution of neutrons.

3. Experimental method and measurement

3.1. Slowing-down time and energy

The relation between neutron slowing-down time and energy in the KULS has been measured in the bismuth hole and the lead hole at the opposite upper position to the bismuth hole, as shown in Fig. 1. For the investigation of the experimental reliability, two types of detectors were employed: one was a BF₃ counter (12 mm in diameter, 50 mm in length, 1 atm. pressure) for the neutron transmission measurement through a resonance filter which gave the dip structure in the slowing-down time spectrum, and the other was an Ar gas counter (12.7 mm in diameter, 63.5 mm in length, 1 atm. pressure) for the capture γ -ray measurement with a resonance filter which showed the bump structure in the slowing-down time spectrum. The detector was placed at the bottom of the bismuth or the lead hole covered with and without the resonance filter and the setting position was about 40 cm distant from the photoneutron target in the KULS. Table 1 shows the resonance filters and their main resonance energies used in the present measurement. Since the resonance energies for these filters are well known [24], we can calibrate the relation between slowing-down time t at the center of the dip spectrum by the BF₃ counter or of the bump spectrum by the Ar gas counter and its energy E , as a function of $E = K/(t + t_0)^2$, where K is slowing-down constant and t_0 is constant for the zero time correction.

Output pulses from the BF₃ or the Ar gas counter were transmitted through the pre-amplifier, the main amplifier and the discriminator and were stored in a multi-channel analyzer of 4096 channels as a function of the neutron slowing-down time. The channel width of 62.5 to 500 ns

Table 1

Resonance filters and their main resonance energies used in the present measurement

Material	Energy [eV]	Thickness [mm]	Form
In	1.46	0.2	foil
Te	2.33	7.0	powder
Ta	4.28	0.2	foil
Ta	10.4		
Au	4.91	0.05	cylinder
Ag	5.19	0.5	cylinder
Ag	16.3		
Cd	27.5	0.3	cylinder
Mo	44.9	7.0	powder
Co	132	0.3	cylinder
Cu	230	1.0	cylinder
Cu	579		
Mn	336	7.0	powder

was selected. Another BF₃ counter was set in a lead hole as seen in Fig. 1, to monitor the neutron source intensity during the experiment.

3.2. Energy resolution

The energy resolution of neutrons in the KULS has been experimentally obtained from the dip or the bump spectrum, as performed in the above measurements, making use of the BF₃ and the Ar gas counters. The dip or the bump spectrum was fitted with a Gaussian function to give the energy resolution at full width at half maximum $(\Delta E/E)_{FWHM} = 2.35(\Delta\sigma/\sigma)_{Gaussian}$ using the standard deviation. In the transmission measurement with a resonance filter, corrections are required for the dip spectrum broadened by certain width of the resonance cross section and by the certain thickness of the resonance filter. Then, the capture γ -ray measurement using a sharp resonance peak like a delta function would be better to determine the energy resolution, because one can derive the energy resolution without any corrections in the measured data. Table 1 lists not only the big resonance filters but also the Cu and Cd filters with sharp resonances at 230, 579 and 27.5 eV, respectively.

3.3. Neutron spectrum and flux distribution measured by activation method

With the photoneutron target of lead placed near the center of the KULS, we have irradiated eleven kinds of activation foils at the distance of 12.5 cm behind the target, as seen in Fig. 1. During the irradiations, lead plugs were put into the through hole. Table 2 shows the activation foils and the fourteen nuclear reactions used in the present measurement. Gamma-rays from these induced activities were measured with a HPGe detector, whose detection efficiency was calibrated using a mixed radioactive standard source. The linac operations were performed with a

Table 2

Nuclear reaction, half life, gamma-ray energy and its intensity used for the present data processing

No.	Reaction	Half life ^a	Gamma-ray ^a energy [MeV]	Gamma-ray ^a intensity [%]
1	$^{197}\text{Au}(n,\gamma)^{198}\text{Au}$	2.694 d	0.412	95.5
2	$^{55}\text{Mn}(n,\gamma)^{56}\text{Mn}$	2.579 h	0.847	98.93
3	$^{59}\text{Co}(n,\gamma)^{60}\text{Co}$	5.271 y	1.173	99.90
4	$^{186}\text{W}(n,\gamma)^{187}\text{W}$	23.85 h	0.686	29.3
5	$^{24}\text{Mg}(n,p)^{24}\text{Na}$	14.66 h	1.369	100.0
6	$^{27}\text{Al}(n,p)^{27}\text{Mg}$	9.462 m	0.844	73.0
7	$^{27}\text{Al}(n,\alpha)^{24}\text{Na}$	14.66 h	1.369	100.0
8	$^{46}\text{Ti}(n,p)^{46}\text{Sc}$	83.83 d	0.889	99.98
9	$^{47}\text{Ti}(n,p)^{47}\text{Sc}$	3.341 d	0.159	68.2
10	$^{48}\text{Ti}(n,p)^{48}\text{Sc}$	1.821 d	0.984	100.0
11	$^{58}\text{Ni}(n,p)^{58}\text{Co}$	70.92 d	0.811	99.53
12	$^{54}\text{Fe}(n,p)^{54}\text{Mn}$	312.2 d	0.835	99.98
13	$^{64}\text{Zn}(n,p)^{64}\text{Cu}$	12.70 h	0.511	35.8
14	$^{115}\text{In}(n,n')^{115\text{m}}\text{In}$	4.486 h	0.336	45.8

^aThe nuclear data were taken from Ref. [25].

pulse width of 33 ns, a repetition rate of 30 Hz, an electron peak current of about 2 A and an electron energy of 32 MeV, respectively.

The activation data were analyzed by spectrum adjustment method employing the NEUPAC and the SAND-II codes [17,18]. The NEUPAC code contains energy dependent group cross sections of 135 groups from 0.01 eV to 16.4 MeV, including the error matrices [26] for neutron dosimetry reactions in ENDF/B-V. For the SAND-II code, the original code was revised to produce the analytical uncertainties using the Monte Carlo method [27,28]. Moreover, a subroutine program was added for the self-shielding correction in the foil. The group cross sections of 642 energy bins were used and taken from the JENDL Dosimetry File [29]. As an initial spectrum for the adjustment with the NEUPAC and the SAND-II codes, the spectral result calculated with the MCNP code was used, as described later.

Neutron flux distribution in the KULS was measured in the radial irradiation holes and the through hole. Nickel wires of 1 mm in diameter were radially set in the experimental holes to measure fast neutron fluxes by the $^{58}\text{Ni}(n,p)^{58}\text{Co}$ reaction. Gold foils, each of 5 mm×10 mm and 50 μm thick, were put on the nickel wire in every 10 cm distance for the measurement of slow neutrons by the $^{197}\text{Au}(n,\gamma)^{198}\text{Au}$ reaction. At the position of 12.5 cm behind the neutron source and the bottom of the bismuth and the lead holes, neutron fluxes were also measured with Ni foils (12.7 mm in diameter and 0.5 mm thick) and Au foils (12.7 mm in diameter and 50 μm thick). With the Au foils and Mn–Cu foils (Mn:Cu=88:12, 12.7 mm in diameter, 0.2 mm thick), cadmium ratio measurement (Cd-cover: 0.5 mm thick) was made in the bismuth and the lead holes by their (n, γ) reactions. These induced activities were measured with the above HPGe detector.

3.4. Neutron spectrum measured by TOF method

Making use of the Ta photoneutron target, angular neutron flux spectrum of $\mu = 0$ ($\theta = 90^\circ$) to the incident electron beam was measured from a few eV to 10 MeV by the neutron TOF method. The experimental arrangement is shown in Fig. 2. A horizontal through hole of 8 cm in diameter was stuffed with a lead plug in the backward region to make a re-entrant hole and to extract neutrons at the position of $r = 12.5$ cm from the photoneutron target.

In order to experimentally investigate the reproducibility of the neutron spectrum measurement, different types of two neutron detectors were employed: one was composed of a bank of three ^6Li glass (12.7 cm in diameter and 1.27 cm thick) scintillation detectors at the 22 m station and the other was ^{10}B -vaseline-plug NaI(Tl) (12.7 cm in diameter and 5.08 cm thick) scintillation detectors at the 24 m station. When the ^{10}B -vaseline-plug NaI(Tl) detectors were used for the spectrum measurement, the ^6Li glass detectors were removed from the TOF neutron beam. Relative detection efficiencies for these neutron detectors were experimentally calibrated by making use of a borated graphite standard pile [30]. The background measurement was performed by removing the backward lead plug to make a through hole. Through the amplifiers and the discriminator, output signals from the detectors were fed into a time digitizer, which was initiated by the linac electron burst, and the TOF data were stored in a data acquisition system. The channel width was 20 ns to 0.25 μs and the number of channel was 4096.

The linac was operated with the pulse width of 10 ns, the repetition rate of 180 Hz, the electron peak current of about 1 A and the electron energy of about 32 MeV, respectively. A BF₃ counter was set in an experimental hole of the KULS to monitor the neutron intensity between

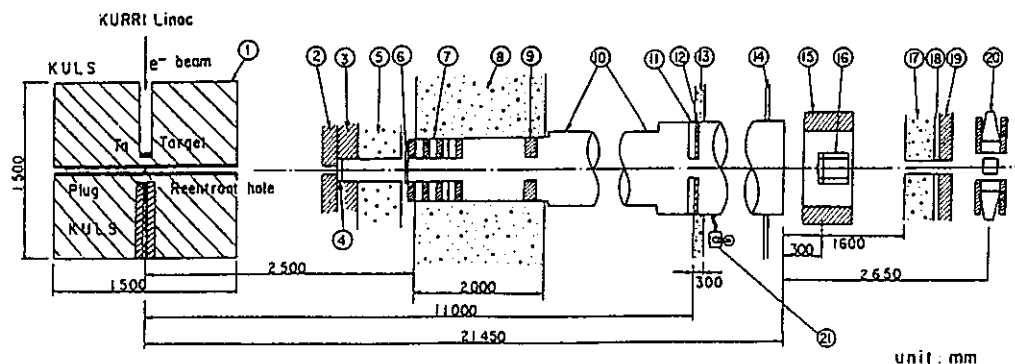


Fig. 2. Experimental arrangement for the linac TOF method. (1) KULS, (2) Pb collimator, (3) Pb shield, (4) U-filter, (5) Heavy concrete (6) Cd-filter, (7) Pb + B₄C collimator, (8) Concrete wall, (9) Pb collimator, (10) Flight tube, (11) B₄C collimator, (12) Pb collimator, (13) Concrete wall, (14) Wall of measuring house, (15) Detector shield of Pb, (16) ⁶Li glass detectors, (17) Concrete shield, (18) Cd shield, (19) Pb shield, (20) ¹⁰B-vaseline-plug NaI(Tl) detectors, (21) Rotary pump.

the experimental runs. An uranium filter of 2 cm in thickness was placed in the TOF beam to shield the neutron detectors against the intense γ -ray flash from the linac burst. Moreover, a Cd-filter of 0.5 mm in thickness was placed in the TOF beam to suppress overlap of thermal neutrons from the previous pulses. The relation between neutron TOF and its energy was calibrated with resonance energies of 132 eV for Co, of 336 eV and 2.37 keV for Mn and of 27.7 keV for Fe filters. Good linearity was found between the neutron TOF and the channel number.

4. Calculations

The continuous energy Monte Carlo code MCNP [16] has been employed to analyze the time-dependent spectrum of slowing-down neutrons in the KULS. This code can track the time behavior of neutrons every 10^{-8} s. The calculations were performed with three dimensional Cartesian coordinate, and the geometrical parameters and/or size of the KULS were referred as the spectrometer was. For the calculations, the photoneutron source spectrum was taken from the experimental data, which were previously measured by the neutron TOF method [20]. Tally boxes of $10 \times 10 \times 10$ cm³ for the MCNP calculations were put at the positions of the bismuth and the lead holes. Fig. 3 shows the calculated time-dependent neutron spectra for average energies from 70 keV to 3.6 eV at the bismuth hole about 40 cm distant from the Ta photoneutron source. In the figure, the mean time in μ s after the pulsed neutron burst is shown for the each corresponding spectrum. The time behavioral spectra seem to be asymptotic form at energies below a few keV and after that, the spectrum form is kept in the slowing-down process, although small dips are observed at 0.8, 2.31 and 12.09 keV due to the sharp

resonances of bismuth. From the calculated time-dependent spectra, we can obtain the relation between neutron slowing-down time and its average energy and also the energy resolution at FWHM.

The time-dependent spectra were integrated over a few tens of milliseconds to get the steady state neutron spectrum from about 0.1 eV to 10 MeV. For these calculations, one million random histories were performed. The statistical errors were poor in the lower energy region and 20 to 30% at neutron energies of a few eV, although the error was about 1% at hundreds of keV. There was scarcely difference in shape between the scalar neutron flux and the angular neutron flux in the lead hole. Activation data support the fact that the angular flux distribution of neutrons is almost symmetric around the neutron source in the KULS, as described later.

The MCNP code has its own nuclear data libraries, which were generated from the evaluated nuclear data files of ENDF/B-IV [21] and ENDL-85 [22]. New data library [31] generated from JENDL-3 [23] was also available for the MCNP calculations. Comparison of the calculated neutron spectrum and the measured one would be useful for the integral investigation of the nuclear data for lead, to understand the characteristics of the lead slowing-down spectrometer.

5. Results

5.1. Slowing-down time and energy

The measured relation between the neutron slowing-down time t in μ s and the average neutron energy E in keV is summarized in Fig. 4. By the least squares fitting with these measured data, the slowing-down constant K appeared in the relation of $E = K/(t_0 + t)^2$ was obtained to be

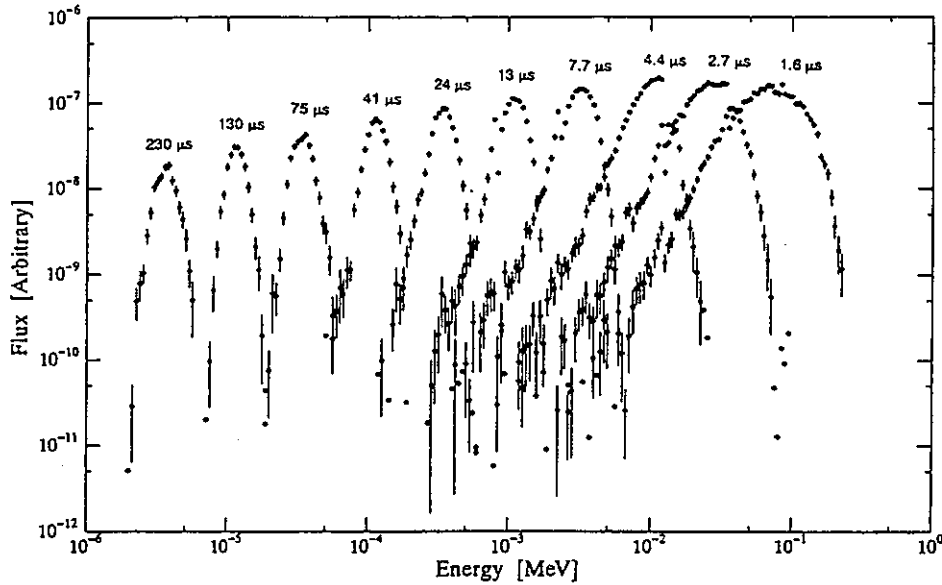


Fig. 3. Calculation of time dependent neutron spectra in the Bi hole after the pulsed neutrons were driven into the Ta target.

190 ± 2 ($\text{keV } \mu\text{s}^2$) for the bismuth experimental hole and 156 ± 2 ($\text{keV } \mu\text{s}^2$) for the lead one in the KULS, respectively. For both experimental holes, the constant t_0 was derived to be 0.2 to 0.3 μs . The present value of the constant K for the lead hole is in good agreement with 155 ($\text{keV } \mu\text{s}^2$), which was obtained by Wakabayashi et al. [5] before it was transferred from the University of Tokyo to KURRI. The bismuth hole was originally provided at KURRI.

As seen in Fig. 3, the time-dependent spectra from a few eV to hundreds keV calculated with a certain time bin were fitted with a Gaussian function, especially near the peak region. Making use of the slowing-down time corre-

sponding to the Gaussian peak, the constant K for the bismuth hole was derived as 191 ± 3 ($\text{keV } \mu\text{s}^2$), which was in excellent agreement with the experimental results mentioned above. In the same manner, the constant K for the lead hole was obtained with the calculations. The resultant value for the lead hole is 157 ± 4 ($\text{keV } \mu\text{s}^2$), which is in good agreement with the present experimental value and that measured by Wakabayashi et al.

5.2. Energy resolution

After the neutron transmission data measured by the BF_3 counter were corrected for the resonance width and the sample filter thickness, neutron energy resolution of the KULS was obtained by fitting the resonance dip data in the slowing-down time spectrum, and derived from the FWHM in the Gaussian distribution. Resonance capture measurements using the Ar gas counter could give the appropriate energy resolution at sharp and narrow resonances of 230 and 579 eV for copper and 27.5 eV for cadmium without any corrections for the resonance peak width. Fig. 5 illustrates the present results measured in the bismuth hole. It is seen that the measured energy resolution is about 40% at energies from a few eV to about 500 eV and that the resolution is going to be larger in the lower and the higher energy regions. The results for the lead hole were in good agreement with those for the bismuth hole measured by the BF_3 and the Ar gas counters, as shown in Table 3.

The time-dependent spectra calculated with the MCNP code were also fitted with a Gaussian function. The resultant energy resolutions at FWHM are summarized in

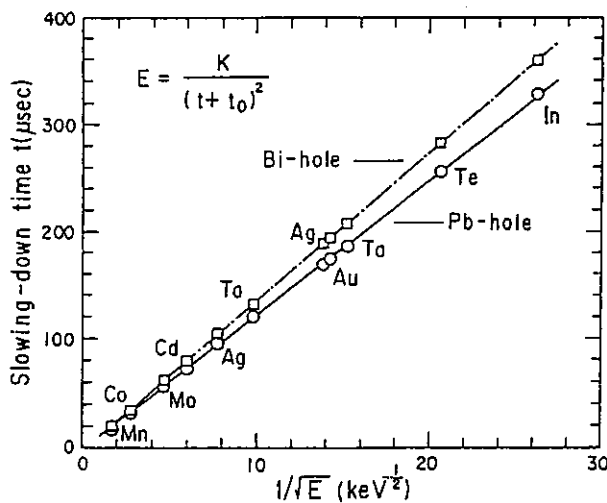


Fig. 4. Relation between neutron slowing-down time and mean energy in Bi and Pb holes of the KULS.

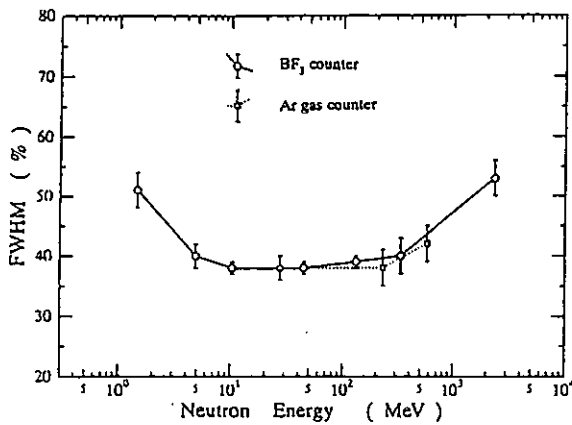


Fig. 5. Energy resolution measured by resonance filters in Bi hole of the KULS. (—○—) neutron transmission method using the BF_3 counter. (---□---) capture gamma-ray measurement using the Ar gas counter (Error lines are indicated).

Table 3 and are compared with the measured data using the BF_3 and the Ar gas counters in the bismuth and the lead holes, respectively. Although good agreement can be seen between the measured energy resolutions in both holes, the calculated values are generally lower by about 10% than the measured ones. It may be said that the difference is due to some other effects, such as impurity in the KULS.

5.3. Neutron spectrum and flux distribution measured by activation method

Making use of fourteen kinds of activation data, neutron spectrum from the lead target has been obtained in the energy region from 0.01 eV up to 20 MeV by the SAND-II code and up to 16.4 MeV by the NEUPAC code. The initial

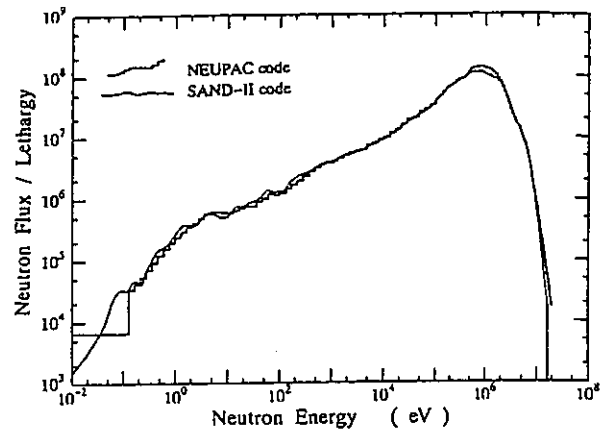


Fig. 6. Neutron spectra obtained by the activation data analysis for the lead photoneutron source.

spectrum for both analysis codes has been taken from the MCNP calculation, and the adjusted results are shown in Fig. 6. In the figure, neutron fluxes are given by the absolute values from the activation reaction rates. The spectral uncertainties in these results are 2 to 3% at least and 7 to 8% above 10 MeV and below a few hundreds keV where the activation responses are poor. Both spectra, adjusted with different type of analysis codes, are in general agreement with each other except for energies around 1 MeV, although small deviations are observed in the resonance neutron energy region within the order of analysis error. The discrepancy around 1 MeV would be due to the difference between the dosimetry cross section libraries for some threshold reactions. In the MeV energy region, the spectral shape is close to that of lead photoneutron source and harder than that of $1/E$ spectrum in the slowing-down neutron energy region. From the Cd-ratio

Table 3
Energy resolution [%] in Bi and Pb holes of the KULS

Measurements				Calculations		
Energy	BF_3 counter	Ar gas counter		Energy	MCNP code	
[eV]	Bi hole	Bi hole	Pb hole	[eV]	Bi hole	Pb hole
1.46	51±3			3.02		35.7
4.9	40±2			3.56	37.4	
10.4	38±1			10.0		28.5
27.5		38±2	37±2	11.6	31.6	
44.9	38±1			29.8		28.2
132	39±2			33.8	35.7	
230		38±3	40±3	99.1		29.8
336	40±3			113	34.5	
579		42±3	42±4	298		33.7
2370	53±3			339	38.3	
				990		38.1
				1091	43.2	
				2988		50.3
				3208	51.8	

measurements using Au and Mn–Cu foils, it was found that there existed scarcely thermal neutrons in the KULS as displayed in Fig. 6, since the Cd-ratio was almost unity.

By the $^{58}\text{Ni}(n,p)^{58}\text{Co}$ reaction used in the above activation measurement, fast neutron flux was obtained at $r = 12.5$ cm behind the neutron source (at the center of the horizontal through hole). Making use of the spectrum-averaged cross section for the KULS, the resultant fast neutron flux was 2.9×10^8 n/cm²/s, which was the result normalized to 100 W operation of the linac, although the linac power was about 63 W during the irradiation. This neutron flux is in good agreement with the normalized integral value between 1 keV and 20 MeV, appeared in Fig. 6. Fast neutron fluxes at the bottom of the bismuth and the lead holes ($r = 35$ to 50 cm from the source) were also measured with nickel foils. The results were 1.8×10^7 to 7.1×10^6 n/cm²/s/100 W depending upon the distance from the source, respectively. Experimental uncertainties for these neutron fluxes were 5 to 7%.

The spatial distribution of neutrons in the KULS was experimentally determined by the activation method. The results are given in Fig. 7 for the epi-thermal neutron flux distribution by the $^{197}\text{Au}(n,\gamma)^{198}\text{Au}$ reaction and in Fig. 8 for the fast neutron flux distribution by the $^{58}\text{Ni}(n,p)^{58}\text{Co}$ reaction. Although the epi-thermal neutron flux may be higher by 5 to 10% in the forward direction, it is seen that not only flux distribution of epithermal neutrons but also that of fast neutrons are approximately symmetric in the KULS. From Figs. 7 and 8, in addition, it may be realized that the neutron flux distribution in the KULS is not affected by the room-return neutrons, at least, at the position to set the detector in the experimental hole.

5.4. Neutron spectrum measured by TOF method

The angular neutron flux spectrum of $\mu = 0$ was measured at the position of $r = 12.5$ cm behind the Ta photoneutron target in the KULS, making use of the ^6Li

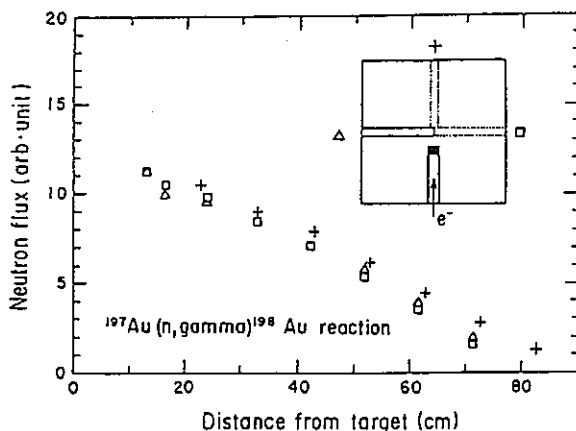


Fig. 7. Spatial distribution of epi-thermal neutrons measured by the $^{197}\text{Au}(n,\gamma)^{198}\text{Au}$ reaction in the KULS.

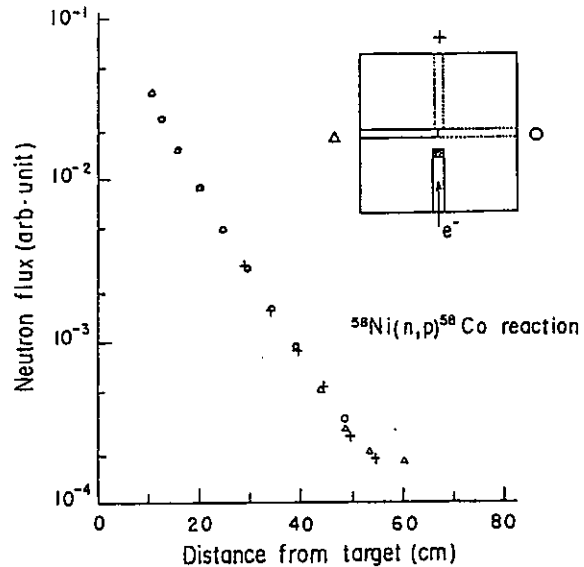


Fig. 8. Spatial distribution of fast neutrons measured by the $^{58}\text{Ni}(n,p)^{58}\text{Co}$ reaction in the KULS.

glass detectors from a few eV up to 4.5 MeV and of the ^{10}B -vaseline-plug NaI(Tl) detectors from a few eV up to 10 MeV. The results are shown in Figs. 9 and 10 and are compared with the time-integrated spectra calculated by the MCNP code. By the MCNP calculations, we have also found that the angular neutron fluxes and scalar neutron fluxes are in general agreement in spectral shape.

The measured data were summed with energy interval of $\Delta u = 0.1$ in lethargy unit to give better statistics. The statistical errors were 2 to 10%, in general, and about 50% at worst at lower energies as seen in the figures. The neutron source normalization was made for the calculated spectra, and the measured spectrum was normalized to the calculated ones by the spectrum integration above 100 keV in Figs. 9 and 10, respectively. Fluctuations in the calculated spectra are caused by poor statistics in the Monte

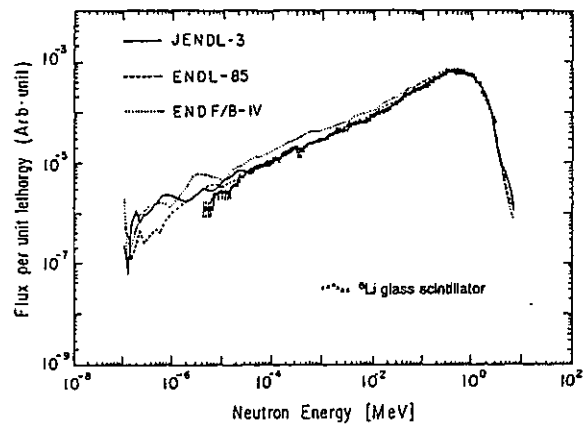


Fig. 9. Neutron spectra measured with ^6Li glass scintillators and calculated with the MCNP code for the Ta photoneutron source.

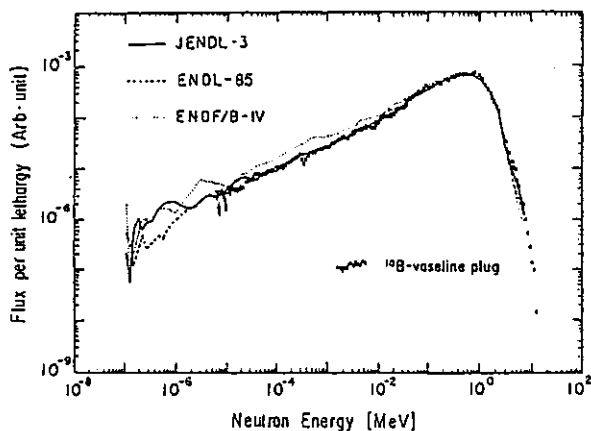


Fig. 10. Neutron spectra measured with ^{10}B -vaseline-plug NaI(Tl) detectors and calculated with the MCNP code for the Ta photo-neutron source.

Carlo calculations, especially below 10 eV the uncertainties are about 300%. As seen in Figs. 9 and 10, good agreement is obtained in general between the measured spectrum and those calculated with the evaluated nuclear data libraries of JENDL-3 and ENDL-85, while the ENDF/B-IV spectrum is higher below 100 keV than the measured and the other calculated spectra. The difference is about 25% around 10 keV and 50% around 100 eV, respectively, for both ^6Li glass and ^{10}B -vaseline-plug NaI(Tl) detectors' measurements. It has also been found that the agreement is good between the experimental results by the detectors. This fact implies that the systematic uncertainty in the measured spectrum may be small.

Around 336 eV in the measured spectra in Figs. 9 and 10 one can see a dip structure due to the big resonance of manganese, which is included as an impurity in the steel case of lead plug. In the MCNP calculations, the manganese impurity has not been considered. If the antimony impurity exists in lead of the KULS, this may absorb lower energy neutrons and make the fluxes lower in the lower energy region. Moreover, the measured TOF data had poor counting rate and the background counting rate was almost half of the foreground one. Lower neutron fluxes near 10 eV may be due to the neutron absorption by Sb, poor counting rate or inappropriate background subtraction for the TOF measurement.

In Fig. 11, the neutron spectra by the NEUPAC and the MCNP codes are compared. In the slowing-down energy region below 100 keV, these spectra are in general agreement with each other, although the lead target produces higher energy neutrons than the Ta target above several hundreds of keV [20]. The ENDF/B-IV spectrum below about 100 keV is also higher than that analyzed by the activation data, as seen in Figs. 9 and 10, although large deviations are observed among the spectra. From the comparison of the results in Figs. 6, 9–11, good agreement

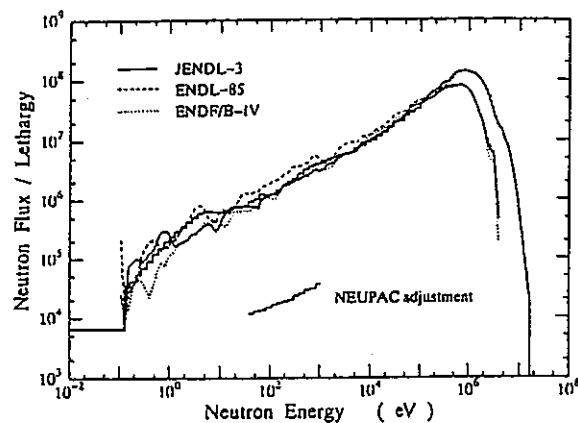


Fig. 11. Comparison of neutron flux spectra analyzed by the NEUPAC code and calculated by the MCNP code.

can be seen between the TOF spectra and the MCNP calculations by the JENDL-3 and the ENDL-85 data, so that it may be said that the NEUPAC and the SAND-II spectra by the activation data are in good agreement with the TOF spectra in the slowing-down energy region.

6. Discussion

In the present study on the characteristics of the KULS, good agreement can be seen in general between the experiments and the calculations related to the neutron slowing-down time and its energy and to the energy resolution. It has been also found that the energy resolution of the KULS is larger than 27% for the theoretically predicted value at FWHM [1,2]. Making use of the MCNP code, we have more investigated the KULS characteristics from the points of 1) the spectrometer size, 2) the impurities in lead blocks, and 3) the spectral shape of the neutron sources.

At first, we have tried to make one dimensional calculations for the neutron fluxes and energy spectra not only in the KULS of $1.5 \times 1.5 \times 1.5 \text{ m}^3$ (effective radius = 93.1 cm) but also in lead slowing-down spectrometers of $1.2 \times 1.2 \times 1.2 \text{ m}^3$ (effective radius = 74.4 cm), $1.8 \times 1.8 \times 1.8 \text{ m}^3$ (effective radius = 112 cm) and $2.0 \times 2.0 \times 2.0 \text{ m}^3$ (effective radius = 124 cm) as typical cases of the spectrometer size, respectively. At the radial positions of more than 10 cm from the photoneutron source, it is found that the relation of neutron slowing-down time and energy is almost independent of the size of the spectrometer and of the distance from the neutron source, except for the neutron intensity. Even in case that the neutron source position shifts 10 cm from the KULS center, the relation of slowing-down time and energy and the energy resolution are almost same as before at 10 cm from the source. Neutron leakage with the KULS is higher than those with the bigger spectrometers, and the neutron fluxes in the 30

to 40 cm region from the neutron source of the KULS are about 70% and 35% of those in the bigger spectrometer of radius = 112 cm at 10 keV and 10 eV, respectively. From the point of the spectrometer size, one can see that the energy resolution in the KULS (1.5 m cubic) is larger than those in other bigger spectrometers, especially in the higher energy region as appeared in Fig. 12.

If the KULS is made of bismuth material only, the slowing-down constant K becomes larger and can be calculated as $308 \text{ (keV } \mu\text{s}^2)$. In the KULS, 10 to 15 cm thick layers of bismuth blocks are partially used and those blocks may make the slowing-down constant larger than that made by lead material only. One may be able to understand the reason why the slowing-down constant K in the bismuth hole is larger than that in the lead hole.

Concerning the impurities which may contribute to the energy resolution of the KULS, we have taken account of antimony (0.05% Sb in weight) added to the lead as hardener and of water (10 to 1000 ppm of H_2O in weight) adhered to the lead surface. From the calculated results, we found that the Sb impurity was effective in absorbing epi-thermal neutrons and made the neutron fluxes lower, although the impurity did not give a severe influence to the energy resolution. In Figs. 9 and 10, the reason why the experimental spectra deviate from the MCNP calculations below about 30 eV would be explained by the neutron absorption of Sb. Fig. 13 shows the FWHM data depending upon the Sb and water impurities in the KULS. From the results, it is said that the energy resolution is not affected much by the adhered water up to 100 ppm. Even if the lead blocks were oxidized or some water was adhered to the lead, more than 10 ppm water would not be considered because the blocks were carefully cleaned to pile up.

As far as the neutron energy spectrum in the KULS is concerned, good agreement can be seen between the calculations and the TOF measurements, although the impurities in the KULS are not considered. However, the

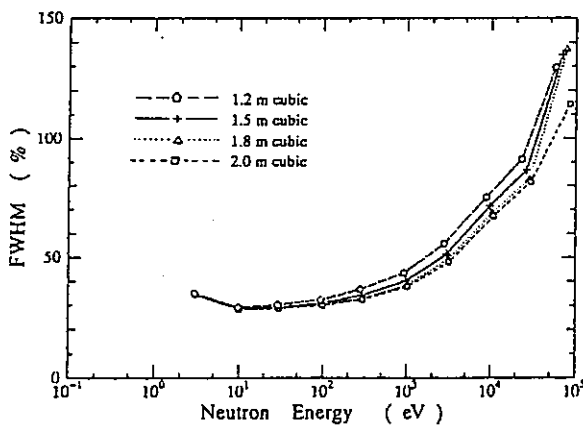


Fig. 12. Comparison of the calculated FWHM with different sizes of lead slowing-down spectrometers.

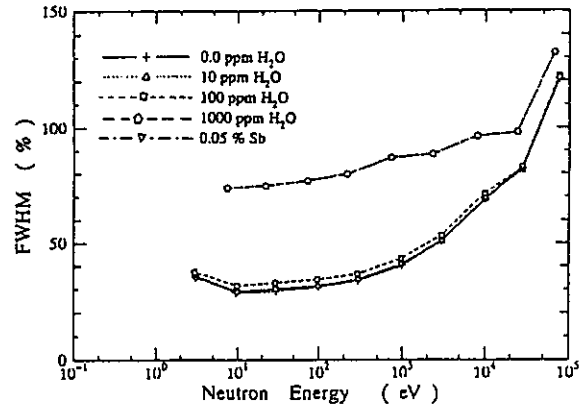


Fig. 13. Comparison of the calculated FWHM with Sb and H_2O impurities in the KULS.

calculated energy resolutions of the KULS are 5 to 10% lower than the measured ones, as given in Table 3. The difference may be due to some effects by such as small amount of impurities which are not considered in the present calculations.

With the different types of neutron source spectra, neutron behavior in the KULS has been investigated. We have selected the following spectra: 1) Ta photoneutron source, 2) 14 MeV neutrons, and 3) 500 keV neutrons whose energy is lower than the threshold level (0.57 MeV) for the inelastic scattering cross section of lead. The 14 MeV neutrons are widely spread after a few interactions with lead, and the slowing-down time spectrum may become similar to that from the Ta photoneutrons. The slowing-down time spectrum by the 500 keV neutrons already shows asymptotic form above 1 keV, as seen in Fig. 14, and the calculated energy resolution at 100 eV, for example, is about 28% at FWHM, while the energy resolution obtained with the Ta photoneutron source is about 30% in the lead hole. This fact implies that the energy resolution of the KULS is broadened by the inelastic scattering processes with lead. In the lower energy region, up-scattering neutrons may also broaden the energy resolution.

As we have investigated above, main factors to make the energy resolution broadened are thought to be the effects due to the size of the KULS, the inelastic scattering of fast neutrons and the impurities in the KULS. It may be said that the practical energy resolution of the KULS was broadened by the superposition of these effects.

As seen in Figs. 6, 9 and 10, it may be realized that there scarcely exist thermal neutrons in the KULS and that the neutron spectrum is close to that obtained in a large core of fast breeder reactors [32]. The neutron spectral shape in the KULS is simple and no structure can be observed. We have characterized the neutron spectrum in the KULS through the present experiments and the calculations. It can be expected to use the KULS in future not

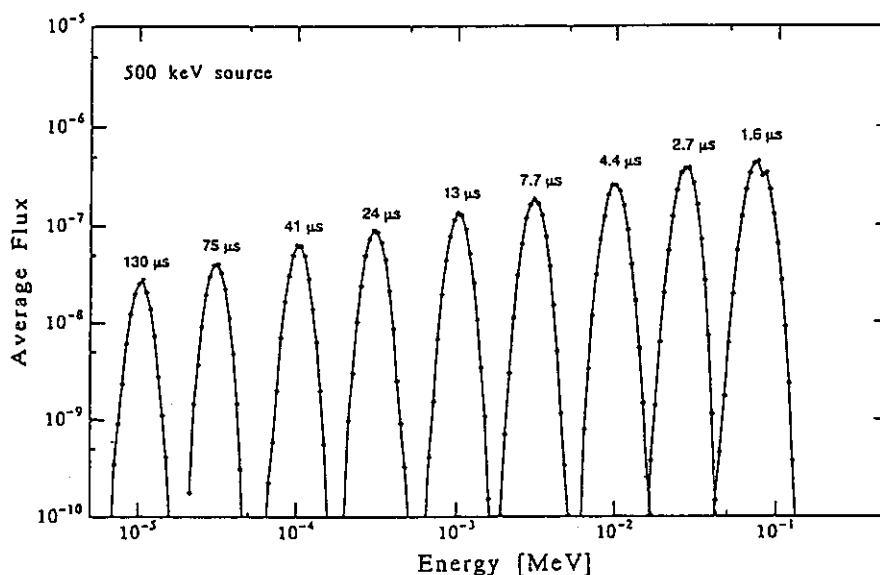


Fig. 14. Calculation of time dependent neutron spectra in the KULS driven by 500 keV neutrons.

only for measurements of energy dependent nuclear data but also for integral experiments as a reference neutron spectrum field.

7. Conclusion

The characteristic behavior of neutrons in the Kyoto University Lead Slowing-down Spectrometer, KULS of $1.5 \times 1.5 \times 1.5 \text{ m}^3$, was obtained by the experiments using resonance neutron filters and by the calculations with the MCNP code. The slowing-down constant K in the relation of $E = K/t^2$ was experimentally determined to be $190 \pm 2 \text{ (keV } \mu\text{s}^2)$ for the bismuth hole and $156 \pm 2 \text{ (keV } \mu\text{s}^2)$ for the lead hole, respectively. The energy resolution of the KULS was obtained to be around 40% in the relevant energy region for the bismuth and the lead holes, making use of the Ar gas counter for the sharp resonances at 230 and 579 eV of Cu and at 27.5 eV of Cd, and of the BF_3 counter for the neutron transmission measurement using resonance filters.

Monte Carlo calculations using the MCNP code were also performed to determine the relation between the neutron slowing-down time and its average energy and to obtain the energy resolution and the neutron spectrum in the KULS. The calculated results agreed in general with these measurements, and the calculated energy resolutions were lower by about 10% than the measured ones.

Spatial distribution of neutrons in the KULS was measured by the activation method and the results showed almost symmetric around the photoneutron source. The neutron flux spectrum in the KULS was obtained by the spectrum adjustment method with activation data in the energy range from 0.01 eV to 20 MeV. The angular neutron

spectrum was also measured by the TOF method from 4 eV to 10 MeV, and the TOF measurement was compared with the spectra calculated with the JENDL-3, the ENDL-85 and the ENDF/B-IV cross section data. The calculated spectra are in general agreement with the measured one except for that the ENDF/B-IV spectrum seems to be 25 to 50% higher than the TOF measurement below about 100 keV. The present result would be useful for the integral investigation of lead cross section which is related to the neutron transport in the lead slowing-down spectrometer. The neutron flux spectrum per unit lethargy in the KULS is proportional to the square root of energy in the slowing-down neutron energy region and show similar spectral tendency to the TOF measurement and the activation analysis. Since there exist scarcely thermal neutrons in the KULS, the neutron field there would be expected to be a quasi-standard field for integral measurements in the epithermal/resonance neutron energy region.

Acknowledgments

The authors would like to express their sincere thanks to Prof. M. Nakazawa of University of Tokyo for the reconstruction of the lead slowing-down spectrometer. They are also indebted to Mr. K. Nishio of Kyoto University for his kind assistance in the Monte Carlo calculations.

This study was supported by the Grant-in-Aid of Scientific Research from the Ministry of Education, Science and Culture (No. 03452302 and No. 63460234) and by the Cooperative Use Program of KURRI. The calculations were carried out with the FACOM M-Series Computers at the Data Processing Center of Kyoto University.

References

- [1] K.H. Beckurts and K. Wirtz, *Neutron Physics* (Springer, New York, 1964) p. 342.
- [2] A.A. Bergman, A.I. Isacoff, I.D. Murin, F.L. Shapiro, I.V. Shtraniikh and M.V. Cazamovsky, *Proc. 1st Int. Conf. on Peaceful Uses for Atomic Energy, United Nations, P/642, Vol. 4* (1955) p. 135.
- [3] Y.P. Popov, *Proc. Lebedev Phys. Inst., Academy of Sci., USSR, Vol. 24* (1964) p. 111.
- [4] F. Mitzel and H.S. Plendl, *Nukleonik* 6 (1964) 371.
- [5] H. Wakabayashi, A. Sekiguchi, M. Nakazawa and O. Nishino, *J. Nucl. Sci. Technol.* 7 (1970) 487.
- [6] A.A. Bergman, A.E. Samsonov, Yu. Ya. Stavisskii, V.A. Tolstikov and V.B. Chelnokov, *Proc. Nuclear Constants, Obninsk Reports, Vol. 7* (1971) p. 37.
- [7] M. Fujino, F. Takahashi and H. Yamamoto, *J. Nucl. Sci. Technol.* 13 (1976) 566.
- [8] J.A. Harvey (ed.), *Experimental Neutron Resonance Spectroscopy* (Academic Press, New York and London, 1970).
- [9] R.E. Slovacek, D.S. Cramer, E.B. Bean, J.R. Valentine, R.W. Hockenbury and R.C. Block, *Nucl. Sci. Eng.* 62 (1977) 455.
- [10] Y. Nakagome, R.C. Block, R.E. Slovacek and E.B. Bean, *Phys. Rev. C* 43 (1991) 1824.
- [11] H.T. Maguire, Jr., C.R.S. Stopa, R.C. Block, D.R. Harris, R.E. Slovacek, J.W.T. Dabbs, R.J. Dougan, R.W. Hoff and R.W. Loughheed, *Nucl. Sci. Eng.* 89 (1985) 293.
- [12] B. Alam, R.C. Block, R.E. Slovacek and R.W. Hoff, *Nucl. Sci. Eng.* 99 (1988) 267.
- [13] Y. Danon, R.E. Slovacek, R.C. Block, R.W. Loughheed, R.W. Hoff and M.S. Moore, *Nucl. Sci. Eng.* 109 (1991) 341.
- [14] E.C. Vanterpool, R.E. Slovacek, D.R. Harris and R.C. Block, *Nucl. Sci. Eng.* 110 (1992) 186.
- [15] N.M. Abdurrahman, R.C. Block, D.R. Harris, R.E. Slovacek, Y. Lee and F. Rodriguez-Vera, *Nucl. Sci. Eng.* 115 (1993) 279.
- [16] MCNP – A General Monte Carlo Code for Neutron and Photon Transport, Version-3A, LA-7396-M, Rev.2, Los Alamos National Laboratory (1986).
- [17] M. Nakazawa and A. Sekiguchi, *Proc. 2nd ASTM-Euratom Symp. on Reactor Dosimetry, NEUREG/CP-0004, Vol. 3* (1977) p. 1423.
- [18] W.N. McElroy, S. Berg and G. Gigas, *Nucl. Sci. Eng.* 27 (1967) 533.
- [19] S.A. Hayashi, I. Kimura, K. Kobayashi, S. Yamamoto, H. Nishihara, T. Mori and S. Kanazawa, *J. Nucl. Sci. Technol.* 24 (1987) 702.
- [20] K. Kobayashi, I. Kimura and T. Mori, *Nucl. Sci. Eng.* 99 (1988) 157.
- [21] D. Garber (ed.), BNL-17541 (ENDF-201) (1975).
- [22] R.J. Howerton, D.E. Cullen, R.C. Haight, M.H. MacGregor, S.T. Perkins and E.F. Plechaty, UCRL-50400, Vol. 15 (1975).
- [23] K. Shibata, T. Nakagawa, T. Asami, T. Fukahori, T. Narita, S. Chiba, M. Mizumoto, A. Hasegawa, Y. Kikuchi, Y. Nakajima and S. Igarasi, JAERI 1319 (1990).
- [24] S.F. Mughabghab, M. Divadeenam and N.E. Holden, *Neutron Cross Sections, Vol. 1, Neutron Resonance Parameters and Thermal Cross Sections, Part A* (Academic Press, Inc., New York, 1981); and S.F. Mughabghab, *Neutron Cross Sections, Vol. 1, Neutron Resonance Parameters and Thermal Cross Sections, Part B* (Academic Press, Inc., New York, 1984).
- [25] E. Browne and R.B. Firestone, *Table of Radioactive Isotopes* (Wiley-Interscience, New York, 1986).
- [26] T. Iguchi, Private communication (1985).
- [27] Z. Li, Y. Wang and J. Gao, *Measurements of Neutron Flux Spectra in SPR, Japan-China Symp. on Research and Test Reactor, UT-1, JAERI* (1988).
- [28] K. Kobayashi, I. Kimura, Z. Li and Y. Wang, *Proc. 7th ASTM-Euratom Symp. on Reactor Dosimetry*, eds. G. Tsotridis et al. (Kluwer, London, 1992) p. 263.
- [29] M. Nakazawa, K. Kobayashi, S. Iwasaki, T. Iguchi, K. Sakurai, Y. Ikeda and T. Nakagawa, JEARI 1325 (1992).
- [30] I. Kimura, K. Kobayashi, S.A. Hayashi, S. Yamamoto, M. Ando, S. Kanazawa, H. Nishihara and Y. Higashihara, *Nucl. Instr. and Meth.* 137 (1976) 85.
- [31] K. Kosako, Y. Oyama and H. Maekawa, JAERI-M 91-187 (1991).
- [32] A.E. Waltar and A.B. Reynolds, *Fast Breeder Reactors* (Pergamon, New York, 1981).

付録 B

Journal of NUCLEAR SCIENCE and TECHNOLOGY, 30(9), pp. 863~869 (September 1993).

Measurement of Fission Cross Section of Neptunium-237 in Resonance Region with Electron Linac—Driven Lead Spectrometer

Akihiro YAMANAKA[†], Itsuro KIMURA, Satoshi KANAZAWA,

*Department of Nuclear Engineering, Kyoto University**

Katsuhei KOBAYASHI, Shuji YAMAMOTO, Yoshihiro NAKAGOME,
Yoshiaki FUJITA and Tadaharu TAMAI^{††}

*Research Reactor Institute, Kyoto University***

Received December 14, 1992

Making use of a lead neutron slowing-down spectrometer combined with an electron linear accelerator and back-to-back type double fission chambers, we measured the fission cross section of ^{237}Np relative to that of ^{235}U from about 1 eV to about 5 keV with energy resolution ($\Delta E/E$) of about 40%. The experimentally obtained result has been compared with two newly evaluated data files, JENDL-3 and ENDF/B-VI, and with previously measured values by Plattard *et al.* and by Hoffman *et al.* Although the shape of the present energy dependent cross section agrees with that of ENDF/B-VI, that of JENDL-3 below 120 eV and that of Plattard *et al.*, the absolute values of above three are from 3 to 4 times smaller than those of the present data. However the Hoffman *et al.*'s data are rather closer to the present data.

KEYWORDS: fission cross sections, neptunium 237, subthreshold fission, fission ratio, uranium 235, lead slowing-down spectrometer, KULS, double fission chambers, transmutation, ENDF/B-VI, JENDL-3, energy resolution, energy dependence, comparative evaluations

I. INTRODUCTION

Recently, several methods for the transmutation or the incineration of long-lived fission products and transuranium actinides have been proposed and studied. For the evaluation of the feasibility of those methods, basic data especially precise nuclear data are required.

Among several transuranium actinides produced by power reactors, neptunium-237 (^{237}Np) is thought to be one of the most burdensome ones, because of its large production rate in a reactor, very long half-life (2.14×10^6 yr) and α activities in its decay chain. In order to transmute ^{237}Np to nuclides with much shorter half-lives, it is proposed to use the $^{237}\text{Np}(n, f)$ and $^{237}\text{Np}(n, \gamma)^{238}\text{Np}$ reactions.

The cross section for the $^{237}\text{Np}(n, f)$ reaction increases above its threshold energy, and the precision of its cross section data in the MeV region is practically sufficient enough to evaluate the transmutation of ^{237}Np . Below the threshold energy of this reaction, Fubini *et al.*⁽¹⁾ found an intermediate structure from which the double humped barrier for the subthreshold fission of ^{237}Np was demonstrated. Several groups have measured this cross section below the threshold so far^{(2)~(6)}. Jiacoletti

* Yoshidahonmachi, Sakyo-ku, Kyoto 606-01.

** Kumatori-cho, Osaka-fu 590-04.

[†] Present address: Nucl. Power Plant Eng. Dept., Hitachi Works, Hitachi Ltd., Saiwai-cho, Hitachi-shi 317.

^{††} Deceased in August, 1992.

et al. and Hoffman *et al.* measured it by the neutrons from the Physics 8⁽³⁾⁽⁴⁾ and Plattard *et al.* did with an electron linear accelerator⁽⁵⁾. However the absolute value of the data by the former two is about 3 times larger than that by the latter. In two newly evaluated data files, JENDL-3⁽⁷⁾ and ENDF/B-VI⁽⁸⁾, the data are close to those of Plattard *et al.* High resolution measurement of this cross section was carried out by Auchampaugh *et al.*⁽⁶⁾, who mentioned that the experimental data of Plattard *et al.* were too low by a factor of 3. Therefore it has been strongly requested to check these data for the evaluation of the transmutation system by the $^{237}\text{Np}(n, f)$ reaction.

For the purpose of precise evaluation of nuclear data such as the fission cross section of ^{237}Np , required are; (1) a neutron source with clearly known spectrum and with sufficient intensity, and (2) a detector with systematic errors as low as possible. In this work we utilized a lead neutron slowing-down spectrometer with an electron linear accelerator as an intense neutron source. The lead spectrometer affords more than 1,000 times higher neutron flux than an ordinary neutron time-of-flight system, although the energy resolution of the former is inferior to that of the latter. The lead spectrometer is not applicable to obtain individual resonance parameters but suitable to measure the absolute value of cross sections with very small amount sample mass. Before carrying out the fission cross section measurement, we obtained the neutron characteristics of the lead spectrometer very carefully. A special experimental hole covered by a bismuth layer was used to eliminate photofissions. For a detector with low systematic error, we adopted to use back-to-back type double fission chambers with a sample deposit of ^{237}Np and a reference one of ^{235}U and to measure the cross section for the $^{237}\text{Np}(n, f)$ reaction relative to that for the $^{235}\text{U}(n, f)$ reaction of which cross section can be thought to be quite precise.

II. EXPERIMENTAL METHOD

1. Lead Slowing-down Spectrometer

After pulsed fast neutrons are generated at the center in a sufficiently large lead pile, neutrons are initially slowed down by the $(n, 2n)$ reaction, inelastic scattering or elastic scattering. Below the threshold energies of the former two reactions, only the elastic scattering predominates the slowing-down process. Since the elastic scattering cross section for lead is nearly constant in the intermediate and epithermal regions, its absorption cross section is quite small and the mean logarithmic energy loss per an elastic scattering in lead is quite small as 0.0096, neutrons slow down continuously with asymptotically constant energy resolution $\Delta E/E$ and the slowing-down time t is simply related to energy E as below:

$$E = \frac{K}{(t+t_0)^2}.$$

Therefore we can use it as a neutron spectrometer⁽⁹⁾. Several groups have made lead spectrometers with a conventional pulsed neutron source^{(10)~(13)} and have used them for capture cross section measurement and so forth. Slovacek *et al.* utilized an electron linear accelerator as a more intense pulsed neutron source for a lead neutron spectrometer⁽¹⁴⁾, with which they succeeded in measuring very small cross sections such as the subthreshold fission of ^{238}U .

In this work, we took over a lead spectrometer of the University of Tokyo, named LESP⁽¹¹⁾, and reconstructed it beside an electron linear accelerator of Research Reactor Institute, Kyoto University (KURRI). This resuscitated lead spectrometer, abbreviated as KULS, was made by cleaning, polishing and reassembling lead blocks with the purity of 99.9%, covered by Cd sheet 0.5 mm thick and put on a movable steel table. The size and the weight of this lead spectrometer are 1.5 m cubic and about 38 t, respectively. An air cooled photoneutron source which consists of 12 Ta discs is placed at its center. We made 11 experimental holes, which were filled with lead blocks unless one was used for an experiment.

One of these holes was covered with a Bi layer about 10 to 15 cm thick to suppress high energy γ -rays from the neutron capture of $\text{Pb}^{(15)}$. The cross-sectional view of KULS is shown in Fig. 1.

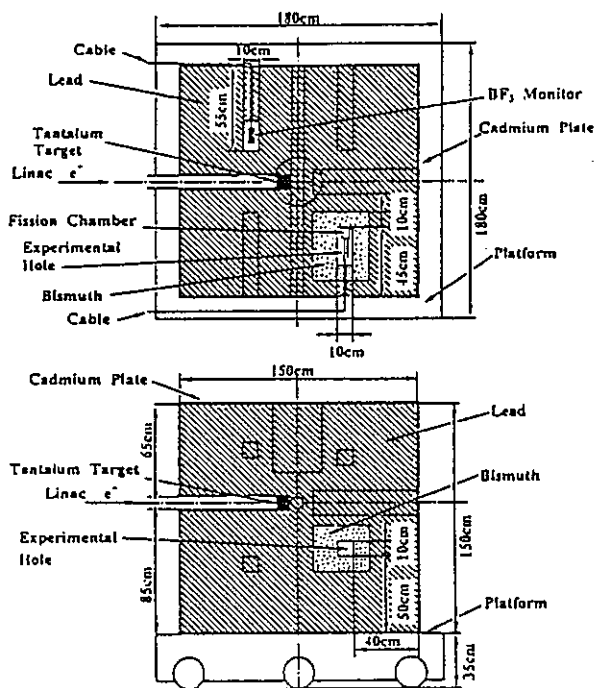
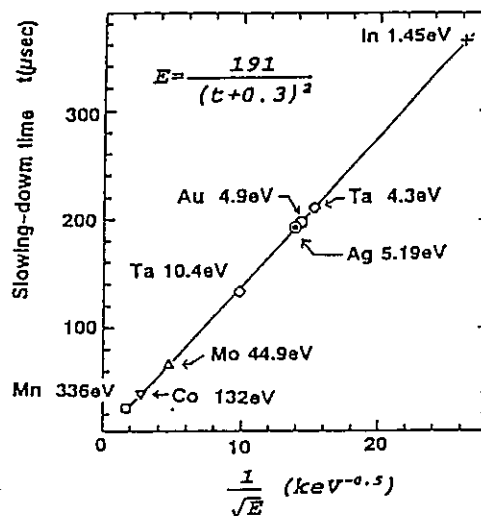


Fig. 1 Cross sectional view of Kyoto University Lead Spectrometer, KULS

The slowing-down characteristics of this lead spectrometer KULS were obtained with a BF_3 counter and an argon filled proportional counter with and without resonance filters (In, Ta, Au, Ag, Mo, Co or Mn). The measured slowing-down time behavior is depicted in Fig. 2. The energy resolution at 27.5 eV shows $39 \pm 1\%$. The details of the characterization of KULS were given elsewhere⁽¹⁶⁾. Since the size of KULS is smaller than most of other lead spectrometers, we could measure the fission cross section for the $^{237}\text{Np}(n, f)$ reaction about 1 eV. Upper limit of the neutron energy is thought to be about 5 keV.

2. Fission Chambers

The fission chambers employed in this work have two identical parallel plate type ionization chambers as shown in Fig. 3⁽¹⁷⁾. These chambers were originally designed for the incore fission ratio measurement in FCA of Japan Atomic Energy Research Institute. Since



Solid line was obtained by the least square fitting ($K=191$ and $t_0=0.3$)

Fig. 2 Relation between slowing-down time and energy of neutrons in Bi covered hole of KULS

the back sides of a sample deposit on a stainless steel plate and a reference one are faced each other, it is called back-to-back type. The chambers were made of Al and filled with a mixed gas of 97%Ar and 3%N₂ at the pressure of 1 atm. The distance between the two electrodes was 8 mm. The operation voltage was 400 V.

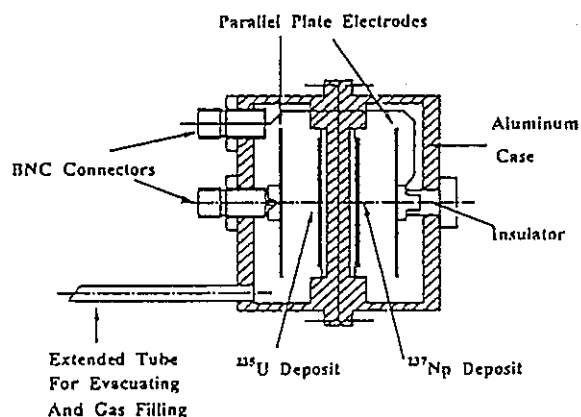


Fig. 3 Cross-sectional view of back-to-back type fission chambers

Neptunium oxide (NpO_2) of about 2 mg with high purity imported from Harwell Establishment of UKAEA was dissolved in hydrochloric acid of 0.2 N and 0.1 ml of this solution was mixed into 2-propanol of 5 ml. Therewith we electrodeposited NpO_2 on a stainless steel plate

28 mm in diameter and 0.2 mm thick. The applied voltage and the electric current were about 200 V and 2 mA, respectively. Electrodeposition was performed for 1 h. The diameter of the deposit was 2 cm. Highly enriched (99.91%) uranium oxide (UO_2) which we had purchased from Oak Ridge National Laboratory, USA was similarly electrodeposited on the stainless steel plate. After the electrodeposition, each plate was sintered with a gas burner, and the reference deposit became U_3O_8 .

The number of atoms in the sample deposit and that in the reference one together with those of impurities were determined by the α -ray spectrometry with a Si surface barrier detector in vacuum. The numbers of ^{237}Np in the sample deposit and that of ^{235}U in the reference one are $(1.99 \pm 0.02) \times 10^{17}$ and $(4.12 \pm 0.09) \times 10^{17}$, respectively. In this determination, (1) statistical error, (2) uncertainties in the decay data, and (3) uncertainty introduced

by background subtraction, 1% for ^{237}Np and 2% for ^{235}U , were taken into account. The thicknesses of the NpO_2 and U_3O_8 deposits are about 25 and 50 $\mu\text{g}/\text{cm}^2$, respectively.

In the sample deposit, we found small amounts of ^{238}Pu and ^{239}Pu , and their contents were 0.320 ± 0.003 and 1.10 ± 0.13 ppm, respectively. The α -rays from ^{234}U was counted for the reference deposit, and the content of ^{234}U became 464 ± 5 ppm.

3. Electronic Circuits

Two identical electronic circuits were prepared for both sample and reference chambers. As seen in Fig. 4 the start signal for timing was taken from the electron linear accelerator. The channel number and time width of each time analyzer were 4,096 and 125 ns, respectively. Since we used quite thin sample and reference deposits, fission pulses were clearly discriminated from background pulses caused by α -rays.

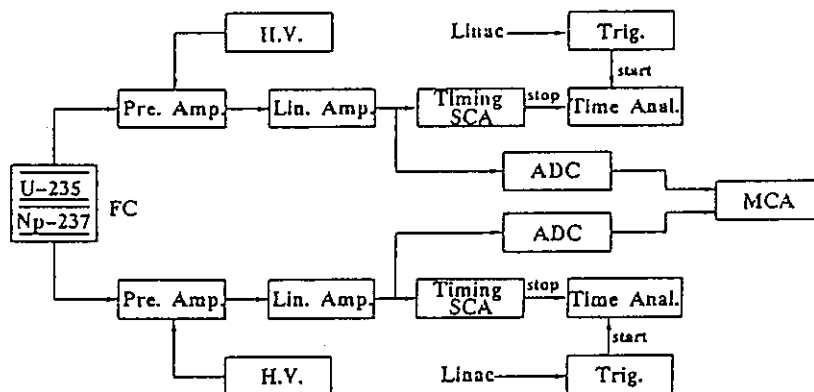


Fig. 4 Block diagram of electronic circuits to measure time dependent fission counts from double fission chambers

4. Fission Rate Measurement

Measurement of the fission ratio of ^{237}Np to ^{235}U was carried out in the Bi-covered experimental hole of KULS. The main reason to use this hole is to suppress the photofission of ^{237}Np and ^{235}U . The electron linear accelerator was operated by the following conditions: pulse repetition=180 pps, pulse width=33 ns, peak electron current=2A, accelerating energy=32 MeV, average neutron yield= 10^{11} n/s and total operation time=50 h.

Background run was carried out by making use of the fission chambers without sample

and reference deposits, and few background counts were observed.

III. RESULTS AND DISCUSSION

From the fission counts of the sample and the reference, the cross section for the ^{237}Np (n, f) reaction is obtained by

$$\sigma_{\text{Np}}(E) = \frac{C_{\text{Np}}}{C_{\text{U}}} \cdot \frac{N_{\text{U}}}{N_{\text{Np}}} \sigma_{\text{U}}(E),$$

where C_{Np} : Fission counts of ^{237}Np
 C_{U} : Fission counts of ^{235}U
 N_{U} : Number of ^{235}U atoms in reference deposit

N_{Np} : Number of ^{237}Np atoms in sample deposit
 $\sigma_{\text{U}}(E)$: Energy dependent fission cross section of ^{235}U .

We cited the numerical values of $\sigma_{\text{U}}(E)$ from ENDF/B-VI.

As it was described that the contents of ^{238}Pu and ^{239}Pu in the sample deposit were 0.32 and 1.10 ppm, respectively, the contribution of their fission counts to σ_{Np} was about 0.05%, and was neglected. The contribution of ^{234}U to σ_{U} is also estimated to be 0.01%.

Since we utilized the experimental hole

covered by Bi, the highest energy of the capture γ -rays is about 4.6 MeV which is much smaller than that of Pb, 6.7 MeV. The photofission cross sections for ^{237}Np is in the order of $100 \mu\text{b}$ at 4.6 MeV and the shapes of both photofission cross sections for ^{237}Np and for ^{235}U are similar in their rise-up region. Therefore we can neglect the contribution of the photofission counts to σ_{Np} .

Grundl *et al.*⁽¹⁸⁾ obtained the mean range of fission fragments in UO_2 to be 8.29 mg/cm^2 . By using this value, Obu⁽¹⁷⁾ showed the losses of fission fragments in the UO_2 layers 10, 20

Table 1 Obtained cross section data for $^{237}\text{Np}(n,f)$ reaction

Energy (eV)	Cross section (mb)	Error (mb)	Energy (eV)	Cross section (mb)	Error (mb)
1.05	35.6	5.3	73.7	61.9	3.9
1.17	35.0	5.1	82.7	68.1	4.2
1.32	32.6	4.4	92.7	88.3	5.1
1.48	21.0	3.1	104	98.7	5.6
1.66	15.5	2.4	117	95.6	5.4
1.86	10.6	1.9	131	91.3	5.2
2.08	13.1	2.2	147	114	6.2
2.34	10.0	2.2	165	148	7.7
2.62	11.7	2.3	185	152	7.9
2.94	13.7	2.5	207	134	7.1
3.30	19.6	3.0	233	112	6.0
3.70	19.3	2.9	261	97.9	5.3
4.16	25.0	3.3	293	88.7	4.9
4.66	38.2	4.7	329	77.4	3.9
5.23	50.7	5.7	369	64.0	3.3
5.87	51.8	5.7	413	54.5	2.9
6.58	48.4	5.5	464	51.4	2.9
7.39	45.3	5.0	520	49.9	2.9
8.29	36.0	4.1	584	51.8	3.1
9.30	31.2	3.5	655	48.1	3.0
10.4	25.8	3.1	735	55.3	3.5
11.7	24.0	2.9	824	55.9	3.6
13.1	22.2	2.8	925	52.5	3.6
14.7	20.0	2.4	1,040	53.7	3.8
16.5	24.7	2.6	1,160	44.0	3.1
18.5	44.5	3.8	1,310	39.8	2.8
20.8	87.0	5.9	1,470	38.4	2.6
23.3	159.4	9.1	1,640	31.4	2.1
26.2	270	14	1,840	37.6	2.5
29.4	432	21	2,070	39.2	2.6
32.9	618	30	2,320	31.4	2.1
37.0	680	33	2,600	34.0	2.2
41.5	530	26	2,920	32.4	2.1
46.5	326	17	3,280	29.7	1.9
52.2	196	11	3,680	27.7	1.7
58.5	116.7	6.7	4,120	32.6	2.0
65.7	80.0	4.9	4,630	37.9	2.3

and $50 \mu\text{g}/\text{cm}^2$ thick. The loss of fission fragments in the both deposits was calculated by interpolating the above data, and was found to be negligible.

Angular distribution of fission fragments against the direction of an incident neutron beam shows an anisotropy for fast neutrons, but those for the neutrons in resonance region can be thought to be isotropic. Therefore we did not correct the data for the effect by the anisotropy of fission fragments. We compared the fission ratios of ^{237}Np and ^{235}U for two configurations; one case for which the sample deposit was placed at the inner position in the experimental hole and the other the opposite. The result shows little difference between them.

Loss of the fission counts for ^{237}Np and ^{235}U below the pulse height discrimination levels was determined by linearly extrapolating the fission count peaks.

After the above corrections, we obtained the result of the cross section for the $^{237}\text{Np}(n, f)$ reaction as Table 1, in which (1) the statistical error for the fission, (2) the error in the determination of the numbers of ^{237}Np and ^{235}U , (3) 2% as systematic error, and (4) the uncertainty in the fission cross sections for ^{235}U were taken into account.

In Fig. 5, the present result is compared with the evaluated values in JENDL-3 and in ENDF/B-VI. Since the energy resolution of the original data in both evaluated data files is much higher than that of the present experiment, we processed the evaluated data values by multiplying a resolution function of which energy resolution function is assumed to be a Gaussian with 40% of its full width at half maximum. In this figure, shown are the processed values of both files.

From this figure, it can be seen that (1) the evaluated values in both JENDL-3 and ENDF/B-VI are about 3 times smaller than the present result, (2) the gross shape of the present result is very similar to that of ENDF/B-VI in all range and to that of JENDL-3 below 120 eV, and (3) above 120 eV, the cross section in JENDL-3 is flat and differs from the present result.

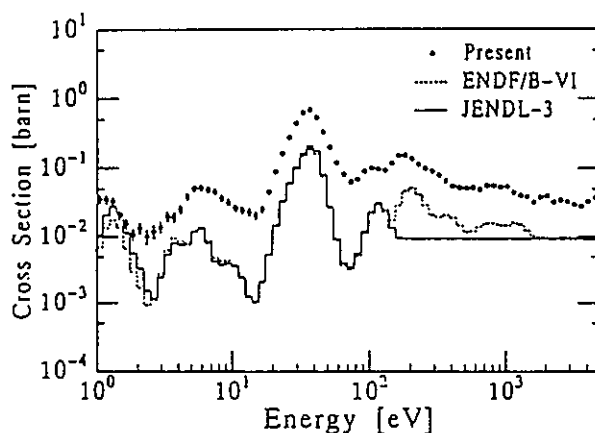


Fig. 5 Experimentally obtained cross section of $^{237}\text{Np}(n, f)$ reaction compared with those in evaluated data files

The present result is compared with earlier experimental data and is shown in Fig. 6. The original point wise data have been also processed as the same manner as the above. The data obtained by Hoffman *et al.*⁽⁴⁾ are close to the present ones, but those measured Plattard *et al.*⁽⁶⁾ are much smaller than the present ones. Too low normalization of Plattard *et al.*'s data was pointed out by Auchampaugh *et al.*, which is supported by the present result.

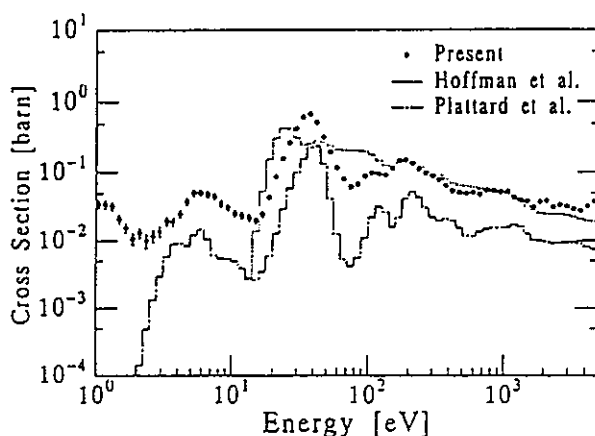


Fig. 6 Experimentally obtained cross section of $^{237}\text{Np}(n, f)$ reaction compared with two previously measured data

Reevaluation of the $^{237}\text{Np}(n, f)$ cross section in resonance and intermediate regions is recommended. If this cross section increases factor 3, the efficiency of the transmutation of ^{237}Np by the fission in resonance region would improve almost the same factor.

IV. CONCLUSION

We have measured the cross section for the $^{237}\text{Np}(n, f)$ reaction from about 1 eV to about 5 keV, normalized to that for the $^{235}\text{U}(n, f)$ reaction with back-to-back type fission chambers by making use of a newly constructed lead neutron slowing-down spectrometer KULS. The absolute values of the data by Hoffman *et al.* are close to the present ones, but those by Plattard *et al.* are from 3 to 4 times less than the present ones. Gross shape of the present result is very similar to that of ENDF/B-VI in all range and that of JENDL-3 below 120 eV, however the absolute values in both files are also from 3 to 4 times smaller than those of the present data. Therefore we recommend to reevaluate the $^{237}\text{Np}(n, f)$ cross section in resonance and intermediate regions.

ACKNOWLEDGMENT

The authors would like to express hearty thanks to Prof. M. Nakazawa of University of Tokyo for the reconstruction of the lead slowing-down spectrometer and to Dr. M. Nakano of Japan Atomic Energy Research Institute (JAERI) for the supply of the fission chambers. They are also indebted to Mr. T. Nakagawa of the Nuclear Data Center of JAERI for supplying nuclear data. Technical assistance by Mr. K. Nishio of Kyoto University is appreciated.

This work was supported by the Grant-in-Aid of Scientific Research from the Ministry

of Education, Science and Culture (No. 6346023 to Fujita and No. 03452302 to Tamai) and by the Cooperative Use Program of KURRI.

REFERENCES

- (1) FUBINI, A., BLONS, J., MICHAUDON, A., PAYA, D.: *Phys. Rev. Lett.*, 20, 1373 (1968).
- (2) BROWN, W.K., DIXON, D.R., DRAKE, D.M.: *Nucl. Phys.*, A156, 609 (1970).
- (3) JIACOLETTI, R.J., BROWN, W.K., OLSON, H.G.: *Nucl. Sci. Eng.*, 48, 412 (1972).
- (4) SEMON, M.D., HOFFMAN, M., SANDERS, W.M.: *Bull. Am. Phys. Soc.*, 21, 655 (1976).
- (5) PLATTARD, S., BLONS, J., PAYA, D.: *Nucl. Sci. Eng.*, 61, 477 (1976).
- (6) AUCHAMPAUGH, G.F., *et al.*: *Phys. Rev.*, C29, 174 (1984).
- (7) SHIBATA, K., *et al.*: *JAERI* 1319, (1990).
- (8) ROSE, R.F. (ed.): *BNL-NCS-17541* (4th ed.), (1991).
- (9) BERGMAN, A.A., *et al.*: *1st Geneva. Conf.* Vol. 4, 135 (1955).
- (10) MITZEL, F., PLENDL, H.S.: *Nukleonik*, 6, 371 (1964).
- (11) WAKABAYASHI, H., SEKIGUCHI, A., NAKAZAWA, M., NISHINO, O.: *J. Nucl. Sci. Technol.*, 6, 487 (1970).
- (12) CHOU, J.C., WERLE, H.: *J. Nucl. Energy*, 27, 811 (1973).
- (13) SAWAN, M., CONN, R.W.: *Nucl. Sci. Eng.*, 54, 127 (1974).
- (14) SLOVACEK, R.E., *et al.*: *ibid.*, 62, 455 (1977).
- (15) NAKAGOME, Y., BLOCK, R.C., SLOVACEK, R.E., EDGAR, B.B.: *Phys. Rev.*, C43, 1824 (1991).
- (16) YAMANAKA, A., *et al.*: *JAERI-M* 92-027, p. 375 (1992).
- (17) OBU, M.: *JAERI-M* 9757, (1981).
- (18) GRUNDL, J.A., GILLIAM, D.M., DUDEY, N.D., POPEK, R.J.: *Nucl. Technol.*, 25, 237 (1975).

Measurements of Thermal Neutron Cross Section and Resonance Integral for $^{237}\text{Np}(n, \gamma)^{238}\text{Np}$ Reaction

Katsuhei KOBAYASHI,

*Research Reactor Institute, Kyoto University**

Akihiro YAMANAKA† and Itsuro KIMURA

*Department of Nuclear Engineering, Kyoto University***

(Received January 12, 1994)

Making use of a standard neutron spectrum field with a pure Maxwellian distribution, the thermal neutron cross section for the $^{237}\text{Np}(n, \gamma)^{238}\text{Np}$ reaction was measured at a neutron energy of 0.0253 eV by the activation method. The result is 158 ± 3 b, which is obtained relative to the reference value of 98.65 ± 0.09 b for the $^{197}\text{Au}(n, \gamma)^{198}\text{Au}$ reaction. Although the data in JENDL-3 is larger by about 15% than the present value, the recently revised data in JENDL-3.2 is close to the present. The ENDF/B-V, ENDF/B-VI, JEF-2 and Mughabghab's data are also larger by 7~15%. Old measurements are larger by 7~18% than the present data.

The resonance integral for the $^{237}\text{Np}(n, \gamma)^{238}\text{Np}$ reaction was also measured relative to the reference value of $1,550 \pm 28$ b for the $^{197}\text{Au}(n, \gamma)^{198}\text{Au}$ reaction with a $1/E$ standard neutron spectrum field. By defining the Cd cut-off energy as 0.5 eV for the $^{237}\text{Np}(n, \gamma)^{238}\text{Np}$ reaction, the present resonance integral is 652 ± 24 b, which is in good agreement with the JENDL-3, -3.2, ENDF/B-V, -VI, JEF-2 and Mughabghab's data. However, most of the old experimental data are, in general, larger by 24~38% than the present measurement.

KEYWORDS: neptunium 237 target, neutron beams, gamma radiation, neptunium 238, nuclear reactions, gold 197 target, gold 198, thermal neutrons, cross sections, Maxwellian distribution field, resonance integrals, $1/E$ neutron spectrum field, activation method

I. INTRODUCTION

Neptunium-237 is one of the minor actinides with a long half-life, which is abundantly produced in light water reactors. In order to make nuclear power more acceptable and practical, much interest has been paid to the disposal of radioactive waste matter these days^{(1)~(7)}. One of the waste disposal methods for ^{237}Np is to adopt the nuclear transmutation using reactor neutrons⁽⁸⁾. Quite a number of experimental data for the $^{237}\text{Np}(n, f)$ cross section have been obtained in the MeV energy region and these data are rather well evaluated. The fission cross sections are about 10~500 mb at energies below about 500 keV. In this lower energy region, large

discrepancies are seen among the existing experimental data⁽⁹⁾. Very recently, the present authors have measured the $^{237}\text{Np}(n, f)$ cross section by using a lead slowing-down spectrometer coupled to an electron linear accelerator⁽¹⁰⁾. The $^{237}\text{Np}(n, \gamma)^{238}\text{Np}$ reaction cross section, which is a combination of $1/v$ and resonance cross sections in the low energy region, is much higher than the fission cross section, and hence this reaction would be more effective for the nuclear transmutation of ^{237}Np than the $^{237}\text{Np}(n, f)$ reaction in the lower energy region, considering the reaction

* Kumatori-cho, Sennan-gun, Osaka 590-04.

** Yoshida honmachi, Sakyo-ku, Kyoto 606-01.

† Present address: Hitachi Works, Hitachi, Ltd., Saiwai-cho, Hitachi-shi 317.

rates averaged over the energy spectrum of neutrons for light water reactors.

Calculations for fuel burn-up and for the reactor design aiming at the transmutation of high level radioactive materials have been carried out^{(1)~(6)(8)}. In these cases, well-evaluated nuclear data are indispensable⁽¹¹⁾. It is said that the evaluated nuclear data, which would be often based on the experimental results, are not always enough for the estimation of nuclear transmutation, especially for the $^{237}\text{Np}(n, \gamma)^{238}\text{Np}$ reaction. The number of energy dependent cross sections for this reaction is limited. In addition, most of the thermal neutron cross sections and the resonance integrals are rather old^{(12)~(17)}. In the previous measurements, information on the neutron spectrum field used was not always enough as a standard.

In the present study, the thermal neutron cross section and the resonance integral for the $^{237}\text{Np}(n, \gamma)^{238}\text{Np}$ reaction have been measured by the activation method, making use of

standard neutron fields with a pure Maxwellian distribution and a $1/E$ neutron spectrum, respectively.

II. NEUTRON SPECTRUM FIELDS

1. Thermal Neutron Spectrum Field

The Kyoto University Reactor (KUR) of the Research Reactor Institute, Kyoto University (KURRI) is a highly enriched uranium-fueled light water-moderated research reactor, whose nominal power is 5 MW. Beside the core, there is a heavy water thermal neutron facility with a heavy water tank of 1.4 m in length. Outside the heavy water tank, there are a void region of 48 cm in thickness, 40×40 cm square and a removable bismuth layer of 60 cm in diameter and 15 cm in thickness, as illustrated in Fig. 1. The irradiation room is about $2.4 \times 2.4 \times 2.4$ m³ and surrounded by 90 cm thick heavy concrete shields. The leakage neutrons from the heavy water tank can be used as a thermal neutron source of plane-type in a large space.

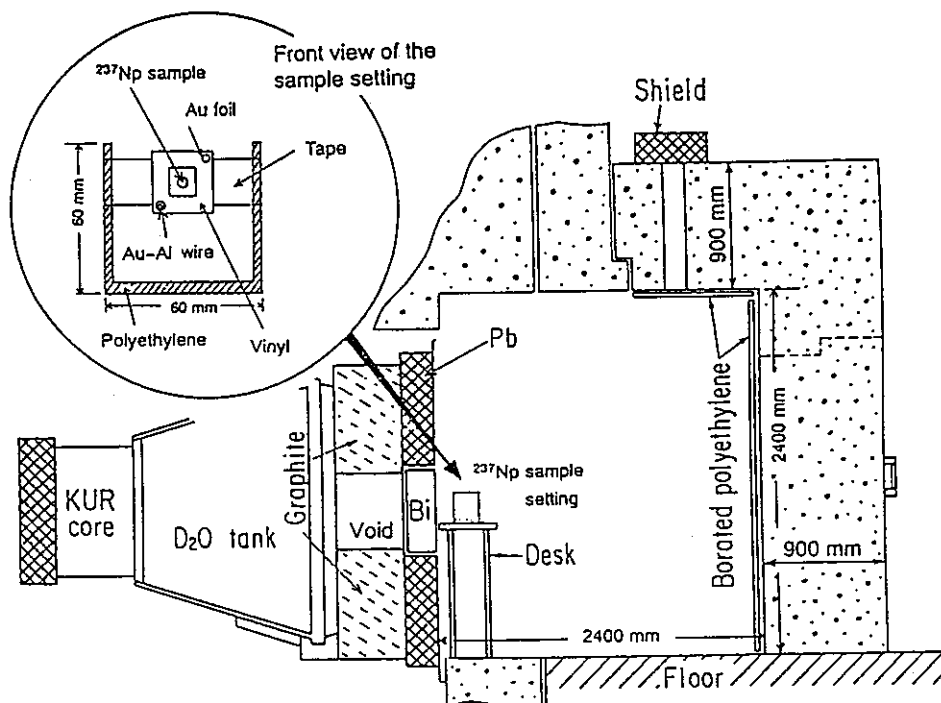


Fig. 1 Experimental arrangement for thermal neutron cross section measurement at heavy water thermal neutron facility of KUR.

The extended figure shows the setting arrangement of the ^{237}Np and the Au samples.

Kanda *et al.* measured the neutron spectrum from the heavy water tank by the time-of-flight technique using a fast chopper⁽¹⁸⁾. The obtained spectrum showed good agreement with a Maxwellian distribution having neutron temperature of 60°C. The Cd-ratio measured by Au foils with and without Cd-cover of 0.7 mm in thickness was more than 5,000 at the bismuth layer, and epi-thermal neutrons could be almost negligible⁽¹⁸⁾⁽¹⁹⁾.

2. $1/E$ Neutron Spectrum Field

The Kinki University Reactor (UTR-KINKI) is a highly enriched uranium-fueled light water-moderated and graphite-reflected research reactor⁽²⁰⁾, which has the separate cores at an interval of 46 cm. The nominal output power is 1 W. At the center of the internal graphite reflector between the two divided cores as shown in Fig. 2, a graphite stringer of 9.6×9.6 cm square and 66 cm long can be withdrawn to make a void region or a central cavity for sample irradiation. The neutron energy spectrum at the central graphite cavity has been calculated⁽²¹⁾ using the SRAC code system⁽²²⁾. In this calculation, geometrical conditions for the separate cores were assumed to be a cylindrical ring. The two-dimensional transport S_N code

TWOTRAN⁽²³⁾ was employed to calculate the neutron spectrum in the central void region. The 122 group constants were produced from ENDF/B-IV data. The results of the neutron spectra are shown in Fig. 3(a),(b). The calculated spectrum satisfactorily agrees with a standard $1/E$ neutron spectrum from about 1 eV to a few 100 keV.

By adjusting the above calculated spectrum with multi-foil activation data for 5 kinds of (n, γ) reactions and 4 kinds of threshold reactions⁽²⁰⁾, the neutron spectrum at the central graphite cavity of the UTR-KINKI was also obtained using the NEUPAC code⁽²⁴⁾. This code contains energy dependent group cross section libraries for important neutron dosimetry reactions in ENDF/B-V. We adopted 144 energy groups from 0.01 eV to 16.4 MeV. The results of the adjusted spectrum are shown in Fig. 3, and compared with the above transport calculations. It has been found that the neutron spectrum at the core center gives a good $1/E$ shape in the relevant energy range. Moreover, the neutron flux distribution is almost flat in the central cavity of the UTR-KINKI⁽²⁰⁾.

The sandwiched foil method has been also employed to measure epi-thermal neutrons at the main resonances for 4 kinds of (n, γ)

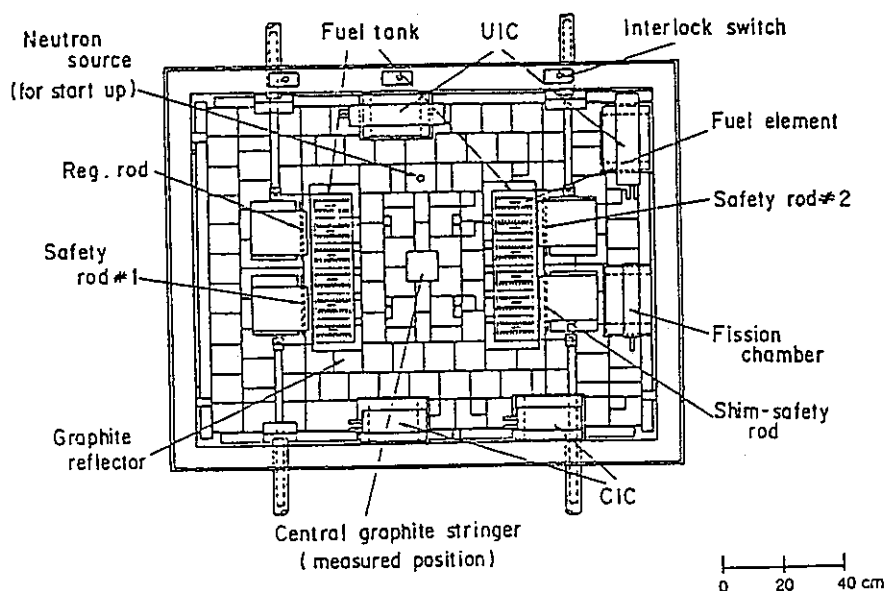


Fig. 2 Top view of UTR-KINKI core for present experiment.
A graphite stringer at the central region can be withdrawn to make a cavity for the sample irradiation.

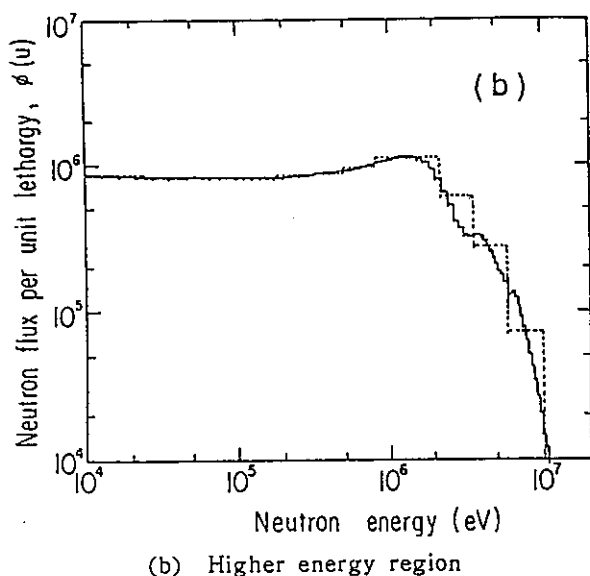
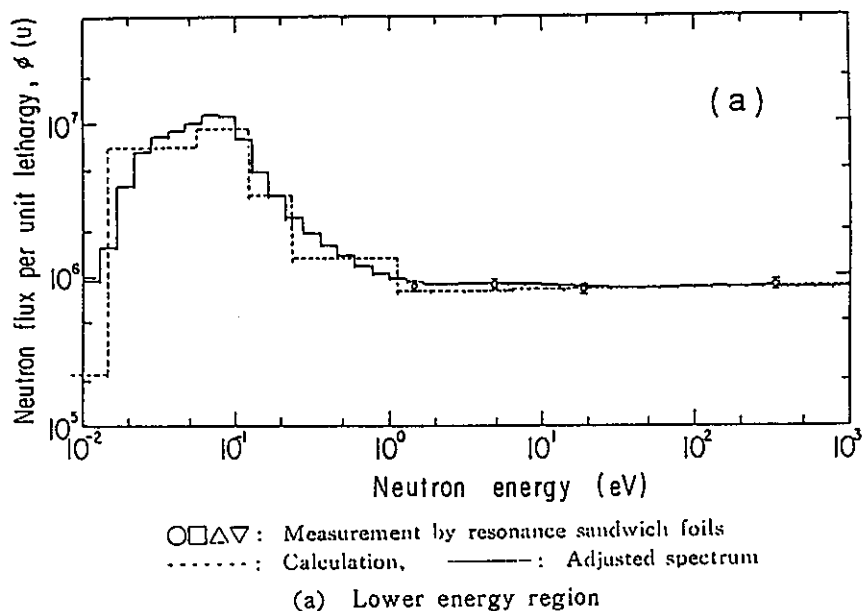


Fig. 3(a),(b) Neutron energy spectra obtained at central graphite cavity of UTR-KINKI⁽²⁰⁾

reactions⁽²⁰⁾. Neutron fluxes at 1.46, 4.94, 18.8 and 337 eV resonances for ^{115}In , ^{197}Au , ^{186}W and ^{55}Mn are shown in Fig. 3(a), respectively. These results are in good agreement with the calculated and the adjusted spectra in the $1/E$ spectrum region.

III. MEASUREMENT OF THERMAL NEUTRON CROSS SECTION

1. Experimental Methods

The heavy water thermal neutron facility of the KUR has been used for the measure-

ment of the thermal neutron cross section for the $^{237}\text{Np}(n, \gamma)^{238}\text{Np}$ reaction. The ^{237}Np samples, which were chemically purified as aqueous solution⁽¹⁹⁾, were prepared in the form of dried filter-paper 1.5×1.5 cm square with drops of the solution. The sample was sealed with vinyl sheet of 0.05 mm in thickness, 2.5×2.5 cm square, and was attached to a 3 mm thick polyethylene holder with adhesive tape, as seen in Fig. 1.

Thermal neutron flux was monitored with an Au foil of 3 mm in diameter and $50 \mu\text{m}$ thick or with a piece of Au-Al alloy wire, 0.5 mm in diameter and 0.0314% in weight of Au. The monitor sample was put on the corner of the vinyl sheet for the ^{237}Np sample and these samples were set at about 10 cm from the Bi surface, as shown in Fig. 1. Irradiation time was about 10 hours during the 5 MW operation of the KUR. Nine irradiations were made, and neutron fluxes for six of them were obtained with the Au-Al alloy wire monitor and the remainings were measured by the Au foil. The thermal neutron flux at the irradiation position in front of the Bi layer reached about $1.5 \times 10^9 \text{ n/cm}^2 \cdot \text{s}$ at the nominal KUR power level of 5 MW.

The total amount of the ^{237}Np atoms was experimentally determined by the γ -ray measurement of 312 keV from ^{233}Pa , which was in radioactive equilibrium to ^{237}Np , and was found

to be $10^{16} \sim 10^{17}$ for each sample. Induced activities of ^{237}Np from the irradiated ^{237}Np sample and the ^{233}Pa were simultaneously measured with a high purity Ge (HPGe) detector. These γ -ray photo-peaks were clearly observed in the pulse height spectrum. Gold samples were also measured with the same Ge detector. These samples were set at a distance of about 5 cm from the detector. Gamma-ray energies and intensities used for the present data processing are shown in Table 1, in which the data used for the determination of number of ^{237}Np atoms are included⁽²⁶⁾. The g -factors⁽²⁶⁾ for both of ^{237}Np and ^{197}Au are also given in the table. The detection efficiency of the Ge detector used was experimentally calibrated by the mixed γ -ray standard sources purchased from Amersham.

Table 1 Nuclear data of ^{237}Np , ^{233}Pa , ^{238}Np , ^{197}Au and ^{198}Au used for present measurements

Isotope	Half-life	γ -ray energy (MeV)	γ -ray intensity (%)	g -factor
^{237}Np	2.14×10^6 yr			0.982
^{233}Pa	27.0 d	0.312	37.0	
^{238}Np	2.12 d	0.984	27.8	
^{197}Au				1.0051
^{198}Au	2.694 d	0.412	95.5	

2. Measurement of Cross Section

The thermal neutron cross section σ_x averaged over the Maxwellian distribution spectrum is defined as

$$\sigma_x = \frac{\sigma_x(v_0)}{1.128} S_x g_x(T_n) \sqrt{\frac{T_0}{T_n}},$$

and the measured reaction rate is given in the following relation:

$$R_x = \varepsilon_x N_x \sigma_x \phi,$$

where $v_0 = 2,200$ m/s, $T_0 = 293.6$ K, T_n is the neutron temperature, S_x the self-shielding coefficient, $g_x(T_n)$ the g -factor, ε_x the detection efficiency, N_x the number of atoms for the relevant reaction and ϕ the neutron flux.

In the present measurement, the thermal

neutron cross section for the $^{237}\text{Np}(n, \gamma)^{238}\text{Np}$ reaction at a neutron energy of 0.0253 eV (corresponding to a velocity of 2,200 m/s) has been measured relative to that for the $^{197}\text{Au}(n, \gamma)^{198}\text{Au}$ reaction as a standard, by re-writing the above relations as follows:

$$\sigma_x(v_0) = \frac{\varepsilon_{\text{Au}}}{\varepsilon_x} \cdot \frac{R_x}{R_{\text{Au}}} \cdot \frac{N_{\text{Au}}}{N_x} \cdot \frac{S_{\text{Au}}}{S_x} \cdot \frac{g_{\text{Au}}(T_n)}{g_x(T_n)} \sigma_{\text{Au}}(v_0),$$

where x and Au denote the parameters for ^{237}Np and ^{197}Au , respectively.

The self-shielding coefficient⁽²⁷⁾ for the Au foil was about 0.9 in our measurement. The coefficients for the Au-Al alloy wire and the ^{237}Np sample were neglected and the corrections were not made for these samples.

IV. MEASUREMENT OF RESONANCE INTEGRAL

1. Experimental Methods

A standard $1/E$ neutron spectrum field at the UTR-KINKI has been used for the measurement of the resonance integral for the $^{237}\text{Np}(n, \gamma)^{238}\text{Np}$ reaction. The ^{237}Np samples were also made in the form of dried filter-paper, which was the same as those used for the thermal neutron cross section measurement. For the neutron flux monitor with Au sample, a metallic foil of 12.7 mm in diameter and 50 μm in thickness was used. Each of the ^{237}Np sample and the Au foil was put in a Cd-cover of 0.5 mm in thickness and stuck on an Al holder, which was set at the central graphite cavity of the UTR-KINKI, as illustrated in Fig. 4. The ^{237}Np sample was set between the Au foils, which were used for the neutron flux monitor. Nine irradiations for the ^{237}Np sample were made for 5 h each together with the Au monitor foils during the 1 W operation of the reactor. Induced activities from the ^{237}Np and the Au foils were measured with a HPGe detector, whose detection efficiency was calibrated with standard γ -ray sources.

The nuclear data used for the present activation measurements were also taken from Table 1. The experimental methods are similar to those for the thermal neutron cross section measurement.

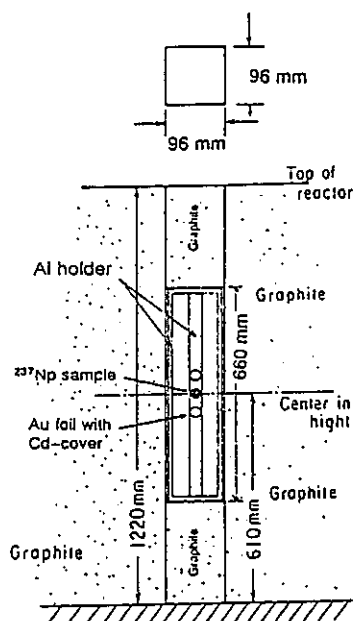


Fig. 4 Experimental arrangement for ^{237}Np and Au samples at central graphite cavity of UTR-KINKI

2. Measurement of Resonance Integral

The resonance integral is defined by the relation;

$$I_x = \int_{E_{Cd}}^{\infty} \sigma_x(E) dE/E,$$

where $\sigma_x(E)$ is the cross section as a function of energy E , and E_{Cd} is a Cd cut-off energy, which is usually defined as 0.5 eV⁽²⁸⁾⁽²⁹⁾. The resonance integral for the $^{237}\text{Np}(n, \gamma)^{238}\text{Np}$ reaction has been measured relative to that for the $^{197}\text{Au}(n, \gamma)^{198}\text{Au}$ reaction, as seen in the following relation:

$$I_x = \frac{\epsilon_{Au}}{\epsilon_x} \cdot \frac{R_x}{R_{Au}} \cdot \frac{N_{Au}}{N_x} \cdot \frac{S_{Au}}{S_x} \cdot I_{Au},$$

where I_{Au} is the standard value of the Au resonance integral, ϵ the detection efficiency, R the reaction rate, N the number of atoms and S the self-shielding coefficient, and the subscripts Au and x mean the data for ^{197}Au and ^{237}Np , respectively. The neutron self-shielding coefficient for the Au foil was obtained by the calculations using the continuous energy Monte Carlo code VIM⁽³⁰⁾. For the ^{237}Np sample, the self-shielding correction was neglected because the sample was diluted in the form of dried filter-paper with the

drops of the ^{237}Np solution.

As seen in Fig. 3, the neutron spectrum at the central graphite cavity of the UTR-KINKI deviates from the $1/E$ standard spectrum below about 1 eV. Moreover, it is noticed that ^{237}Np has a big resonance at 0.49 eV. Making use of the neutron spectrum at the UTR-KINKI, energy dependent reaction rate curve for the $^{237}\text{Np}(n, \gamma)^{238}\text{Np}$ reaction was calculated with the VIM code⁽³⁰⁾. Figure 5 shows the calculated reaction rate which is observed in the energy region above 0.2 eV. In order to derive the resonance integral, which is defined as an integral of the reaction rate for relevant cross section above $E_{Cd}=0.5$ eV, we have made a correction of the measured reaction rate by taking the ratio of the calculated reaction rate integral above 0.5 eV to that above 0.2 eV.

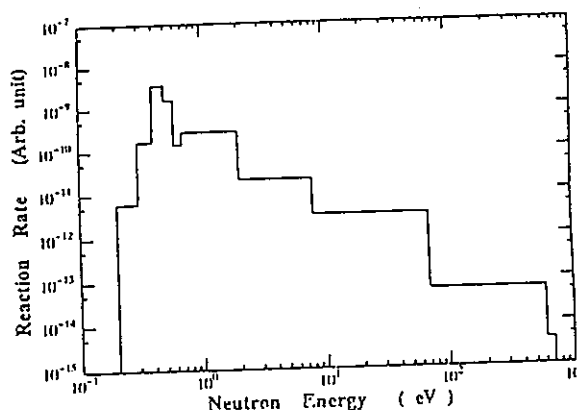


Fig. 5 Calculated reaction rate for $^{237}\text{Np}(n, \gamma)^{238}\text{Np}$ reaction using neutron spectrum obtained at UTR-KINKI

V. RESULTS AND DISCUSSION

1. Thermal Neutron Cross Section

The thermal neutron cross section of $^{237}\text{Np}(n, \gamma)^{238}\text{Np}$ reaction for 2,200 m/s neutrons was obtained, relative to the well known reference cross section value of 98.65 ± 0.09 b for the $^{197}\text{Au}(n, \gamma)^{198}\text{Au}$ reaction. Three of the 9 measured data were obtained with the Au foil monitors and the results were 156.4, 156.5 and 161.3 b, respectively. Other 6 data, which were measured with the Au-Al alloy wire monitors, were in the values from 155.9 to 160.1 b. These 9 data are in good agreement with each other within about 3.4%,

and it is found that there exists consistency between the data measured by the Au foil and the Au-Al alloy wire. Main sources of the uncertainties are due to the statistical errors (1.0~2.0%), the detection efficiencies (1.5~2.2%), number of atoms, especially for ^{237}Np (about 1.8%), geometrical factor for irradiation of the samples (about 0.5%), and errors (0.8~1.2%) including some other corrections. The experimental uncertainties were carefully analyzed and the covariance matrix for the $^{237}\text{Np}(n, \gamma)^{238}\text{Np}$ and the $^{197}\text{Au}(n, \gamma)^{198}\text{Au}$ reactions was derived by considering the correlations between the measured data as done before⁽³⁵⁾. The resultant variance and covariance data gave the standard deviation of about 2% for the $^{237}\text{Np}(n, \gamma)^{238}\text{Np}$ cross section measurement and the off-diagonal element of 0.05, respectively. The present value obtained is shown in Table 2, and compared with the existing experimental and the evaluated data^{(9) (12)~(16) (29) (31)~(34)}.

Table 2 Thermal neutron cross section (2,200 m/s value) for $^{237}\text{Np}(n, \gamma)^{238}\text{Np}$ reaction

Present	158±3 b	
JENDL-3.2 ('93)	164.6	Ref. (33)
JENDL-3 ('90)	181.0	Ref. (29)
ENDF/B-VI ('91)	181.0	Ref. (32)
ENDF/B-V ('79)	169.1	Ref. (31)
JEF-2 ('93)	181.0	Ref. (34)
Mughabghab ('84)	175.9±2.9	Ref. (9)
Gryntakis ('87)	169±3	Ref. (16)
Weston ('81)	180±6	Ref. (15)
Eberle ('71)	187±6	Ref. (14)
Hellstrand ('70)	172±3	Ref. (13)
Schuman ('69)	185±12	Ref. (12)

In order to check the effect on the undesirable $^{237}\text{Np}(n, \gamma)^{238}\text{Np}$ reaction by epi-thermal neutrons, we have also made a neutron irradiation of the ^{237}Np sample with a Cd-cover of 0.5 mm in thickness at the heavy water thermal neutron facility of the KUR. We have found no induced activities of ^{238}Np in the ^{237}Np sample.

As seen in Table 2, previous measurements of the thermal neutron cross section are between 169 and 187 b and are larger by 7~18% than the present value. The Mugh-

abghab's datum is larger by 11%. The evaluated data in JENDL-3, ENDF/B-V, -VI and JEF-2 whose libraries are based on experimental data, are also larger by about 7~15% than the present measurement. These discrepancies may be due to the fact that the previous measurements are not always good enough from the points of the experimental technique, purity of the sample prepared and the neutron spectrum field used as a standard. Very recently, the evaluated cross sections of ^{237}Np in JENDL-3 have been revised as JENDL-3.2⁽³³⁾ by taking account of recent data. The thermal neutron cross section in JENDL-3.2 is closer to our present data.

2. Resonance Integral

The resonance integral for the $^{237}\text{Np}(n, \gamma)^{238}\text{Np}$ reaction was obtained by normalizing the measured data to the reference value of $1,550\pm 28$ b for the $^{197}\text{Au}(n, \gamma)^{198}\text{Au}$ reaction. All of the 9 experimental data were between 644 and 671 b and showed good agreement with each other. The experimental uncertainties are due to the statistical counts (5~10% for ^{237}Np and 0.5~1% for ^{197}Au), the reference value for the $^{197}\text{Au}(n, \gamma)^{198}\text{Au}$ reaction, the Cd cut-off correction in the ^{237}Np reaction (about 1%) and the self-shielding effect for the Au foil (1.2%). Some of other uncertainties due to the detection efficiencies, number of atoms, geometrical factor and other corrections are almost similar to those in the thermal neutron cross section measurement. Considering the correlations between the measured data as described above, the experimental uncertainties were analyzed⁽³⁵⁾ to obtain the variance and covariance matrix for the $^{237}\text{Np}(n, \gamma)^{238}\text{Np}$ and the $^{197}\text{Au}(n, \gamma)^{198}\text{Au}$ reactions. The experimental uncertainty derived from the variance data is 3.7% for the $^{237}\text{Np}(n, \gamma)^{238}\text{Np}$ reaction, and the off-diagonal element in the covariance matrix is 0.48. The present result is given in Table 3 and compared with the previous data^{(9) (12) (13) (16) (17) (29) (31)~(34)}.

Since ^{237}Np has a big resonance at 0.49 eV, the effective Cd cut-off energy is much lower than 0.5 eV whose value is used for the definition of the resonance integral. In the

Table 3 Resonance integral for
 $^{237}\text{Np}(n, \gamma)^{238}\text{Np}$ reaction

Present	652 ± 24 b	
JENDL-3.2 ('93)	662.0	Ref. (2)
JENDL-3 ('90)	663.0	Ref. (2)
ENDF/B-VI ('91)	655.0	Ref. (3)
ENDF/B-V ('79)	662.6	Ref. (3)
JEF-2 ('93)	655.0	Ref. (3)
Mughabghab ('84)	640 ± 50	Ref. (9)
Gryntakis ('87)	821.5 ± 58.0	Ref. (10)
Hellstrand ('70)	640 ± 50	Ref. (13)
Schuman ('69)	807 ± 40	Ref. (12)
Scoville ('68)	900 ± 300	Ref. (17)

experimental determination of the resonance integral for the $^{237}\text{Np}(n, \gamma)^{238}\text{Np}$ reaction, therefore, the measured data were corrected. In the present measurement, the correction factor for the reaction rate due to the difference from the Cd cut-off energy of 0.5 eV was estimated to be 0.7 by the Monte Carlo calculations using the VIM code. Without this correction, the resonance integral is 931 ± 35 b.

We have investigated the effect which is observed in the resonance integral by changing the Cd cut-off energy, and found that a 10% change with energy results in only a 0.2% shift in the integral data, if the cross section is assumed to be $1/v$ shape. Moreover, we have made corrections for the fact that the neutron energy spectrum in the UTR-KINKI deviates from the ideal $1/E$ spectrum, especially at energies below 1 eV.

Recent evaluations of JENDL-3, -3.2, ENDF/B-V, -VI, JEF-2 and by Mughabghab are in good agreement with the present measurement, as shown in Table 3. However, most of the experimental values which are rather old are larger by 24~38% than the present value, except for that by Hellstrand. The reason why the old experimental data are much larger than the present value may be due to the fact that the Cd cut-off energy correction was not made properly. Moreover, another problem may be due to the use of the irradiation field deviating from a $1/E$ neutron spectrum as a standard.

VI. CONCLUSION

The thermal neutron cross section for the $^{237}\text{Np}(n, \gamma)^{238}\text{Np}$ reaction at 0.0253 eV was

measured with the pure Maxwellian distribution field at the heavy water thermal neutron facility of the KUR, and the resonance integral for the same reaction was measured with the $1/E$ neutron spectrum field at the central graphite cavity of the UTR-KINKI, relative to the $^{197}\text{Au}(n, \gamma)^{198}\text{Au}$ reaction cross section for both ^{237}Np cross section measurements. For the thermal neutron cross section measurement, most of the previous experimental data are larger by 7~18% than the present data (158 ± 3 b), and the evaluated values in JENDL-3, ENDF/B-V, -VI and JEF-2 are also larger by 7~15% than the present result. The Mughabghab's evaluation is also larger by 11%. The value in JENDL-3.2 (164.6 b) is close to the present measurement. On the other hand, the evaluated resonance integrals in JENDL-3, -3.2, ENDF/B-V, -VI, JEF-2 and by Mughabghab are in good agreement with the present result (652 ± 24 b). However, some of the old measurements are larger by 24~38% than the present value.

ACKNOWLEDGMENT

The authors would like to express their sincere thanks to Prof. R. Miki of Kinki University for his useful discussions and great encouragement to carry out this work.

This study was supported by the Grant-in-Aid of Science Research from the Ministry of Education, Science and Culture (No. 03452302). A part of this work was also performed by the Visiting Research Program of the Kinki University Atomic Energy Research Institute under the support and cooperation by the Section of Kinki University Cooperation Research Use, Faculty of Engineering, Osaka University.

The authors are much indebted to the Nuclear Data Center of Japan Atomic Energy Research Institute for supplying the nuclear data of ^{237}Np . The Monte Carlo calculations were carried out with the FACOM M-Series Computers at the Data Processing Center of Kyoto University.

—REFERENCES—

- (1) MUKAIYAMA, T., *et al.*: Conceptual study of actinide burner reactors, *Proc. of 1988 Int.*

- Reactor Phys. Conf., Jackson Hole*, Vol. IV, 369.
- (2) BERWALD, D.H., DUDERSTADT, J.J.: *Nucl. Technol.*, 42, 34 (1979).
 - (3) TAKANO, H., *et al.*: Concept of actinide transmutation with intense proton accelerator, *Proc. of 6th Int. Conf. on Emerging Nuclear Energy Systems, Monterey, USA*, (1991).
 - (1) JOURNET, J., *et al.*: Minor actinides transmutation in oxide fueled fast reactors, *Proc. of Int. Conf. and Technol. Exposition on Future Nuclear System; Emerging Fuel Cycles and Waste Disposal Options*, p. 99 (1993), ANS.
 - (5) DOBBIN, K.D., *et al.*: Evaluating the efficacy of a minor actinide burner, *ibid.*, p. 131.
 - (6) BULTMAN, J.H.: Actinide breeding and burning in metallic and oxide fueled ALMR cores, *ibid.*, p. 170.
 - (7) KONING, A.J., *et al.*: Nuclear data evaluation for accelerator-based transmutation of radioactive waste, *ibid.*, p. 437.
 - (8) PRONIER, C., *et al.*: Some specific aspects of homogeneous Am and Np based fuels transmutation through the outcomes of the superfact experiment in PHENIX fast reactor, *ibid.*, p. 158.
 - (9) McLANE, V., *et al.*: "Neutron Cross Sections", Vol. 2, Neutron Cross Section Curves, (1988), Academic Press.
 - (10) YAMANAKA, A., *et al.*: *J. Nucl. Sci. Technol.*, 30(9), 863 (1993).
 - (11) HAAS, M.N.: Nuclear fuel cycle data needs, Ref. (4), p. 435.
 - (12) SCHUMAN, R.P., BERREGUI, J.R.: Resonance integral measurements, *IN-1296*, (1968).
 - (13) HELLSTRAND, E., *et al.*: Studies of the capture cross section of ^{237}Np and ^{241}Am in different reactor spectra, *BNL 50242*, (1970).
 - (14) EBERLE, S.H., *et al.*: Project actiniden, *KFK-1456*, (1971).
 - (15) WESTON, L.W., TODD, J.H.: *Nucl. Sci. Eng.*, 79, 184 (1981).
 - (16) GRYNTAKIS, E., *et al.*: "Handbook on Nuclear Activation Data", Technical Rep. Ser. No. 273, p. 199 (1987), IAEA.
 - (17) SCOVILLE, J.J., ROGERS, J.W.: Resonance integrals measured in the advanced reactivity measurement facilities, *IN-1195*, (1968).
 - (18) KANDA, K., *et al.*: *Nucl. Instrum. Methods*, 148, 535 (1978).
 - (19) KOBAYASHI, T.: Private communication, (1983).
 - (20) KOBAYASHI, K., *et al.*: *Annu. Rep. Kinki Univ., At. Energy Res. Inst.*, 25, 21 (1988).
 - (21) MIKI, R., ITOH, T., TOTAKA, M.: *ibid.*, 23, 33 (1986).
 - (22) TSUCHIHASHI, K., *et al.*: *JAERI 1285*, (1983).
 - (23) LATHROP, K.D., BRINKLEY, F.W.: *LA-4848-MS*, (1973).
 - (24) NAKAZAWA, M., SEKIGUCHI, A.: *Proc. of 2nd ASTM-Euratom Symp. on Reactor Dosimetry, NUREG/CP-0004*, Vol. 3, 1423 (1977).
 - (25) BROWNE, E., FIRESTONE, R.: "Table of Radioactive Isotopes", (1986), John Wiley & Sons, New York.
 - (26) MUGHABGHAB, S.F.: "Neutron Cross Sections", Vol. 1, Neutron Resonance Parameters and Thermal Cross Sections, Part B, (1984), Academic Press.
 - (27) HELM, F.H.: *Nucl. Sci. Eng.*, 16, 235 (1963).
 - (28) MUGHABGHAB, S.F., *et al.*: "Neutron Cross Section", Part A, (1981), Academic Press.
 - (29) SHIBATA, K., *et al.*: Japanese Evaluated Nuclear Data Library, Version-3, JENDL-3, *JAERI 1319*, (1990).
 - (30) BLONQUIST, R.N., *et al.*: *ORNL/RSIC-44*, p. 31 (1980).
 - (31) KINSEY, R. (Ed.): ENDF/B Summary Documentation, *BNL-NCS-17541*, (3rd Ed.) (ENDF/B-V), (1979).
 - (32) ROSE, R.F. (Ed.): *ibid.*, (4th Ed.) (ENDF/B-VI), (1991).
 - (33) JAERI Nuclear Data Center: JENDL-3.2, Rev. 2 of JENDL-3, Private communication, (1993).
 - (34) OECD/NEA Data Bank, (1993).
 - (35) KOBAYASHI, K., KIMURA, I., MANNHART, W.: *J. Nucl. Sci. Technol.*, 19(5), 341 (1982).

Fission Cross Section Measurements of Am-241 between 0.1 eV and 10 keV
with Lead Slowing-down Spectrometer and at Thermal Neutron Energy

Shuji Yamamoto¹, Katsuhei Kobayashi¹, Mitsuharu Miyoshi^{2*}, Itsuro Kimura²,
Ikuo Kanno², Nobuo Shinohara³, and Yoshiaki Fujita¹

1 Research Reactor Institute, Kyoto University

Kumatori-cho, Sennan-gun, Osaka 590-04, Japan

2 Department of Nuclear Engineering, Kyoto University

Yoshida-honmachi, Sakyo-ku, Kyoto 606-01, Japan

* Present address: GE and Yokogawa Medical System Inc.

4-chome, Asahigaoka, Hino-shi, Tokyo 191, Japan

3 Department of Radioisotopes, Japan Atomic Energy Research Institute

Tokai-mura, Naka-gun, Ibaraki 319-11, Japan

ABSTRACT

Making use of back-to-back type double fission chambers and a lead slowing-down spectrometer coupled to an electron linear accelerator, the cross section for the $^{241}\text{Am}(n,f)$ reaction has been measured relative to that for the $^{235}\text{U}(n,f)$ reaction in the energy region from 0.1 eV to 10 keV. To avoid the interference between the ^{241}Am and the ^{235}U resonances, the relative fission cross section below 1 keV was measured to that for the $^{10}\text{B}(n,\alpha)$ reaction with a BF_3 counter, and the result obtained was normalized to the absolute value by the ^{235}U reference data between 200 eV and 1 keV. The measured result has been compared with (1) the evaluated nuclear data appeared in ENDF/B-VI and JENDL-3.2, and (2) the existing experimental data, whose evaluated and measured data were broadened by the energy resolution function of the spectrometer.

General agreement was seen between the evaluated data and the present measurement, although some discrepancies were found in the energy region with the dip and bump cross section shapes. The JENDL-3.2 data are underestimated by 1.2 to 2.3 times between 22 and 140 eV, while the recent data by Dabbs et al. and in ENDF/B-VI are in good agreement with the measurement. Some of the previous experimental data which were measured partially in the relevant energy region are not always in agreement with the present measurement.

The fission cross section for thermal neutrons was also measured in a pure Maxwellian neutron spectrum field with the double fission chambers. The result at 0.0253 eV is 3.15 ± 0.097 b, which is obtained relative to the reference value of 586.2 b for the $^{235}\text{U}(n,f)$ reaction. The ENDF/B-VI data is in good agreement with the present measurement, while the JENDL-3.2 value is lower by 4.2 %. The ratios of the earlier experimental data to the present value are distributed between 0.89 and 1.02.

付録D

Americium-241 is one of the burdensome minor actinides which are abundantly produced in power reactors. The nuclear data for ^{241}Am are of great importance for the design of reactors with MOX or Pu fuels and for the system design of spent fuel reprocessing. In addition the fission cross section of ^{241}Am is also of interest for its transmutation from the stand point of the disposal of radioactive waste¹⁻⁵⁾.

Although the fission cross section of ^{241}Am rises around 500 keV up to about 2 barns like a threshold reaction function, ^{241}Am has fission cross sections to a certain extent in the thermal, intermediate and resonance energy regions. Then, one may not be able to take no account of fission rates occurring in thermal reactors. Up to now, although numerous measurements of the cross section for the $^{241}\text{Am}(n,f)$ reaction have been made, there still exist marked discrepancies among the measured data below 300 keV⁶⁻¹²⁾. Dabbs et al. measured the fission cross section in the wide energy range from 0.02 eV to 20 MeV by neutron time-of-flight (TOF) method. Before them, several experimental groups had partially provided the cross section in less broad energy regions. Two newly evaluated data appeared in ENDF/B-VI¹³⁾ and JENDL-3.2¹⁴⁾ are close to those obtained by Dabbs et al.⁶⁾. However, other experimental data by Leonard et al.⁷⁾, Bowman et al.⁸⁾, Gerasimov et al.⁹⁾, Seeger et al.¹⁰⁾, Derrien et al.¹¹⁾, and Gayther et al.¹²⁾ are not always in agreement with those evaluated data. Concerning the thermal neutron fission cross section of ^{241}Am , the evaluated values are in general agreement with each other¹³⁻¹⁶⁾. Most of the experimental data were obtained from 1950's to 1970's, and they were distributed between 2.8 and 3.2 b¹⁷⁻²²⁾.

The difficulty to measure the fission cross section of ^{241}Am has been often caused by strong alpha-particle activity or pileup pulses due to its short half-life of 432 years as alpha-decay. In addition, the fission cross section in the energy region from 1 to 300 keV is lower than 0.1 b. Therefore, an intense neutron source is required for the cross

section measurement, especially in the intermediate or resonance energy region, to have enough signal-to-background ratio. A lead slowing-down spectrometer is a powerful tool and is often used for this kind of fission cross section measurements because of about 10^4 increase in neutron flux comparing to the conventional TOF experiment at a 5 m flight path²³⁾, although energy resolution of the spectrometer is about 35 % at full width at half maximum (FWHM).

Another problem for fission cross section measurements of trans-uranium nuclides is often due to the lack of isotopically pure samples, though the utilization of high purity samples is one of the most important things for nuclear data measurement. Wagemans suggests the usefulness of thermal neutron experiments to check the sample quality²⁴⁾. We had an experience in obtaining the larger fission cross section of ^{241}Am with the sample on the market²⁵⁾. Through the careful and steady investigation of the ^{241}Am sample by the alpha-ray spectrometry, we found that the problem was mainly caused by the plutonium impurities in the sample²⁶⁾.

In the present measurement, we have prepared a pure ^{241}Am sample by anion-exchange method to remove impurities of trans-uranium nuclides. The chemical solution of the sample was electrolyzed and the ^{241}Am layer was deposited on a stainless steel disk, which was put into back-to-back (BTB) type fission chambers²⁷⁾ together with that of ^{235}U . The fission cross section for the $^{241}\text{Am}(n,f)$ reaction was measured at energies between 0.1 eV and 10 keV relative to that for the $^{235}\text{U}(n,f)$ reaction by making use of the double fission chambers and the lead slowing-down spectrometer coupled to 46 MeV electron linear accelerator (linac) of Research Reactor Institute, Kyoto University (KURRI)²⁸⁾. In order to avoid the interference between the ^{241}Am and ^{235}U resonances, the relative fission cross section was measured to that for the $^{10}\text{B}(n,\alpha)$ reaction using a BF_3 counter below 1 keV, and the result was normalized to that measured with the BTB chambers at energies between 200 eV and 1 keV. The experimental technique is almost the same as that of the previous measurement of fission cross section for ^{237}Np ²⁹⁾. The

present measurement is compared with the evaluated data in ENDF/B-VI and JENDL-3.2, and with the existing experimental data.

The thermal neutron cross section for the $^{241}\text{Am}(n,f)$ reaction was also measured with the above fission chambers at a standard neutron spectrum field of pure Maxwellian distribution of the Kyoto University Reactor (KUR) at KURRI³⁰⁾. The result is compared with the evaluated and the previous experimental data.

II. Experimental Method

2.1. Lead Slowing-down Spectrometer

The lead slowing-down spectrometer was installed coupling to the 46 MeV electron linac at KURRI. This Kyoto University Lead Slowing-down Spectrometer (KULS) is composed of 1600 pieces of lead blocks (each size : $10 \times 20 \times 20 \text{ cm}^3$, and purity : 99.9 %) and these are piled up to make a cube of $1.5 \times 1.5 \times 1.5 \text{ m}^3$ (about 40 tons) without any structural materials²⁸⁾. The KULS is covered with Cd sheets of 0.5 mm in thickness. At the center of the KULS, we have set an air-cooled photoneutron target of Ta to produce pulsed fast neutrons. Four sets of thermocouples were attached on the surface of the photoneutron target case to monitor the temperature. The linac was operated to keep the temperature less than 300 °C. The KULS has eight experimental/irradiation holes ($10 \times 10 \text{ cm}^2$, 55 or 45 cm in depth), and one of the holes is covered by bismuth layers of 10 to 15 cm in thickness to shield high energy gamma-rays (6 to 7 MeV) produced by the $\text{Pb}(n,\gamma)$ reaction in the spectrometer²⁸⁾. The cross sectional view of the KULS is shown in Fig. 1.

Characteristic behavior of neutrons in the KULS was studied by calculations with the continuous energy Monte Carlo code MCNP³¹⁾ and by experiments with resonance filter method²⁸⁾. There exists the relation of $E = K/t^2$ in the neutron slowing-down time t in μs

and the energy E in keV, where K is slowing-down constant^{32,33)}. The neutron slowing-down time and the energy resolution of the KULS were measured with a BF_3 counter (12 mm in diameter, 50 mm in length, 1 atm.) and an Ar gas counter (12.7 mm in diameter, 63.5 mm in length, 1 atm.) which were covered with and without resonance filters of In, Te, Ta, Au, Cd, Mo, and Mn. In order to calibrate the neutron slowing-down time and the energy, the BF_3 counter was used for the neutron transmission measurement with the filters and the Ar gas counter was applied to the capture gamma-ray measurement with the filters. The dips or the bumps which were observed in the slowing-down time spectrum corresponded to their resonance energies of the filter. It was found that the slowing-down constant K in the relation of $E=K/t^2$ was determined to be 190 ± 2 and 156 ± 2 ($\text{keV } \mu\text{s}^2$) for the bismuth and the lead experimental holes, respectively²⁸⁾. The energy resolution was around 40 % for both experimental holes at energies from a few eV to about 500 eV and was larger in the lower and the higher energy regions²⁸⁾. The relation between neutron slowing-down time and energy and the energy resolution were also obtained by the MCNP calculations and the results were in good agreement with those measured by the BF_3 and the Ar gas counters. More detailed characteristics of the KULS are given in other literatures^{28,29)}

2.2. ^{241}Am and ^{235}U Samples

Americium solution obtained from IAEA was purified at Isotope Products Laboratory, Japan Atomic Energy Research Institute by the anion-exchange method using nitric acid-methyl alcohol mixed media³⁴⁾, in order to remove uranium, neptunium, plutonium and curium from the americium sample. The purified americium solution and isopropyl alcohol were mixed thoroughly and electrolyzed on a stainless steel disk (28 mm in diameter and 0.2 mm in thickness) for preparing an americium deposit (radioactive area of 20 mm in diameter)³⁵⁾. After electrodeposition, the sample was sintered with a gas burner to fix the americium layer on the disk by making americium oxide.

The alpha-rays from the deposit were measured with a silicon surface barrier detector. Impurities of ^{237}Np , $^{238-240}\text{Pu}$, ^{243}Am and ^{242}Cm on the americium deposit were not observed in the measured alpha-ray spectrum. Therefore, the isotopic composition of ^{241}Am for the deposit was estimated to be greater than 99.9 %. The number of the ^{241}Am atoms was determined by analyzing the alpha-rays with 5.322 to 5.544 MeV. The 59.5 keV gamma-ray from ^{241}Am was also measured with a HPGe detector. The number of ^{241}Am atom was determined by both detectors and the result was $(1.734 \pm 0.020) \times 10^{16}$, as given in Table 1, where the errors were estimated by taking account of (i) statistics of the activity measurements, (ii) geometrical detection efficiencies and (iii) uncertainties of the decay data used.

The deposit of highly enriched uranium oxide (99.91 % of ^{235}U) purchased from ORNL was prepared as almost the same technique as the americium sample and was electrodeposited on the stainless steel disk at KURRI. This ^{235}U sample was used to monitor the neutron flux in this study as a well-known reference cross section of the $^{235}\text{U}(n,f)$ reaction. Alpha-ray and gamma-ray spectrometries were carried out to determine the number of the uranium atom as well as the americium sample. By the analyses of the alpha-rays with 4.152 to 4.597 MeV and the 185.7 keV gamma-ray from ^{235}U , the number of ^{235}U atoms was determined to be $(3.283 \pm 0.036) \times 10^{17}$, as shown in Table 1.

Uniformity of the electrodeposited layer was investigated by using a solid state track detector of CR-39³⁶⁾. The exposure times for measuring the tracks from ^{241}Am and ^{235}U were a few seconds and two hours, respectively, under the condition that the distance between the layer and the track detector was 0.5 mm. After etching the exposed plastics with KOH solution, the detector surface was examined with a microscope, and the number of the etched pits was counted in every area of $3 \times 3 \text{ mm}^2$. The number of pits per the unit area were between about 25 and 40 for ^{241}Am and between about 60 and 75 for ^{235}U except at the edge of the radioactive region of the deposit. Considering the layer thickness of $2.5 \mu\text{g}/\text{cm}^2$ for the ^{241}Am and $41 \mu\text{g}/\text{cm}^2$ for the ^{235}U deposits, most of the

fission fragments can easily pass through the layers, so that the non-uniformity in the present deposits could not disturb the fission cross section measurement.

2.3. Fission Chambers

The fission chambers which are employed in the present experiment are composed of two identical parallel plate-type ionization chambers, as shown in Fig. 2. These chambers were originally designed for the incore fission ratio measurements²⁷⁾. Since the back sides of the Am deposit on the stainless steel plate and of the reference one are faced each other, it is called back-to-back (BTB) type. The double fission chambers were made of aluminum and filled with a mixed gas of 97 % Ar and 3 % N_2 at the pressure of 1 atm. In this gas pressure, the mean range of alpha particles reaches 36 mm, while that of fission fragments is about 20 mm. Therefore, the fission chambers were designed so as to collect most of the whole energy of fission fragments, although the chambers could not collect that of alpha particles, in order to get good discrimination between the alpha and the fission fragment pulses. The distance between the electrode and the deposit layer was designed to be 8 mm. The operation voltage was 400 volts. Figure 3 shows a typical pulse height distribution of fission fragments by five hours' measurement for the Am layer. Since we used the thin ^{241}Am and the thin ^{235}U deposits, fission pulses were clearly discriminated from background ones caused by the alpha-rays.

2.4. BF_3 Counter

The $^{10}\text{B}(n,\alpha)$ reaction is well known to be one of the standard cross sections and is often applied to cross section measurements as a reference. The BF_3 counter, which was purchased from Mitsubishi Electric Co., Ltd., was used for the fission cross section measurement of ^{241}Am in the resonance interference energy region of ^{241}Am and ^{235}U fission cross sections. The counter was a cylindrical type, 50 mm in effective length, 12 mm in diameter and 1 atm. and its high voltage bias was 1100 V. Instead of the fission

chamber of ^{235}U in the BTB chambers, the BF_3 counter was employed to measure the energy dependence of the neutron flux spectrum in the resonance energy region of the $^{235}\text{U}(\text{n},\text{f})$ cross section.

2.5. Fission Ratio Measurement

The fission cross section of ^{241}Am has been measured as ratio to that of ^{235}U by making use of the BTB chambers in the bismuth hole. As both of ^{241}Am and ^{235}U nuclei have neutron resonances in the relevant energy region, the fission ratio data may be interfered with each other. Then, we have employed not only the BTB chambers but also the BF_3 counter which is well known as a good $1/v$ detector for the present measurement. The relative fission cross section of ^{241}Am was measured below 1 keV with the BF_3 counter and the result was normalized to the fission cross section between 200 eV and 1 keV measured by the $^{235}\text{U}(\text{n},\text{f})$ reaction using the BTB chambers.

The lead slowing-down spectrometer KULS was driven by the 46 MeV electron linac at KURRI, and the typical operating conditions during the experiments were as follows: pulse repetition rate of 150 Hz, pulse width of 22 ns, electron peak current of about 0.8 A, and the energy of about 31 MeV. After the linac was operated for more than 120 hours, the deposited plates of ^{241}Am and ^{235}U in the BTB chambers were exchanged each other, and another measurement was made for about 130 hours in the bismuth hole. After the chambers were inserted into the bismuth hole, the hole space was filled with bismuth bricks not to let neutron leak.

2.6. Electronics and Data Taking

Two identical electronic circuits were employed for both fission chambers, as seen in Fig. 4. Through the amplifiers and the discriminators, signals from the fission chambers were fed into a time digitizer, which was initiated by the linac electron burst, and the slowing-down time data of neutrons were stored every about 5 hour measurement in a

data acquisition system, Canberra's Series-88 MPA analyzer. Two sets of 4096 channels were allotted to the slowing-down time measurements for the BTB chambers with 62.5 ns/channel to 0.5 μs /channel. Pulse height distributions of fission events from the ^{241}Am and the ^{235}U deposits were also measured with each 4096 channel analyzer in parallel with the slowing-down time measurements.

For the measurement of relative fission cross section of ^{241}Am , output signals from the BF_3 counter were also led to the time digitizer through the amplifiers and the discriminators. The data of the slowing-down time of neutrons were stored as the same as the BTB chambers.

III. Fission Cross Section Measurement

3.1. Fission Cross Section

The fission counts at the slowing-down time t (in μs) can be converted to those at energy E (in keV) by using the relation of $E = 190/(t + t_0)^2$, where, t_0 is a constant for zero time correction²⁸⁾. From the fission counts of the ^{241}Am and the ^{235}U deposits, the energy dependent cross section for the $^{241}\text{Am}(\text{n},\text{f})$ reaction is obtained by

$$\sigma_{\text{Am}}(E) = \frac{C_{\text{Am}}(E)}{C_{\text{U}}(E)} \frac{N_{\text{U}}}{N_{\text{Am}}} \sigma_{\text{U}}(E)$$

where, $C_{\text{Am}}(E)$: fission counts of ^{241}Am at energy E ,

$C_{\text{U}}(E)$: fission counts of ^{235}U at energy E ,

N_{U} : number of ^{235}U atoms in the ^{235}U deposit,

N_{Am} : number of ^{241}Am atoms in the ^{241}Am deposit,

$\sigma_{\text{U}}(E)$: energy dependent fission cross section of ^{235}U .

We cited the numerical values of $\sigma_{\text{U}}(E)$ from ENDF/B-VI¹³⁾, whose accuracy of the fission cross section value was estimated as seen in Table 2. The reference data were

broadened by the energy resolution function which was fitted to the previous measurements in the relevant energy region²⁸⁾, although the original fission cross section in ENDF/B-VI had sharp resonances at energies from eV to keV. Below 200 eV, since neutron resonances are found in the fission cross sections of ^{241}Am and ^{235}U , we have employed the $^{10}\text{B}(n,\alpha)$ reaction which shows smooth and good $1/v$ energy dependence in the relevant energy region, instead of the $^{235}\text{U}(n,f)$ reaction. In the relative cross section measurement with the BF_3 counter, $C_U(E)$ and $\sigma_U(E)$ in the above relation can be interpreted to be the counts and the cross section for the $^{10}\text{B}(n,\alpha)$ reaction. The ratio of N_U/N_{Am} can be thought to be a constant in this case. For the data processing, we have made programs written in Fortran language for the personal computer.

Systematic difference between the ^{241}Am and the ^{235}U deposit positions in the BTB chambers was experimentally investigated by exchanging the positions each other. Before and after the both deposits were exchanged, the measured ratio for $C_{\text{Am}}(E)/C_U(E)$ was about 1.06 ± 0.05 , which was almost independent of neutron energy. For the derivation of the fission cross section, we took the average value for the $C_{\text{Am}}(E)/C_U(E)$ ratios obtained by exchanging the positions for the ^{241}Am and the ^{235}U deposits.

3.2. Backgrounds

As the pulse height of fission events is bigger in principle, it may be easy to distinguish fission pulses from noise pulses or alpha-pulses of the sample deposit. Since the radioactivity of the ^{241}Am deposit was about 8.8×10^5 Bq, pile up problem of the alpha pulses might be also negligible. Background counts due to the overlap neutrons from the previous pulses of the linac may be negligible because of low pulse repetition rate of 150 Hz and of low thermal neutron flux in the KULS²⁸⁾. The background due to the fission events has to be taken into account in the data analysis. Since the BTB chambers were put into the bismuth hole, background counts due to the photofission of ^{235}U and ^{241}Am by the $\text{Pb}(n,\gamma)$ reaction in the KULS could be reduced.

Background run was carried out by making use of the BTB chambers without sample deposit. Very limited number of counts in total were observed in the slowing-down time spectrum for more than thirty hours' run. It was found that the background counts for the ^{241}Am chamber might affect the minimum cross section region for the $^{241}\text{Am}(n,f)$ reaction by 0.2 to 0.4 % in average at most, although the background counts for the ^{235}U chamber could be negligible comparing to the foreground counts.

Neutrons may be scattered by structural materials of the BTB chambers before arriving at the deposit layers. The inscattered neutrons, which are not directly observable, may cause another background for the present measurement. In order to investigate the inscattered background, we have made calculations using a continuous energy Monte Carlo code, MCNP³¹⁾. The BTB chambers are made of aluminum and the size is 40 mm in diameter, 39 mm in length and about 2 mm in thickness for the chambers' case, as seen in Fig. 2. The electrodes, deposit layers, backing plates and their supports by which neutrons may be scattered are set inside of the chambers. Calculation geometry for the MCNP code was referred to dimension as the chambers were, and it was assumed that the neutrons entered the chambers almost isotropically from the surrounding. The energy dependent reaction ratio data for ^{241}Am to ^{235}U were calculated with 5,000,000 random histories to see how the measured cross section was affected by the inscattered neutrons. The present calculations have shown that very small correction may be required to make the $^{241}\text{Am}(n,f)$ cross section lower by 2-6 % at most in the energy region from 1 eV to 10 eV and to make it larger by about 7 % at most at energies between 0.3 and 0.8 eV, even if taking account of the calculation uncertainties. Other small corrections were also made around 100 eV.

IV. Measurement of Thermal Neutron Cross Section

4.1. Thermal Neutron Spectrum Field

The Kyoto University Reactor (KUR) at KURRI has a thermal neutron facility with a heavy water tank of 1.4 m in length^{30,37}. The irradiation room is about 2.4 x 2.4 x 2.4 m³ and is surrounded by 90 cm thick heavy concrete shields. The leakage neutrons from the heavy water tank can be used as a thermal neutron source of plane-type in a large space.

Kanda et al. measured the neutron spectrum from the heavy water tank by the time-of-flight technique using a fast chopper³⁷. The obtained spectrum showed good agreement with a Maxwellian distribution having neutron temperature of 60°C. The Cd-ratio measured by Au foils with and without Cd-cover of 0.7 mm in thickness was more than 5,000 and epi-thermal neutrons could be negligible³⁷.

4.2. Experimental Methods

The heavy water thermal neutron facility has been employed for the measurement of the thermal neutron cross section for the ²⁴¹Am(n,f) reaction, making use of the BTB type double fission chambers. The chambers were set in the irradiation room and exposed to thermal neutrons for about 10 hours during the nominal power operation of 5 MW of the KUR. The irradiation was repeated by exchanging the ²⁴¹Am and the ²³⁵U sample positions. Fission pulses from the samples were led to their 2048 channel pulse height analyzers through the amplifiers and the discriminators. Each of the fission counts was obtained by integrating the pulse height distribution above the discrimination level.

4.3. Measurement of Cross Section

The thermal neutron cross section σ_{th} averaged over the Maxwellian distribution spectrum is defined as

$$\sigma_{th} = \frac{\sigma_{th}(v_0)}{1.128} g(T_n) \sqrt{\frac{T_0}{T_n}}$$

where $v_0=2,200$ m/s, $T_0=293.6$ K, T_n is the neutron temperature, and $g(T_n)$ the g-factor.

The thermal neutron cross section σ_{Am} for the ²⁴¹Am(n,f) reaction at a neutron energy of 0.0253 eV (corresponding to a velocity of 2,200 m/s) is obtained almost same as the case for the KULS, by rewriting the relations as follows:

$$\sigma_{Am} = \frac{C_{Am}}{C_U} \frac{N_U}{N_{Am}} \frac{g_U(T_n)}{g_{Am}(T_0)} \sigma_U$$

where, C_{Am} : fission counts of ²⁴¹Am,

C_U : fission counts of ²³⁵U,

$g_U(T_n)$: g-factor of ²³⁵U,

$g_{Am}(T_0)$: g-factor of ²⁴¹Am,

σ_U : fission cross section at 0.0253 eV of ²³⁵U.

The reference fission cross section was taken from the evaluated data file of ENDF/B-VI, and the g-factors for ²⁴¹Am(0.996) and ²³⁵U(0.9761 ± 0.0012) were referred to the literature¹⁶, although Gryntakis³⁸ gave 1.0220 and 0.9665 values, respectively. The ratio of C_{Am}/C_U data obtained by exchanging the deposit positions of ²⁴¹Am and ²³⁵U in the BTB chambers was 1.04 ± 0.03. We took an average of the values before and after the deposits were exchanged to derive the fission cross section.

V. Results and Discussion

Making use of the BTB chambers and the KULS, the cross section for the ²⁴¹Am(n,f) reaction was measured relative to that for the ²³⁵U(n,f) reaction at energies from 0.1 eV to 10 keV. In the resonance energy region for ²⁴¹Am and ²³⁵U below 1 keV, the relative fission cross section of ²⁴¹Am was measured to that for the ¹⁰B(n,α) reaction and was normalized to the absolute value between 200 eV and 1 keV obtained by the ²³⁵U(n,f) reaction, to avoid the resonance interference between ²⁴¹Am and ²³⁵U. The present result from 0.1 eV to 10 keV is shown in Fig. 5, and is compared with the ENDF/B-VI and the

JENDL-3.2 data, which are broadened by the energy resolution function of the KULS.

Dead time correction for the ^{235}U fission chamber was less than 0.03 % and that for the ^{241}Am was negligibly small. Concerning the effects of (1) loss of the fission fragments in the ^{241}Am and the ^{235}U deposits, (2) anisotropic angular distribution of the fission fragments, and (3) photofission in the deposits on the resultant fission cross section of ^{241}Am , we have assumed that they may be negligible as mentioned before²⁹⁾. Since the pure ^{241}Am sample was carefully prepared and the impurity was not observed, we could take no account of the impurity effect in the fission cross section measurement.

The cross section data were obtained by summing up the slowing-down time data to give about 0.115 lethargy width. The experimental uncertainties for the present measurement are summarized in Table 2. The discrimination level was set in the minimum count region between the fission and the noise counts in the pulse height distribution. Uncertainty to determine the fission counts was estimated to be 1.9 % for ^{241}Am and 0.65 % for ^{235}U , respectively. Considering the gain shift in the detection system, the discrimination level was checked and determined every 10 to 20 hours during the experiment. The number of atoms in the ^{241}Am and the ^{235}U deposits were derived from the mean average by the alpha- and gamma-ray measurements. The gamma-ray measurement supported the result by the alpha-ray measurement within the experimental uncertainty, as seen in Table 1. Uncertainties for the reference cross sections of the $^{235}\text{U}(n,f)$ and the $^{10}\text{B}(n,\alpha)$ reactions^{13,39)} were estimated to be 2 to 4 % and 2 % in the relevant energy region, respectively.

Good agreement can be seen in general shape and absolute values, as seen in Fig. 5, between the present measurement and the evaluated data in ENDF/B-VI and JENDL-3.2, and both of the evaluated data show good agreement with each other, except at energies from about 22 eV to about 140 eV. Some discrepancies can be seen between the evaluated data and the measurement in the dip and the bump cross section region. The both evaluated data in the energy range of 2 to 4 eV are lower by about 30 %.

Comparing the evaluated values with the present measurement, the JENDL-3.2 data between 22 and 140 eV are underestimated by 1.2 to 2.3 times, while the ENDF/B-VI data are in good agreement with the measurement.

The existing experimental data have been also broadened by the energy resolution function of the KULS, and compared with the present data in Fig. 6. The data measured by Dabbs et al., whose result is mainly referred to the evaluation for the ENDF/B-VI file, are in general agreement with the present values. The fission cross sections obtained by Gayther et al. are higher above 55 eV by 50 to 100 % than the present measurement. The data by Bowman et al., Gerasimov et al., and Derrien et al. are close to the present cross section below several tens of eV, although Bowman et al. gave two times higher data above 200 eV. Leonard et al. gave higher values between 2 and 5 eV. Seeger et al. measured the cross section with a nuclear explosion technique and obtained much higher values than the present data above 20 eV.

In Table 3, comparisons are performed for mean values of the ^{241}Am fission cross section from the present work with results from ENDF/B-VI, JENDL-3.2 and the data by Dabbs et al. As seen in the table, the agreement between the present measurement and the ENDF/B-VI data are good in general. The JENDL-3.2 data shows good agreement with the measurement except for the 20 to 200 eV region. The data by Dabbs et al. seem to be higher a little than the two evaluated data and the present values, especially in the lower energy region. The present result above 1 keV is higher by about 5 % than the evaluations and the Dabbs' data.

The cross section of $^{241}\text{Am}(n,f)$ reaction for 2,200 m/s neutrons was obtained relative to the reference value of 586.2 b appeared in ENDF/B-VI. The present result at 0.0253 eV is 3.15 ± 0.097 b, which is close to the extrapolated value of the KULS data as seen in Fig. 5. Fission counts were determined by linearly extrapolating the pulse height distribution curve near the discrimination level. Main sources of the uncertainties in the present measurement are due to the statistical error (0.04 to 0.4 %), assignment of C_{Am}

and C_U by integrating the pulse height spectrum above the discrimination level (estimated to be about 1.5 % for C_{Am} and 1.1 % for C_U , respectively), the g-factors for ^{241}Am and ^{235}U , the reference cross section for the $^{235}U(n,f)$ reaction (estimated to be less than 1 %)^{13,16)}, the number of atoms in the deposit samples as seen in Table 1, and the correction assigned for the setting position of ^{241}Am and ^{235}U deposits in the BTB chambers (0.25 %). We have estimated that the uncertainty of the g-factor for ^{241}Am is ± 1.3 %, because we could see such a difference between the g-factors by Mughabghab¹⁶⁾ and Gryntakis³⁸⁾, while the g-factor for ^{235}U is well determined¹⁶⁾. Some other uncertainties and corrections may be small and be negligible as those in the above KULS experiment. The total experimental uncertainty of the thermal neutron cross section for the $^{241}Am(n,f)$ reaction was derived to be about 3.1 % as the root of square sum of the above uncertainties.

The measured result is given in Table 4, and is compared with earlier evaluated and experimental data. The evaluated value in ENDF/B-VI is in good agreement with the present result, and the JEF-2.2 and the Mughabghab's data are also close to the measurement. The data appeared in JENDL-3.2 and measured by Dabbs et al. are lower by 4.2 % and 2.9 %, respectively. Although the average value of other six earlier experimental data is in agreement with the present measurement within the uncertainty, the data by Gavrilov et al. seems to be lower by 11 % than the present data.

Since we carefully prepared the ^{241}Am sample and used the pure sample, the measured cross section may not be disturbed by the undesirable reactions due to the impurities. This would be implied by the fact that the present measurement of the thermal neutron cross section for the $^{241}Am(n,f)$ reaction is in good agreement with most of the recent evaluated values at 0.0253 eV, as mentioned above. The present result may also reveal that the KULS data with the ^{241}Am sample are not affected by the impurities in the sample.

VI. Conclusion

The cross section for the $^{241}Am(n,f)$ reaction has been measured from 0.1 eV to 10 keV relative to that for the $^{235}U(n,f)$ reaction, making use of the BTB type double fission chambers and a lead slowing-down spectrometer coupled to the KURRI electron linac. The present measurement shows good agreement with the ENDF/B-VI data and the data measured by Dabbs et al. The JENDL-3.2 data are also in general agreement with the measurement, although the evaluated values are underestimated by 1.2 to 2.3 times between 22 and 140 eV. These evaluated and measured data were broadened by the energy resolution function of the spectrometer, KULS. Some of the previous experimental data which were measured partially in the relevant energy region are not always in agreement with the present measurement.

Thermal neutron cross section for the $^{241}Am(n,f)$ reaction at 0.0253 eV was obtained to be 3.15 ± 0.097 b, which was measured with the pure Maxwellian distribution field by the BTB chambers. Good agreement can be seen between the present measurement and the values evaluated in ENDF/B-VI, JEF-2.2 and by Mughabghab. The JENDL-3.2 and the Dabbs' data are lower by 4.2 % and 2.9 % respectively than the present value. Most of the experimental data, which were measured from 1950's to 1970's, are close to that of the present result, although the data by Gavrilov, et al. seems to be lower by about 11 %.

Acknowledgement

The authors would like to express their sincere thanks to Prof. M. Nakazawa of University of Tokyo for the reconstruction of the lead slowing-down spectrometer for this

work. They are grateful to Prof. T. Tsuruta of Atomic Energy Research Institute, Kinki University for his kind guidance how to make uniformity measurements of the electrodeposited layers using solid state track detectors. They are also indebted to Dr. T. Nakagawa of Nuclear Data Center, Japan Atomic Energy Research Institute for supplying nuclear data. Technical assistance by H. Yamamoto and A. Kohashi of Kyoto University is appreciated.

This study was supported by the Grant-in-Aid of Scientific Research from the Ministry of Education, Science and Culture (No.06452430 and No.06302081) and by the Cooperative Use Program of KURRI.

References:

1. D. Lancaster, "Actinide Burning in a Standard Pressurized Water Reactor", Proc. of the Int'l Conf. and Technol. Exposition on Future Nucl. Systems: Global '93", Sept. 12-17, 1993, p.609, ANS, La Grange Park, Illinois, 1993.
2. J. Tommasi, et al., "Long-Lived Waste Transmutation in Reactor", *ibid.*, p.1252, ANS, La Grange Park, Illinois, 1993.
3. T. Wakabayashi, et al., "Feasibility Studies of an Optimized Fast Reactor Core for MA and FP Transmutation", Proc. of the Int'l Conf. on Evaluation of Emerging Nuclear Fuel Cycle Systems: Global '95", Sept. 11-14, 1995, p.800, CEA, 1995.
4. J. L. Kloosterman and J. M. Li, "Transmutation of Americium in Fission Reactors", Proc. of the Int'l Conf. on Evaluation of Emerging Nuclear Fuel Cycle Systems: Global '95", Sept. 11-14, 1995, p.800, CEA, 1995.
5. T. Mukaiyama, et al., "Research and Developments of Transmutation of High Level Radioactive Waste", J. At. Energy Soc. Japan, H. Sekimoto and T. Ohsawa(Ed.), Vol.37, No.3, p.159 (1995).

6. J. W. T. Dabbs, et al., Nucl. Sci. Eng., 83, 22 (1983).
7. B. R. Leonard Jr., et al., Bull. of the Am. Phys. Soc., 4, 31 (1959).
8. C. D. Bowman, et al., Phys. Rev., 137, B326 (1965).
9. V. F. Gerasimov, Yaderno-Fizicheskie Issledovaniya, 2, 16 (1966).
10. P. A. Seeger, et al., Nucl. Phys., A96, 605 (1967).
11. H. Derrien, et al., Proc. of the Int'l Conf. on Nucl. Cross Sections Technol., Washington D.C., 2, 637 (1975).
12. D. B. Gayther and B. W. Thomas, "Measurement of the Neutron Capture and Fission Cross-Sections of ^{241}Am ", Proc. of the 4-th All-Union Conf. on Neutron Phys., Kiev, Part 3, p.3 (1977).
13. R. F. Rose(Compiled and Edited), "ENDF-201, ENDF/B-VI Summary Documentation", BNL-NCS-17541, 4th Ed. (ENDF/B-VI) 1991.13.
14. T. Nakagawa, et al., J. Nucl. Sci. Technol., Vol.32, No.12, 1259 (1995), and "Evaluation of Nuclear Data for Americium Isotopes", JAERI-M, 89-008 (1989).
15. C. Nordborg and M. Salvatores, "Status of the JEF Evaluated Data Library", Proc. of International Conf. on Nucl. Data for Sci. and Technol., Gatlinburg, USA, 1994, ORNL, Vol.2, p.680 (1994).
16. S. F. Mughabghab, "Neutron Cross Sections", Vol.1, Neutron Resonance Parameters and Thermal Cross Sections, Part B:Z=61-100, Academic Press. Inc., New York (1984).
17. G. C. Hanna, et al., Phys. Rev., 81, 893 (1951).
18. B. B. Cunningham and A. Ghiorso, Phys. Rev., 82, 558 (1951).
19. E. K. Hulet, et al., Phys. Rev., 107, 1294 (1957).
20. M. A. Bak, et al., Atomnaya Energiya, 23, 316 (1967).
21. V. D. Gavrilov, et al., Atomnaya Energiya, 41, 85 (1975).
22. K. D. Zhuravlev, et al., Atomnaya Energiya, Vol.39, No.4, 285 (1975).
23. R. E. Slovacek, et al., Nucl. Sci. Eng., 62, 455 (1977).

24. C. Wagemans, Nucl. Instr. Methods in Phys. Res., A236, 429 (1985).
25. K. Kobayashi, et al., "Fission Cross Section Measurement of Am-241 between 0.1 eV and 10 keV with Lead Slowing-down Spectrometer", Gatlinburg, Tenn., May 1994, J. K. Dickens(Ed.), ORNL, Vol.1, p.242 (1994).
26. M. Miyoshi, "Measurement of Neutron Energy Dependent Fission Cross Section of ^{241}Am ", Master Thesis in Japanese, Department of Nuclear Engineering, Kyoto University, 1995.
27. M. Obu, "Preparation and Characteristics of Fission Chambers with Actinide Nuclides", JAERI-M 9757 (1981).
28. K. Kobayashi, S. Yamamoto, A. Yamanaka, et al., "Characteristics of the Kyoto University Lead Slowing-down Spectrometer Coupled to an Electron Linac", submitted to Nucl. Instr. Methods in Phys. Res.
29. A. Yamanaka, et al., J. Nucl. Sci. Technol., Vol.30, No.9, 863 (1993).
30. K. Kobayashi, et al., J. Nucl. Sci. Technol., Vol.31, No.12, 1239 (1994).
31. "MCNP - A General Monte Carlo Code for Neutron and Photon Transport, Version 3A", LA-7396-M, Rev.2, Los Alamos National Laboratory (1986).
32. A. Bergman, et al., proc. of the 1st Int'l Conf. on Peaceful Users for Atomic Energy, United Nations, p/642, Vol.4, 135 (1955).
33. K. H. Beckurts and K. Wirtz, "Neutron Physics", Springer-Verlag, New York, p.342 (1964).
34. S. Usuda and N. Kohno, Separation Science and Technology, 23, 1119 (1988).
35. N. Shinohara and N. Kohno, Appl. Radiat. Isot., 40, 41 (1989).
36. T. Tsuruta, et al., J. Nucl. Sci. Technol., Vol.29, No.11, 1108 (1992).
37. K. Kanda, et al., Nucl. Instrum. Methods, 148, 535 (1978).
38. E. M. Gryntakis, et al., Radiochimica Acta, 22, 128 (1975).
39. "Nuclear Data Standards for Nuclear Measurements", Technical Reports Series No.227, IAEA, Vienna (1983).

Table 1 Determination of number of atoms for the ^{241}Am and ^{235}U oxide deposits.

Method	^{241}Am deposit	^{235}U deposit
α -spectroscopy	$(1.722 \pm 0.022) \times 10^{16}$	$(3.289 \pm 0.039) \times 10^{17}$
γ -spectroscopy	$(1.796 \pm 0.053) \times 10^{16}$	$(3.253 \pm 0.094) \times 10^{17}$
Weighted mean value	$(1.734 \pm 0.020) \times 10^{16}$	$(3.283 \pm 0.036) \times 10^{17}$

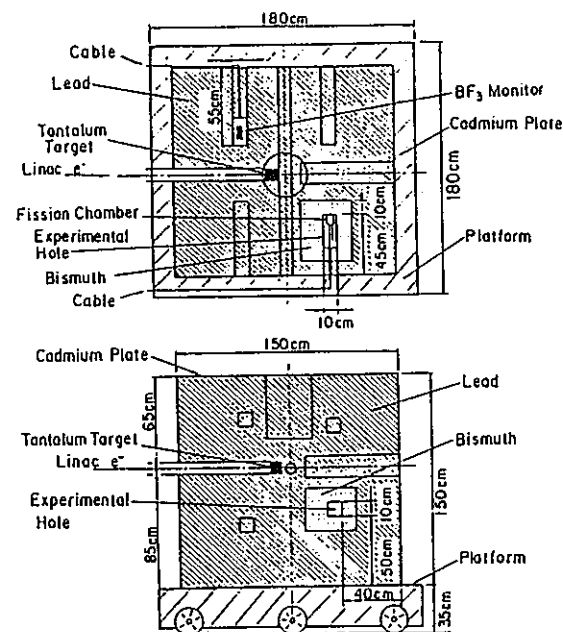


Fig. 1 Cross sectional view of the Kyoto University Lead Slowing-down Spectrometer, KULS.

Table 2 Experimental uncertainties for the present measurement.

Uncertainties due to	Error in %
Statistical error for ^{241}Am for ^{235}U	0.08 – 6.2 0.06 – 1.1
Assignment of fission counts for ^{241}Am for ^{235}U	< 1.9 < 0.65
Number of atoms for ^{241}Am for ^{235}U	1.3 1.2
Reference cross section for the $^{235}\text{U}(n,f)$ reaction	2 – 4
Reference cross section for the $^{10}\text{B}(n,\alpha)$ reaction	2
Correction for setting position of ^{241}Am and ^{235}U deposits in the BTB chambers	0.3
Correction to in-scattered neutrons by the chambers	0.2
Correction to background subtraction	< 0.2 – 0.4

Table 3 Comparison of mean values of the ^{241}Am fission cross section from the present work with those from ENDF/B-VI, JENDL-3.2 and the data by Dabbs et al.

Energy range (eV)	ENDF/B-VI	JENDL-3.2	Dabbs et al.	Present
0.1 – 0.89	4.753+0*	4.724+0	5.133+0	4.897+0
0.89 – 3.55	2.046+0	1.853+0	2.182+0	1.914+0
3.55 – 20.0	7.982-1	7.106-1	8.438-1	7.636-1
20.0 – 200	2.558-1	1.893-1	2.524-1	2.514-1
200 – 1000	9.701-2	9.708-2	10.224-2	10.965-2
1000 – 10000	3.031-2	3.009-2	3.110-2	3.570-2

* read as $4.753 \times 10^{+0}$ Table 4 Thermal neutron cross section (2,200 m/s value) for $^{241}\text{Am}(n,f)$ reaction.

Cross Section (b)	Reference	
3.15 ± 0.097	Present	
3.153	ENDF/B-VI('91)	Ref(13)
3.019	JENDL-3.2('95)	Ref(14)
3.177	JEF-2.2('94)	Ref(15)
3.20 ± 0.09	Mughabghab('84)	Ref(16)
3.06 ± 0.19	Dabbs('83)	Ref(6)
3.0	Hanna('51)	Ref(17)
3.0 ± 0.2	Cunningham('51)	Ref(18)
3.13 ± 0.15	Hulet('57)	Ref(19)
3.15 ± 0.10	Bak('67)	Ref(20)
2.8 ± 0.25	Gavrilov('75)	Ref(21)
3.2 ± 0.15	Zhuravlev('75)	Ref(22)

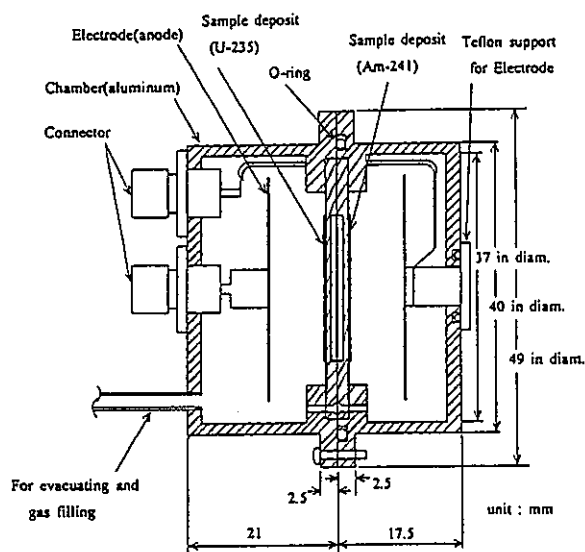


Fig. 2 Cross sectional view of the BTB chambers.

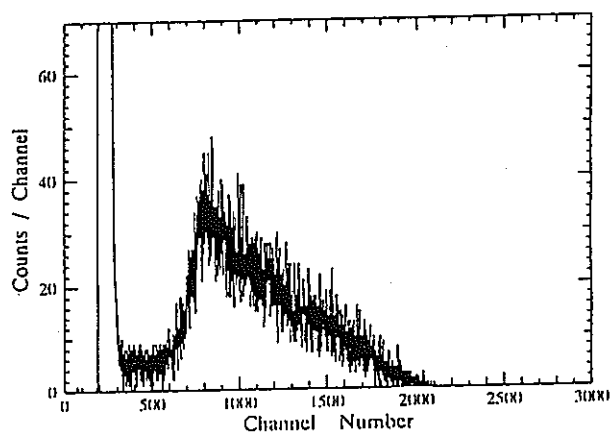


Fig. 3 Pulse height distribution of fission fragments for ^{241}Am with the BTB chambers.

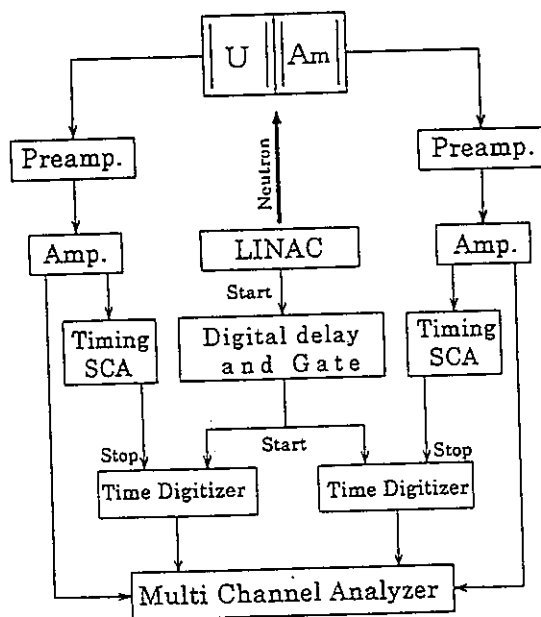


Fig. 4 Block diagram of electronic circuits to measure time dependent fission counts with the BTB chambers.

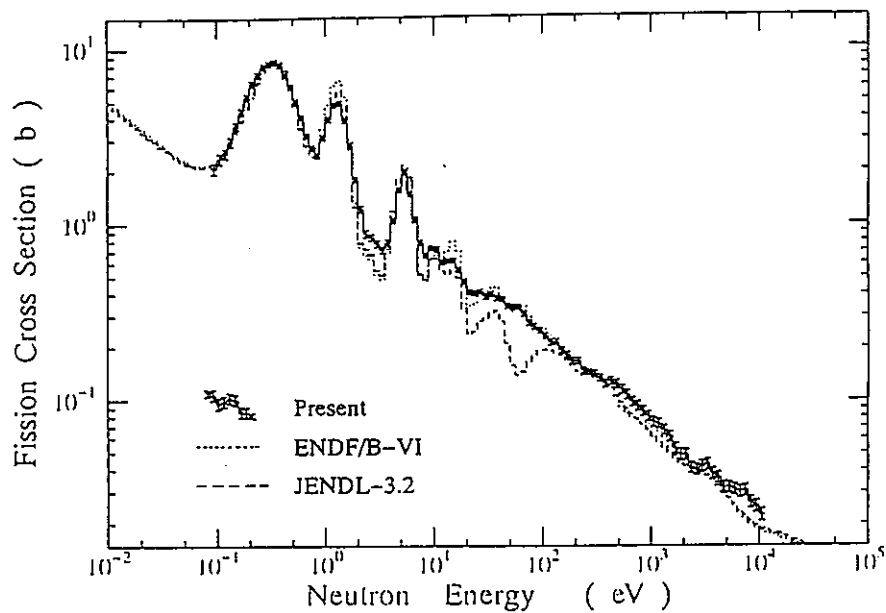


Fig. 5 Comparison of the evaluated fission cross section of ^{241}Am with the present measurement. The evaluated data are broadened by the energy resolution of the KULS.

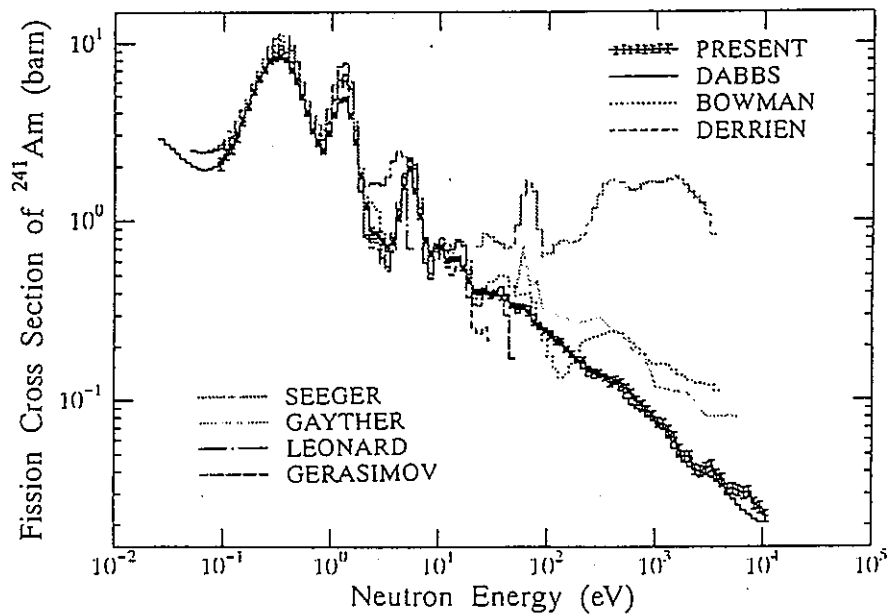


Fig. 6 Comparison of the existing experimental data with the present measurement. The experimental data are broadened by the energy resolution of the KULS.

付録 E

Measurement of Fission Cross Section with Pure Am-243 Sample using Lead Slowing-Down Spectrometer

Katsuhei Kobayashi¹, Shuji Yamamoto¹, T. Kai¹, Yoshiaki Fujita¹,
Hideki Yamamoto², Itsuro Kimura² and Nobuo Shinohara³

- 1 *Research Reactor Institute, Kyoto University
Kumatori-cho, Sennan-gun, Osaka 590-04, Japan*
- 2 *Department of Nuclear Engineering, Kyoto University
Yoshidahonmachi, Sakyo-ku, Kyoto 606-01, Japan*
- 3 *Isotope Products Laboratory, Japan Atomic Energy Research Institute
Tokai-mura, Naka-gun, Ibaraki 319-11, Japan*

By making use of back-to-back type double fission chambers and a lead slowing-down spectrometer coupled to an electron linear accelerator, the fission cross section for the $^{243}\text{Am}(n,f)$ reaction has been measured relative to that for the $^{235}\text{U}(n,f)$ reaction in the energy range from 0.1 eV to 10 keV. The measured result was compared with the evaluated nuclear data appeared in ENDF/B-VI and JENDL-3.2, whose evaluated data were broadened by the energy resolution function of the spectrometer. General agreement was seen between the evaluated data and the measurement except that the ENDF/B-VI data were lower in the range from 15 to 60 eV and that the JENDL-3.2 data seemed to be lower above 100 eV.

1. Introduction

Americium isotopes are minor actinides which are produced subsequently to ^{237}Np nuclide in light water reactors. The nuclear data for the minor actinides are of great interest in the design of reactors with MOX or Pu fuels and for the design of systems for spent fuel reprocessing or waste disposal. The fission cross sections are important for transmutation of the burdensome actinides[1,2].

Numerous measurements of the nuclear data for ^{237}Np and ^{241}Am have been made previously [3]. Recently, the authors have also measured the fission cross sections of ^{237}Np and ^{241}Am in the neutron energy range from 0.1 eV to 10 keV[4,5]. However, the fission cross section for ^{243}Am is not always enough both in quality and in quantity, especially, the measured data have not been reported below 5 keV except for thermal neutron energy[3,6]. In the lower energy region, ^{243}Am has a small subthreshold fission cross section. However, the cross section is still important not only for systematic studies of fission mechanism but also for transmutation in light water reactors because they have higher neutron fluxes at the relevant energies.

In the present study, at first, we have prepared the pure ^{243}Am sample by anion-exchange method to remove the ^{239}Pu impurity produced through the alpha-decay of ^{243}Am . After the chemical purification, the fission cross section for the $^{243}\text{Am}(n,f)$ reaction has been measured

relative to that for the $^{235}\text{U}(n,f)$ reaction by making use of back-to-back type double fission chambers and a lead slowing-down spectrometer coupled to 46 MeV electron linear accelerator (linac) of Research Reactor Institute, Kyoto University (KURRI). The experimental technique is the same as before[4,5]. The measured result is compared with the evaluated data in JENDL-3.2[7] and ENDF/B-VI[8].

2. Experimental Methods

2.1. Lead Slowing-down Spectrometer

The lead slowing-down spectrometer was recently installed coupling to the 46 MeV electron linear accelerator (linac) at Research Reactor Institute, Kyoto University (KURRI). The Kyoto University Lead Slowing-down Spectrometer (KULS) is composed of 1600 pieces of lead blocks (each size : $10 \times 20 \times 20 \text{ cm}^3$, and purity : 99.9 %) and these are piled up to make a cube of $1.5 \times 1.5 \times 1.5 \text{ m}^3$ (about 40 tons) without any structural materials[9], as seen in Fig. 1. At the center of the KULS, we have set an air-cooled photoneutron target of Ta to generate pulsed fast neutrons. Thermocouples were attached on the surface of the target case to monitor the temperature. The linac was operated to keep the temperature less than 300°C . The KULS has eight experimental/irradiation holes ($10 \times 10 \text{ cm}^2$, 55 or 45 cm in depth), and one of the holes is covered by bismuth layers of 10 to 15 cm in thickness to shield high energy gamma-rays (6 to 7 MeV) produced by the $\text{Pb}(n,\gamma)$ reaction in the spectrometer.

Characteristic behavior of neutrons in the KULS was studied by calculations with the continuous energy Monte Carlo code MCNP[10] and by experiments with resonance filter method [4,9]. It was found that the slowing-down constant K in the relation of energy and slowing-down time $E=K/t^2$ was determined to be 190 ± 2 and $156 \pm 2 \text{ (keV } \mu\text{s}^2)$ for the bismuth and the lead experimental holes. The energy resolution was around 40 % for both experimental holes at energies from a few eV to about 500 eV and was larger in the lower and the higher energy regions. More detailed characteristics of the KULS are given elsewhere [4,9].

2.2. ^{243}Am and ^{235}U Samples

The americium sample was purified at Isotope Products Laboratory,

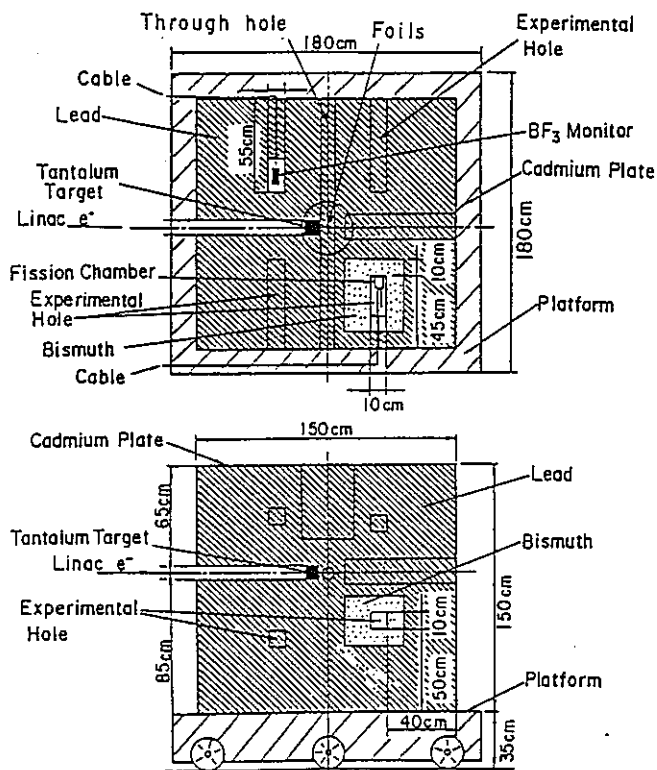


Fig. 1 Cross-sectional view of Kyoto University Lead Spectrometer, KULS.

Japan Atomic Energy Research Institute by anion-exchange method using nitric acid methyl alcohol-mixed media [11], in order to remove uranium, neptunium, plutonium and curium from the americium sample. The purified americium solution and isopropyl alcohol were mixed thoroughly and electrolyzed on a stainless steel disk (28 mm in diameter and 0.2 mm in thickness) for preparing an americium deposit (radioactive area of 20 mm in diameter)[12]. After electrodeposition, the sample was sintered with a gas burner to fix the americium layer on the disk by making americium oxide.

Alpha-ray from the deposit was measured with a silicon surface barrier detector. The pulse height distribution of the ^{243}Am sample is shown in Fig. 2. Although small amount of impurities of ^{241}Am and ^{243}Cm are observed in the figure, their counting rate ratios for $^{241}\text{Am}/^{243}\text{Am}$ and $\text{Cm}/^{243}\text{Am}$ are 0.007 and 0.00004, respectively. We have found that these impurities have no influence on the result of the ^{243}Am (n,f) cross section measurement, considering their cross sections and half-lives or numbers of their atoms.

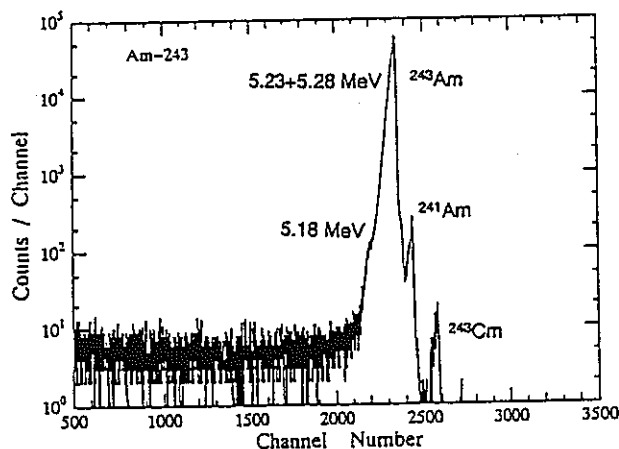


Fig. 2 Alpha-ray spectrum of ^{243}Am .

In addition, 74.7 keV gamma-ray from ^{243}Am was measured with a HPGc detector and the number of ^{243}Am was also determined by analyzing the gamma-ray spectrum obtained. The results measured by both detectors are in good agreement within the uncertainty of 2 %. The number of ^{243}Am atoms is determined to be $(3.33 \pm 0.11) \times 10^{17}$, where the error was estimated by taking into account (i) statistics of the activity measurements, (ii) geometrical detection efficiencies, and (iii) uncertainties of the decay data used.

Highly enriched uranium oxide (99.91 % of ^{235}U) got from ORNL was chemically treated as almost same technique as the americium sample. The uranium deposit on the stainless steel disk was prepared at KURRI by the electrodeposition method. This ^{235}U sample was used to monitor the neutron flux in this study as the well-known reference cross section of the $^{235}\text{U}(n,f)$ reaction. Alpha-ray and gamma-ray spectrometries were carried out to determine the number of the uranium atom as well as the americium sample. From the analyses of the alpha-rays with 4.152 to 4.597 MeV from ^{235}U , the number of ^{235}U atoms was determined to be $(2.81 \pm 0.03) \times 10^{16}$. The gamma-ray measurement by 185.7 keV of ^{235}U showed good agreement within 1.5 % with the alpha-ray measurement.

2.3. Fission Chambers

The fission chambers employed for the present measurement are composed of two parallel plate type ionization chambers[4,5] as shown in Fig. 3. The back sides of a sample deposit (^{243}Am) and a reference one (^{235}U) are faced each other, and it is called back-to-back type. The chambers were made of Al and filled with a mixed gas (97% Ar and 3% N_2) at 1 atm.

2.4. Data Taking and Fission Rate Measurement

The back-to-back type fission chambers were put in the Bi-covered hole of the KULS. Since we used quite thin ^{243}Am ($43 \mu\text{g}/\text{cm}^2$) and ^{235}U ($3.5 \mu\text{g}/\text{cm}^2$) deposits, fission pulses were clearly discriminated from background pulses caused by alpha-rays, and led to the respective time analyzer, as before[4,5]. The start signal for timing was taken from the linac electron burst. The channel number and the time width of each time analyzer were 4096 and 62.5 or 500 ns, respectively. The linac was operated with pulse width of 22–33 ns, repetition rate of 200 Hz, electron peak current of about 1.9 A, and accelerating energy of about 30 MeV. After about 50 hours' experiment, the ^{243}Am and the ^{235}U deposited plates were exchanged each other and had another 30 hours, to eliminate the systematic and statistic uncertainties in the cross section measurement.

The fission cross section of ^{243}Am is obtained by

$$\sigma_{\text{Am}}(E) = \frac{C_{\text{Am}}}{C_{\text{U}}} \frac{N_{\text{U}}}{N_{\text{Am}}} \sigma_{\text{U}}(E)$$

where

C_{Am} : fission counts of ^{243}Am ,

C_{U} : fission counts of ^{235}U ,

N_{Am} : number of ^{243}Am atoms in the sample deposit,

N_{U} : number of ^{235}U atoms in the reference deposit,

$\sigma_{\text{U}}(E)$: energy dependent fission cross section of ^{235}U .

We cited the numerical values of $\sigma_{\text{U}}(E)$ from ENDF/B-VI[8].

Figure 4 shows the cross sections measured at the time when 4 weeks, 5 months and 13 months have passed after the chemical purification. In the neutron energy region around 0.3 eV, one can see that the cross sections are getting higher as the time passes, due to the accumulated impurity of ^{239}Pu by the alpha-decay of ^{243}Am . With the repeated experiments as seen in Fig. 4, we could experimentally investigate the influence of the ^{239}Pu impurity and correct the measured results to give the data at the point of time when the chemical process was done. The details are described elsewhere[13].

3. Results and Discussion

The present result, which has been corrected with the growth influence of the ^{239}Pu impurity, is shown in Fig. 5 and is compared with the evaluated cross sections in JENDL-3.2[7] and

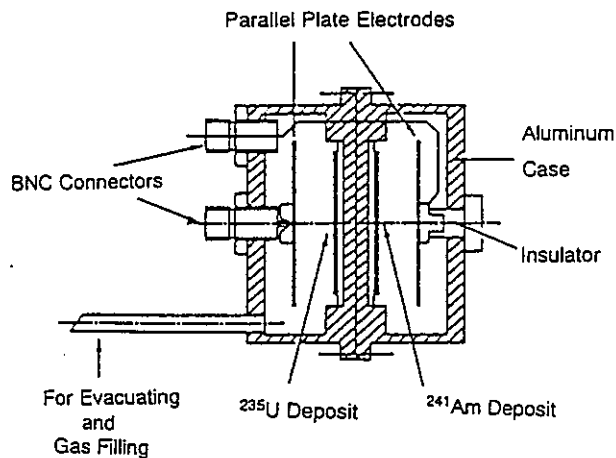


Fig. 3 Cross-sectional view of back-to-back type fission chambers.

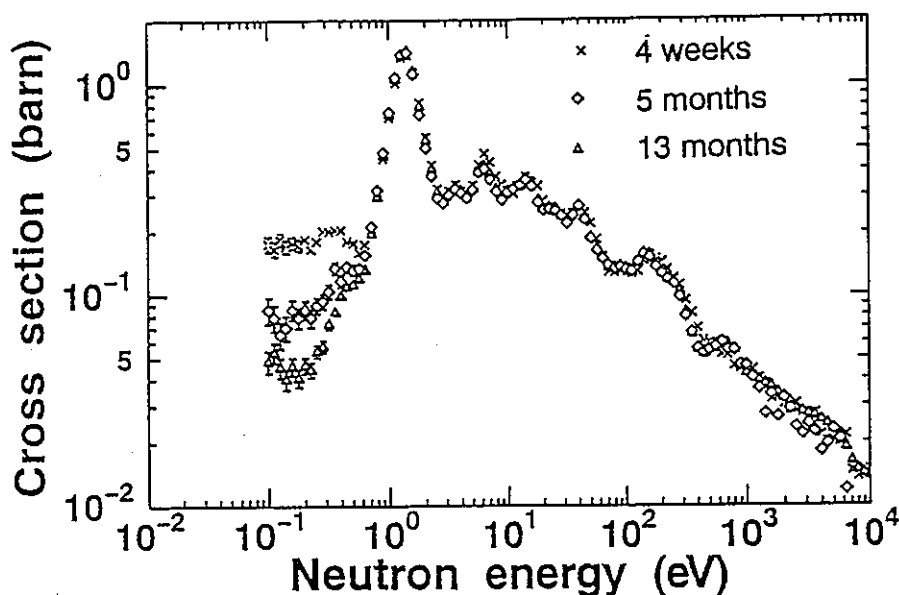


Fig. 4 Comparison of the measured data depending on the time after the chemical purification.

ENDF/B-VI[8], which are broadened by the energy resolution function of the KULS. The experimental uncertainties are considered to be mainly due to (1) the statistical error in fission counts, (2) assignment of fission counts, (3) number of atoms for the ^{243}Am and the ^{235}U deposits, and (4) the reference fission cross section for the $^{235}\text{U}(n,f)$ reaction. Total amount of the experimental uncertainties is 4 to 6 %.

It is seen in Fig. 5 that both of the evaluation data are discrepant each other in the energy regions below 0.3 eV and above 15 eV. Although the ENDF/B-VI data are in general agreement with the present measurement, they are lower at energies between 15 and 60 eV. The JENDL-3.2 data seem to be lower than the measurement in general above 100 eV. At the narrow dip of around 3 eV, one can see discrepancy between the evaluated and the measured data. The reason would be due to the inappropriate resolution function of the lead slowing-down spectrometer.

References

1. D. Lancaster, "Actinide Burning in a Standard Pressurized Water Reactor", Proc. of the Int'l Conf. and Technol. Exposition on Future Nucl. Systems: Global '93", Sept. 12-17, 1993, p.609, ANS, La Grange Park, Illinois, 1993.
2. J. Tommasi, et al., "Long-Lived Waste Transmutation in Reactor", *ibid.*, p.1252, ANS, La Grange Park, Illinois, 1993.
3. V. McLane, et al., "Neutron Cross Sections"; Vol.2, Neutron Cross Section Curves, Academic Press, Inc., London, 1988.
4. A. Yamanaka, et al., J. Nucl. Sci. Technol., 36, 863 (1993).
5. K. Kobayashi, S. Yamamoto, et al., "Measurement of Fission Cross Section with Pure Am-241 Sample using Lead Slowing-down Spectrometer", JAERI-Conf 96-008, p.117 (1996).

6. K. Wisshak and F. Kappeler, Nucl. Sci. Eng., 85, 251 (1983).
7. T. Nakagawa, "Evaluation of Nuclear Data for Americium Isotopes", JAERI-M, 89-008 (1989), and J. Nucl. Sci. Technol., Vol.32, 1259 (1995).
8. R. F. Rose (Ed.), "ENDF/B Summary Documentation", BNL-NCS-17541, 4th Ed. (ENDF/B-VI) 1991.
9. K. Kobayashi, et al., "Characteristic Behavior of Neutrons in the Lead Slowing-down Spectrometer Coupled to Electron Linac", JAERI-M 93-046, p.360, JAERI, 1993, and Nucl. Instr. Methods, Phys. Res. A, in print.
10. "MCNP - A General Monte Carlo Code for Neutron and Photon Transport, Version 3A", LA-7396-M, Rev.2, Los Alamos National Laboratory (1986).
11. S. Usuda and N. Kohno, Separation Science and Technology, 23, 1119 (1988).
12. N. Shinohara and N. Kohno, Appl. Radiat. Isot., 40, 41 (1989).
13. T. Kai, K. Kobayashi, et al., "The Influence of Impurities for Cross Section Measurement of $^{241,243}\text{Am}(n,f)$ Reactions", presented in this Symposium.

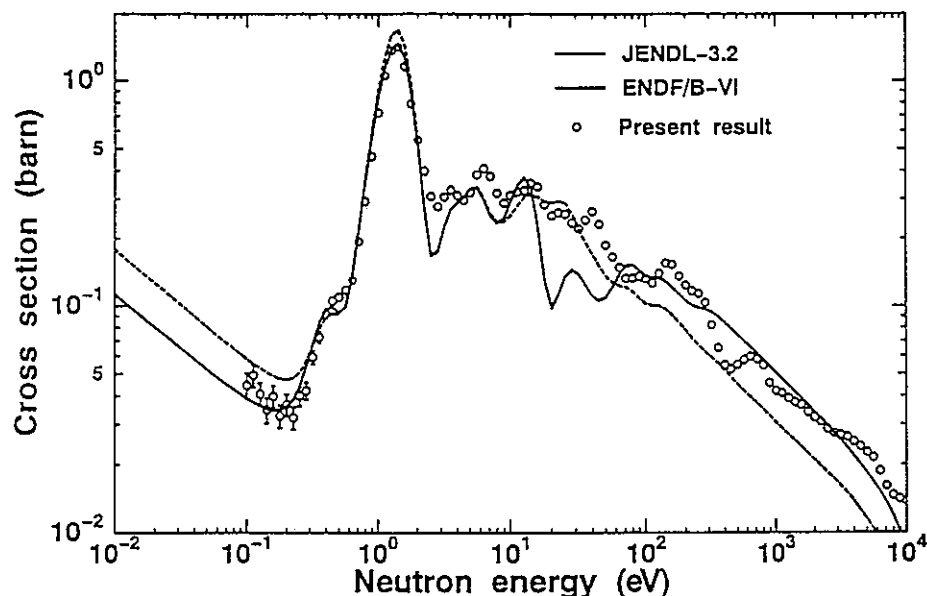


Fig. 5 Comparison of the evaluated fission cross sections of ^{243}Am with the present measurement.

付録 F

The Influence of Impurities for Cross Section Measurement of $^{241,243}\text{Am}(n,f)$ Reactions

Tetsuya Kai¹, Katsuhei Kobayashi¹, Shuji Yamamoto¹, Yoshiaki Fujita¹,
Itsuro Kimura², Mitsuharu Miyoshi², Hideki Yamamoto² and Nobuo Shinohara³

1 Research Reactor Institute, Kyoto University

2 Department of Nuclear Engineering, Kyoto University

3 Japan Atomic Energy Research Institute

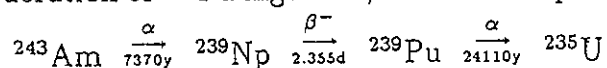
e-mail:tkai@rri.kyoto-u.ac.jp

The influence of the impurities on the fission cross section measurements for ^{241}Am and ^{243}Am has been investigated with the practical results. Following cases have been considered as the influence of impurities; (a) experiments with the ^{241}Am sample that contains impurities originally, and (b) experiments with the ^{243}Am sample that contains impurities produced by α, β decays after the chemical purification. The present study has demonstrated the usefulness of pure samples by the comparison of the experiments using the sample on the market with those using the pure sample processed by the authors. Particularly on the case(b), the correction of the impurity through the periodical measurements was experimentally performed (about 18% around 0.3 eV in 4 weeks after the chemical purification).

1.Introduction

For the nuclear data measurements, in general, cross section value of the sample containing impurities may be bigger than that with the pure sample depending on the amount of impurities and on the nuclear characteristics[1][2]. Particularly, it has to be careful to measure the fission cross sections of minor actinides because many kinds of them are produced and accumulated in the sample through the complicated decay processes. Therefore, the extensive experimental studies have recently been concentrated on the importance of the chemical and isotopic composition of the sample materials and of its physical properties[1][2][3].

In an earlier measurement, we had the experience of obtaining a much larger fission cross section for ^{241}Am , being the measurement made with a sample on the market[4]. Through the careful and systematic investigation of the ^{241}Am sample by α -ray spectrometry, we found that the sample contained the ^{239}Pu impurity of about 0.3%[5]. On the other hand, the measurement of ^{243}Am fission cross section has to be also performed with careful consideration of ^{239}Pu ingrowth, because it is produced through the following decay chain;



This ^{239}Pu ingrowth makes an important contribution to the measured fission cross section even if we have purified the ^{243}Am sample by the chemical processing.

In the present study, following cases have been considered as the influence of impurities for fission cross section measurements with:

(a) the sample which contains impurities originally.

(b) the sample whose decay products are accumulated as impurities after chemical purification.

In practice, the impurity problems have been investigated as typical examples for the measurements of the $^{241}\text{Am}(n,f)$ and $^{243}\text{Am}(n,f)$ cross sections, respectively[4][5][6]. The experiments have been performed by making use of back-to-back type double fission chambers using the Am and the ^{235}U deposits and of a lead slowing-down spectrometer coupled to an electron linear accelerator[7][8].

2. Experimental Methods

2.1. Lead Slowing-down Spectrometer

The fission cross section measurements for ^{241}Am and ^{243}Am have been made in the energy range from 0.1 eV to 10 keV with Kyoto University Lead Slowing-down Spectrometer (KULS)[7]. The KULS is composed of 1600 lead blocks (each size: $10 \times 10 \times 20\text{cm}^3$, purity: 99.9%) and the blocks are piled up to make a cube of $1.5 \times 1.5 \times 1.5\text{m}^3$ (40 tons) without any structural materials. We covered the KULS with Cd sheets of 0.5 mm in thickness. At the center of the KULS, an air-cooled photoneutron source of Ta is set to generate pulsed fast neutrons. One of the experimental holes in the KULS was covered by Bi layers of 10 to 15 cm in thickness to shield high energy gamma-rays (6 to 7 MeV) produced by the $\text{Pb}(n,\gamma)$ reaction in the spectrometer.

The characteristics of the spectrometer (the relation between neutron slowing-down time and energy, and the resolution) have been obtained by the measurements and the calculations. The detailed description is given elsewhere[7].

2.2. ^{241}Am and ^{243}Am Samples

Two kinds of Am samples were used; one was commercially available[4] and the other was prepared by ourselves with the chemical processing using anion-exchange methods. Both types of the Am samples were deposited on stainless steel plates of 28 mm in diameter and 0.2 mm thick (radioactive area: 20 mm in diameter). In the α -ray spectrum of the purified ^{241}Am sample, no other α -ray peak was observed. For the ^{243}Am spectrum measurement, although small amount of impurities of ^{241}Am and ^{243}Cm were observed, the counting rate ratios for $^{241}\text{Am}/^{243}\text{Am}$ and $^{243}\text{Cm}/^{243}\text{Am}$ were 0.007 and 0.00004, respectively. These results were found to be negligible in the $^{243}\text{Am}(n,f)$ cross section measurement at the relevant energies.

2.3. Fission Chambers

The fission chambers employed for the present measurements are composed of two parallel plate type ionization chambers[8]. The back sides of a sample deposit (Am) and a reference one (^{235}U) are faced each other, therefore it is called back-to-back type. The chambers were made of aluminum and filled with a mixed gas (97% Ar and 3% N_2) at 1 atm. Enrichment of the reference ^{235}U sample was 99.91%.

3. Fission Cross Section Measurement

Each of the fission cross section for ^{241}Am and ^{243}Am is obtained by the following

equation;

$$\sigma_{Am}(E) = \frac{C_{Am}}{C_U} \frac{N_U}{N_{Am}} \sigma_U(E)$$

where C_{Am} : fission counts of Am,
 C_U : fission counts of ^{235}U ,
 N_{Am} : number of Am atoms in the sample deposit,
 N_U : number of ^{235}U atoms in the reference deposit,
 $\sigma_U(E)$: energy dependent fission cross section of ^{235}U .

The reference cross section values were cited from ENDF/B-VI[10]. More detailed experimental descriptions are given elsewhere[6][9].

4. Results and discussion

The result with the ^{241}Am sample on the market is shown in Fig. 1, and is compared with the evaluated data in JENDL-3.2[11] and ENDF/B-VI[10], where the evaluated data were broadened by the energy resolution of the KULS. The fission cross section for the pure ^{241}Am sample has also been shown in Fig. 2, where the measurement is in good agreement with the evaluated data. It is clear that the larger cross section for the purchased sample is due to the impurities. We have experimentally investigated the problem and found that the purchased sample contained ^{239}Pu impurity of about 0.3 % at least by the careful α -ray spectrometry. The sample contains some other impurities in addition to ^{239}Pu because the larger cross section has not been corrected properly with the amount of ^{239}Pu impurity except for the energy region around the 0.3 eV resonance. It is shown in Fig. 3 that we have simulated the impurity corrections not only with ^{239}Pu but also with ^{242m}Am . The amount of ^{242m}Am impurity was assumed to be 0.25% to fit the analytical result to the measurement around higher neutron energy region. The result of this correction means that the ^{242m}Am impurity was overestimated and there were any other impurities in the sample because of the inadequate correction around lower neutron energy region.

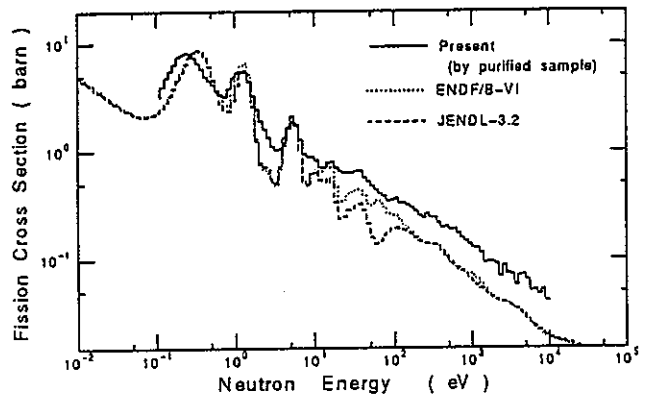


Fig. 1 Comparison of the measured cross section for the purchased sample and the evaluated.

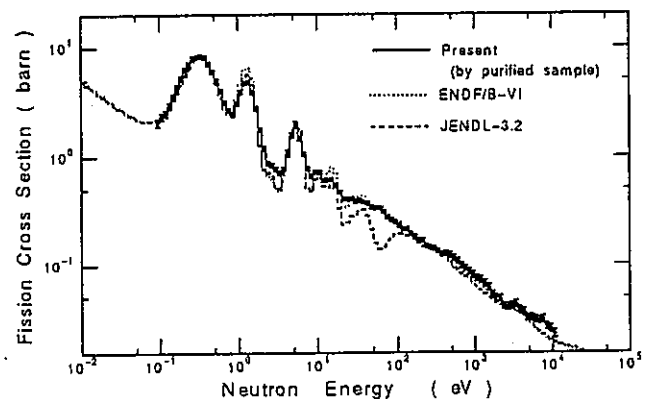


Fig. 2 Comparison of the measured cross section for the purified sample and the evaluated.

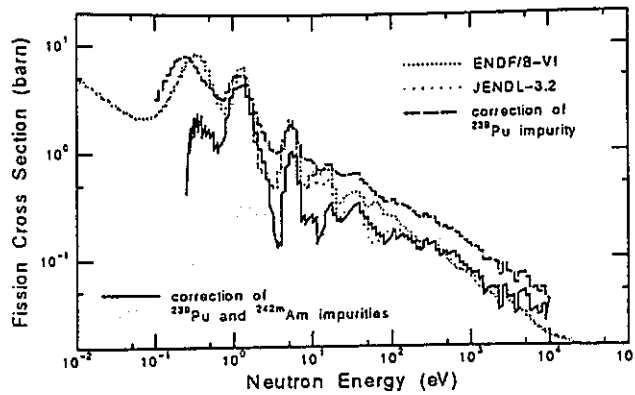


Fig. 3 Corrected cross section for the purchased ^{241}Am sample.

Figure 4 also shows the $^{243}\text{Am}(n,f)$ cross section measured with the sample on the market. There is a remarkable difference between this result and the evaluated data around 0.3 eV, which is clearly caused by ^{239}Pu impurity produced by the α -decay of ^{243}Am . We have followed the growth of ^{239}Pu impurity in the ^{243}Am sample after the chemical purification by the calculation and periodical measurements. In Fig. 5, the results of the measurements performed at 4 weeks, 21 weeks and 55 weeks after the purification is shown. It is obviously observed that the measured values around 0.3 eV increased depending on the time after the purification.

The influence of ^{239}Pu ingrowth around its 0.3 eV resonance is illustrated in Fig. 6, where the solid line means the measured cross sections and the broken line indicates the estimated contribution of ^{239}Pu ingrowth using the cross sections cited from ENDF/B-VI[10]. Good agreement is seen between them. Figure 7 shows the energy dependent influence of the ^{239}Pu ingrowth. As a result, the present cross section for the $^{243}\text{Am}(n,f)$ reaction has been derived and displayed in Fig. 8 with the correction of ^{239}Pu accumulation (about 18 % around 0.3 eV in 4 weeks after the chemical process). Through the present experimental investigation, it is found that the measurement has to be done as soon as possible after the chemical purification not to make the correction large and that the pure sample is indispensable for these kinds of measurements.

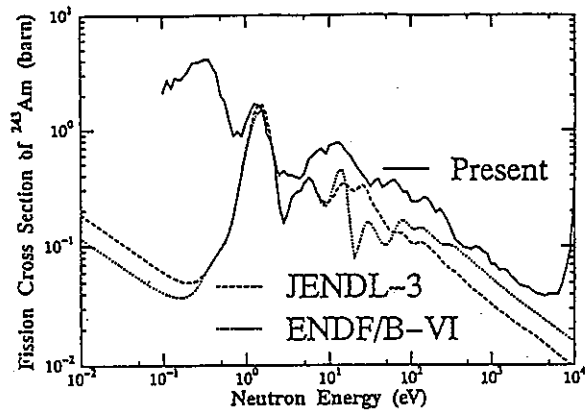


Fig. 4 Comparison of the measured cross section for the purchased sample and the evaluated.

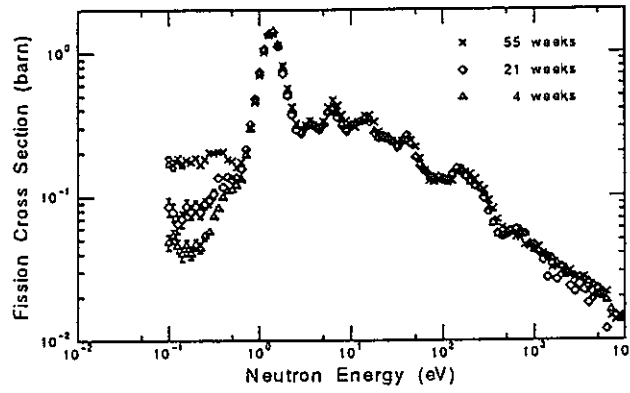


Fig. 5 Ingrowth of ^{239}Pu in $^{243}\text{Am}(n,f)$ cross section after chemical separation.

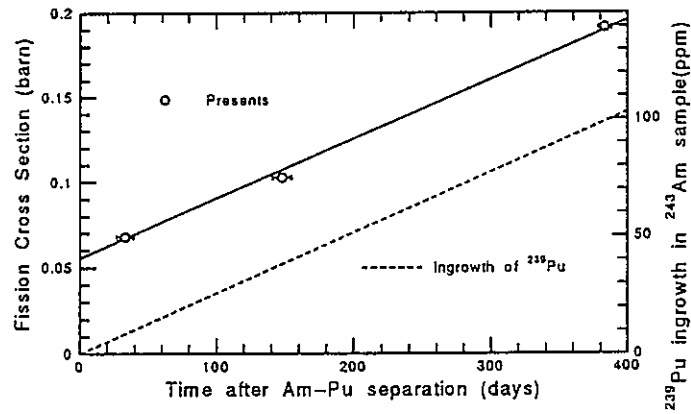


Fig. 6 Contribution of ^{239}Pu around 0.3 eV.

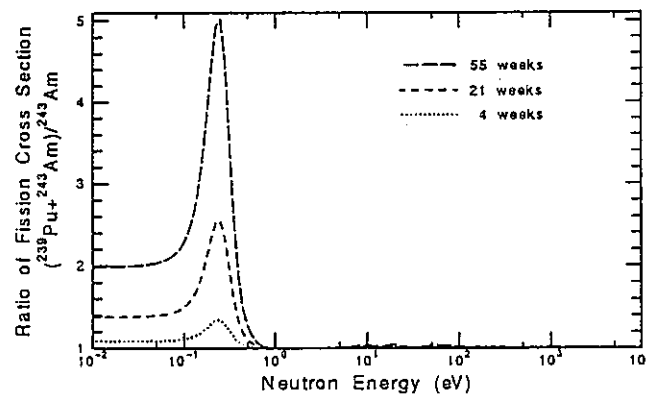


Fig. 7 Energy dependent influence of ^{239}Pu ingrowth.

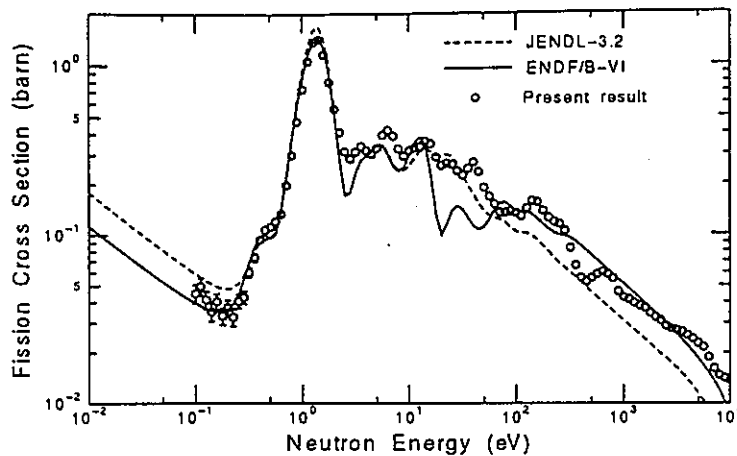


Fig.8 Present $^{243}\text{Am}(n,f)$ cross section with the correction of ^{239}Pu ingrowth.

Reference

- 1) C. Wagemans: *Nucl. Instr. Meth.*, A236, 429(1985).
- 2) C. Wagemans, et al.: *Nucl. Phys.*, A597, 188(1996).
- 3) N. Shinohara: to be published in *J. Nucl. Sci. Technol.*.
- 4) K. Kobayashi, et al.: *Proc. Int'l Conf. on Nucl. Data for Sci. and Technol., Gatlinburg, Vol.1*, p242(1994).
- 5) M. Miyoshi: "Measurement of Nutron Energy Dependent Fission Cross Section of ^{241}Am ", Master Thesis in Japanese, Department of Nuclear engineering, Kyoto University, 1995.
- 6) K. Kobayashi, et al.: "Measurement of Fission Cross Section with the Pure Am-243 Sample using Lead Slowing-Down Spectrometer", presented in this Symposium.
- 7) K. Kobayashi, S. Yamamoto, A.Yamanaka, et al.: "Characteristics of Kyoto University Lead Slowing-down Spectrometer Coupled to an Electron Linac" JAERI-M 93-046,p360(1993) and to be published in *Nucl. Instr. Methods in Phys. Res.*.
- 8) M. Obu: "Preparation and Characteristics of Fission Chambers with Actinide Nuclides" JAERI-M 9757(1981) and to be published in *Nucl. Sci. Eng.*.
- 9) K. Kobayashi, S. Yamamoto, et al.: "Measuement of Fission Cross Section with Pure Am-241 Sample using Lead Slowing-down Spectrometer", JAERI-Conf 96-008, p.117(1996).
- 10) R. F. Rose(Compiled and Edited): "ENDF-201, ENDF/B-VI Summary Documentation", BNL-NCS-17541, 4th Ed. (ENDF/B-VI)(1991.13).
- 11) T. Nakagawa, et al.: *J. Nucl. Sci. Technol.*, Vol.32, No.12, 1259(1995) and "Evaluation of Nuclear Data for Americium Isotopes", JAERI-M, 89-008(1989).

Application of BGO Scintillators to Absolute Measurement of Neutron Capture Cross Sections between 0.01 eV and 10 eV

Shuji YAMAMOTO¹, Katsuhei KOBAYASHI and Yoshiaki FUJITA

*Research Reactor Institute, Kyoto University**

(Received May 7, 1996)

Applying a total energy absorption γ -ray detector composed of 12 bricks ($5 \times 5 \text{ cm}^2$, 7.5 cm thick) of BGO scintillators, the absolute measurement of capture cross sections for Au and Sb has been made in an energy region between 0.01 and 10 eV using the linac time-of-flight method. Incident thermal neutron flux was absolutely determined by using the BGO detection system with a Sm sample. To extend the neutron flux measurement from the thermal neutron region to higher neutron energies, the $^{10}\text{B}(n, \alpha\gamma)$ reaction was applied. Absolute capture yield for the relevant capture sample was obtained by the saturated capture yield at a large resonance of the sample.

Gold was selected to investigate the application of the BGO detection system to the absolute measurement of the capture cross sections, since the $^{197}\text{Au}(n, \gamma)^{198}\text{Au}$ reaction cross section is a well known standard one. The result of the $^{197}\text{Au}(n, \gamma)^{198}\text{Au}$ reaction cross section showed good agreement with the evaluated data in JENDL Dosimetry File and ENDF/B-VI. Then, the detection system was applied to the $\text{Sb}(n, \gamma)$ cross section measurement. Antimony has a large scattering-to-capture cross section ratio comparing to that of gold. The result showed good agreement with the evaluated data in JENDL-3.2 and ENDF/B-VI.

KEYWORDS: BGO scintillator, total energy absorption detector, neutron capture, capture cross section, absolute measurement, time-of-flight method, gold, antimony, eV range 0.01-10

I. INTRODUCTION

Two kinds of measurements are essential for the determination of a neutron capture cross section. One is to measure the neutron flux impinging on a sample, and the other is capture rate measurement occurring in the sample. The capture rate is often obtained by induced-activities from the activation sample or by the detection of prompt γ -rays from the neutron-captured sample. The latter is useful for the energy dependent cross section measurement by a neutron time-of-flight method. For the determination of the number of capture events, however, it is necessary to use a detector of which the detection efficiency for capture events is independent of specific de-excitation cascade modes following the neutron capture⁽¹⁾. For such a purpose, we have developed a total energy absorption detector by employing BGO (bismuth germanate, $\text{Bi}_4\text{Ge}_3\text{O}_{12}$) scintillators⁽²⁾. Similar detectors have been developed and applied to the measurement of neutron capture cross sections by Wisshak⁽³⁾, Block⁽⁴⁾ and Muradyan⁽⁵⁾.

A total energy absorption detector employing BGO scintillators can be a detection system for the absolute measurement of neutron capture cross sections with the following features:

- (1) BGO has a high density (7.13 g/cm^3)⁽⁶⁾; hence, a

large linear absorption coefficient for even higher energy γ -rays. Accordingly, the volume of scintillator which is needed to absorb the major part of capture γ -rays is much smaller (by a factor of about 1,000), than that of an organic-liquid scintillator. This enables a compact setup of the detection assembly including the associated equipment (e.g., detector shielding), and reduces the background counts coming from environmental radiations. Such a system with low background capability may be suitable to give better signal-to-background ratio data for the capture event counting.

- (2) In the case of a large organic-liquid scintillator, a ^{10}B sample cannot be used as a standard to determine the neutron flux impinging on the capture sample since a ^{10}B compound is usually dissolved into the organic liquid so as to reduce the γ -rays produced when the neutrons scattered by the sample are captured by the hydrogen in the scintillator. On the other hand, as for the BGO detector not containing the ^{10}B compound, the $^{10}\text{B}(n, \alpha\gamma)$ reaction may be employed as a standard. A common BGO detection system can be used to measure the neutron flux as well as the capture events. This capability is desirable in capture cross section measurements with high accuracy.
- (3) The low sensitivity to neutrons scattered with a capture sample is one of the most important characteristics of a capture γ -ray detector used in neutron

* Kumatori-cho, Sennan-gun, Osaka 590-04.

¹ Corresponding author, Tel. +81-724-51-2347,

Fax +81-724-51-2602, E-mail: yamamoto@rri.kyoto-u.ac.jp

capture cross section measurements. BGO scintillators have a sensitivity to scattered neutrons which have to be taken into consideration, especially in the case of a sample which has a large value of scattering-to-capture ratio. The authors have overcome the problem by shielding the inner surface of the through hole of the BGO detector with ${}^6\text{LiF}$ tiles of 3 mm in thickness⁽⁷⁾. Lithium-6 has a large cross section for the ${}^6\text{Li}(n, \alpha)$ reaction, especially in the lower energy region, and absorbs the neutrons scattered by the capture sample without γ -ray emission. Below 10 eV the sensitivity to scattered neutrons was sufficiently reduced⁽²⁾.

In the present work, we have experimentally investigated a BGO detection system applied to the absolute measurement of capture cross sections for Au and Sb by making use of a neutron time-of-flight method with the 46 MeV electron linear accelerator (linac) at the Research Reactor Institute, Kyoto University (KURRI). Since the capture cross section for gold is well known as one of the standard neutron cross sections, the cross section measurement may be useful for understanding the applicability of the BGO detection system. Antimony has a large scattering-to-capture cross section ratio (0.82 for Sb, 0.08 for Au at thermal neutron energy)⁽⁸⁾, which means that the Sb may be at a disadvantage for the capture cross section measurement comparing to that of Au.

This paper describes the absolute measurement of neutron capture cross sections for Au and Sb using the BGO detection system as a total energy absorption detector. At first, to determine the neutron flux impinging on a sample, a neutron detection efficiency was calibrated by Sm and ${}^{10}\text{B}$ samples at thermal neutron energy, and the detection efficiency of the capture events occurring in the sample was obtained by the saturated yield method. Finally, the measured results are compared with the evaluated cross section values in JENDL-3.2⁽⁹⁾, JENDL Dosimetry File⁽¹⁰⁾ and ENDF/B-VI⁽¹¹⁾.

II. EXPERIMENTAL METHOD

1. Samples

Samarium sample was a metallic plate of $1.8 \times 1.8 \text{ cm}^2$ and 0.5 mm thick, and the purity was 99.8%. The sample was put into the center of the through hole of the BGO assembly to measure the absolute thermal neutron flux. The sample was thick enough to be black to thermal neutrons.

Boron-10 powder was put into a thin Al case (0.2 mm in thickness) of $1.8 \times 1.8 \text{ cm}^2$ and 8 mm in thickness and the sample thickness was 1.102 g/cm^2 . The enrichment of the ${}^{10}\text{B}$ sample was 90.4%. This sample was set at the center of the BGO assembly instead of the samarium sample to measure the energy dependent neutron flux. The ${}^{10}\text{B}$ sample was black for neutrons below 10 eV.

Gold sample was a metallic plate of $1.8 \times 1.8 \text{ cm}^2$ and the thickness was 0.716 g/cm^2 . The purity was 99.999%. Antimony sample was made of fine powder and packed in an Al case of $1.8 \times 1.8 \text{ cm}^2$ and 5 mm in thickness. The purity was 99.9% and the sample thickness was 1.843 g/cm^2 .

2. BGO Detector

The present BGO assembly consists of twelve scintillator bricks of $5 \times 5 \times 7.5 \text{ cm}^3$, so that the total volume is 2.25 l which corresponds to about 1/1,000 in volume of a large liquid scintillator tank. Twelve bricks are equipped with respective photo-multiplier (PM) tubes and assembled to have a through hole of $2.7 \times 2.7 \text{ cm}^2$ and 15.0 cm in length as shown in Fig. 1. A neutron beam is collimated and led through the hole to a capture sample placed at the center of the BGO assembly. The inside of the hole was covered with enriched ${}^6\text{LiF}$ tiles of 3 mm in thickness, to absorb neutrons scattered by the capture sample⁽²⁾. Also, the BGO detection system is installed in a house made of lead shielding of 5 cm in thickness to reduce background radiation from the surroundings.

Characteristics of the BGO detection system have been investigated both by experimental work and Monte

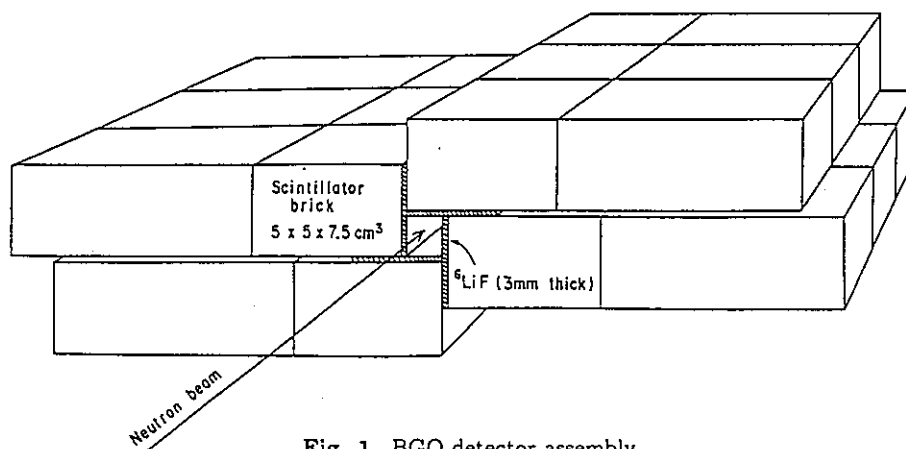


Fig. 1 BGO detector assembly.

Carlo calculations. More detailed description about the pulse height spectra of the $\text{Ta}(n, \gamma)$, $\text{Au}(n, \gamma)$, and $\text{Fe}(n, \gamma)$ reactions, detection efficiency for monoenergetic γ -rays, and sensitivity to neutrons scattered by the capture sample was given in the previous paper⁽²⁾.

3. Experimental Arrangement

Capture cross section measurements in a neutron energy region between 0.01 and 10 eV were carried out by neutron time-of-flight (TOF) technique using the 46 MeV linac at KURRI. The experimental arrangement is shown in Fig. 2. The flight path used in the experiment is in the direction of 135° to the linac electron beam. Photoneutrons from the water-cooled Ta target were directed to a capture sample placed at a distance of 12.7 m from the target. The neutron collimation system was mainly composed of B_4C , Li_2CO_3 and Pb materials, and tapered from about 12 cm in diameter at the entrance of the flight tube to 1.5 cm at the detector so that the neutron beam was collimated to 1.5 cm in diameter upon the sample. The capture sample, which was put on the sample changer, was placed at the center of the BGO assembly. A Pb-shadow shield was put in front of the photoneutron source to reduce the intense gamma-flash produced at the Ta target. The neutron intensity during the TOF experiment was monitored by a BF_3 counter placed in the neutron beam.

4. Pulsed Neutron Source

Making use of the 46 MeV linac at KURRI, bursts of fast neutrons were produced in a water-cooled photoneutron target, which was 5 cm in diameter and 6.1 cm long and composed of 12 sheets of Ta plates with the total thickness of 29 mm⁽¹²⁾. The fast neutrons were moderated in an octagonal water tank, 30 cm in diameter and 10 cm thick, placed beside the target.

During the experimental series for the TOF measurement, the KURRI linac was operated at the repetition rate of 50 Hz, with the pulse width of $3 \mu\text{s}$, electron energy 33 MeV and peak current 0.8 A. In order to prevent overlap of thermal neutrons produced by the previous

linac burst, the pulse repetition rate was set to be as low as 50 Hz in the 12.7 m TOF measurement.

5. Data Acquisition

The block diagram of the data acquisition system is shown in Fig. 3. Output signals from twelve discriminators are led to the coincidence circuit, which makes one output signal when two or more signals from the discriminators are coincided. By using this coincidence technique, the signal-to-noise ratio could be more improved than that without coincidence. In the case of ^{10}B sample, the coincidence technique can not be used because the $^{10}\text{B}(n, \alpha\gamma)$ reaction has no cascade and emits a single γ -ray of 478 keV.

The signals from the BGO detection system were fed into a time digitizer, which was initiated by the KURRI-linac bursts. The TOF data were stored in a data acquisition system, a Canberra's series 88 multi-parameter analyzer which was linked to the PDP-11/34 computer. The sample changer had four sample positions, which were provided for the capture samples of Au, Sb, ^{10}B and

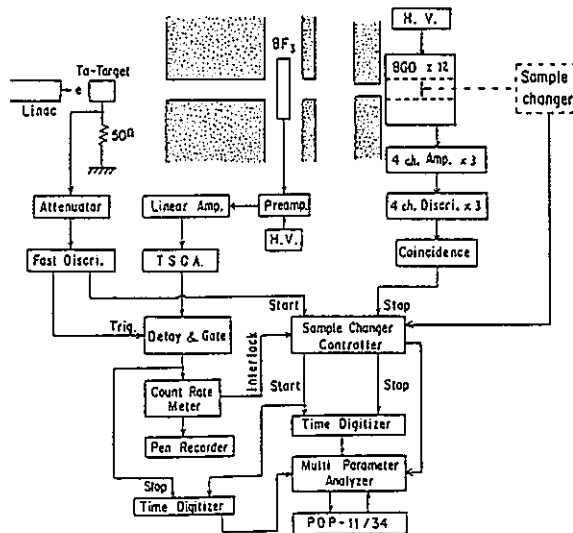


Fig. 3 Block diagram of the data acquisition system.

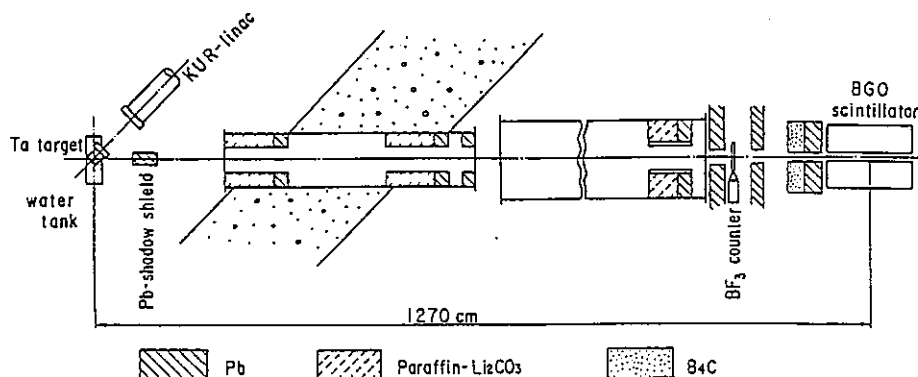


Fig. 2 Experimental arrangement for the capture cross section measurement.

Sm. The multi-channel data were stored as four 2048-channel data which corresponded to individual samples. Another four 2048-channel data areas were used for the measurement of neutron intensity for each sample run using the BF_3 monitor placed in the neutron TOF beam. Neutron monitor counts, which were used to normalize the measured data at each sample position, were obtained by integrating the TOF counts in each channel corresponding to the relevant energy region.

In the case of the present background measurement, a thick ^{10}B plug (1.11 g/cm^2) was placed between the BF_3 counter and the BGO detection system to black out the neutron beam.

III. ABSOLUTE MEASUREMENT OF CAPTURE YIELD

1. Flux Determination with Thermal Neutrons

We have applied the BGO detection system with the samarium sample to the calibration of incident thermal neutron flux.

The counting rate of the BGO detection system for thermal neutrons captured by the samarium sample can be given as follows:

$$C_{\text{Sm}}(E_{th}) = \epsilon_{\text{Sm}}(E_{th})Y_{\text{Sm}}(E_{th})\phi(E_{th}), \quad (1)$$

where C is the counting rate, the subscript "Sm" is for samarium, E_{th} the thermal neutron energy (0.025 eV), ϵ the detection efficiency of the capture event, Y the capture yield, and ϕ the incident neutron flux. Since the Sm has a large thermal neutron capture cross section (5,670 b) and the thick sample can absorb all of incident thermal neutrons, the capture yield $Y_{\text{Sm}}(E_{th})$ is unity. From the following reason, we also assume that the BGO detection efficiency $\epsilon_{\text{Sm}}(E_{th})$ is equal to unity: since samarium has capture cascades with high γ -ray multiplicity (average number of γ -rays per capture=5.6)⁽¹³⁾, it is expected that missing the detection of capture events is very rare in the measurement of capture γ -rays from a Sm sample. This expectation was experimentally verified as described before⁽²⁾. Then, Eq.(1) is rewritten as

$$C_{\text{Sm}}(E_{th}) = \phi(E_{th}). \quad (2)$$

The thermal neutron flux can be absolutely measured as counting rate using the BGO detection system combined with the capture sample of Sm.

2. Calibration of BGO Detector Efficiency for Neutrons

As the ^{10}B sample is also black to thermal neutrons, the following relation is derived:

$$C_{\text{B}}(E_{th}) = \epsilon_{\text{B}}(E_{th})Y_{\text{B}}(E_{th})\phi(E_{th}) = \epsilon_{\text{B}}(E_{th})\phi(E_{th}), \quad (3)$$

where the subscript "B" means ^{10}B . From Eqs.(2) and (3), the detection efficiency $\epsilon_{\text{B}}(E_{th})$ for thermal neutron

capture can be derived as

$$\frac{C_{\text{B}}(E_{th})}{C_{\text{Sm}}(E_{th})} = \epsilon_{\text{B}}(E_{th}) = \epsilon_{\text{B}}. \quad (4)$$

In this calibration, the detection efficiency $\epsilon_{\text{B}}(E_{th})$ was 0.82. It has to be noted that the $\epsilon_{\text{B}}(E_{th})$ is same as those at any other neutron energies, because the $^{10}\text{B}(n, \alpha\gamma)$ reaction emits a single γ -ray of 478 keV independent of incident neutron energy. Therefore, neutron flux $\phi(E)$ at a certain energy E can be measured with the detection efficiency ϵ_{B} , as seen in the following relation:

$$C_{\text{B}}(E) = \epsilon_{\text{B}}Y_{\text{B}}(E)\phi(E). \quad (5)$$

In the present measurement, since the neutron energies are below 10 eV, the ^{10}B sample of 1.102 g/cm^2 in thickness becomes black as the case for thermal neutrons. Therefore it could be considered that the ^{10}B capture yield Y_{B} becomes unity. In addition, the cross section ratio $^{10}\text{B}(n, \alpha\gamma)/(^{10}\text{B}(n, \alpha\gamma) + ^{10}\text{B}(n, \alpha))$ is constant in the relevant energy region⁽¹⁴⁾.

3. Derivation of Capture Yield

When we apply the BGO detector to the absolute measurement of capture cross sections, it may be necessary to select a capture sample which has so large resonance as the sample showing the saturated yield at 4.9 eV. Gold has a very large resonance at 4.9 eV. The capture yield $Y_{\text{Au}}(E_R)$ at the resonance is saturated by the present gold sample of 0.716 g/cm^2 and expected to be unity. The following relation for the Au sample can be also given

$$\begin{aligned} C_{\text{Au}}(E_R) &= \epsilon_{\text{Au}}(E_R)Y_{\text{Au}}(E_R)\phi(E_R) \\ &= \epsilon_{\text{Au}}(E_R)\phi(E_R), \end{aligned} \quad (6)$$

where E_R means the resonance energy and $\phi(E_R)$ can be obtained by the flux measurement using the relation in Eq.(5). From the Eq.(6), the detection efficiency $\epsilon_{\text{Au}}(E_R)$ of capture event for Au was determined to be 0.76. Since the BGO detector is thought to be a total energy absorption detector, we have assumed that the detector efficiency $\epsilon_{\text{Au}}(E_R)$ for Au is not changed from those at any other neutron energies, and can be written as

$$\epsilon_{\text{Au}} = \epsilon_{\text{Au}}(E_R). \quad (7)$$

From the measurement of Au sample, the capture rate at neutron energy E is obtained as

$$C_{\text{Au}}(E) = \epsilon_{\text{Au}}Y_{\text{Au}}(E)\phi(E). \quad (8)$$

Then, the capture yield $Y_{\text{Au}}(E)$ for Au can be given by

$$Y_{\text{Au}}(E) = \frac{C_{\text{Au}}(E)}{C_{\text{B}}(E)} \cdot \frac{\epsilon_{\text{B}}}{\epsilon_{\text{Au}}} Y_{\text{B}}(E). \quad (9)$$

In Eq.(9), $C_{\text{Au}}(E)$ and $C_{\text{B}}(E)$ are measured, ϵ_{B} is calibrated with the Sm experiment using thermal neutrons, and ϵ_{Au} can be determined by the resonance run of Au.

$Y_B(E)$ is unity as mentioned above. In the case of Sb, since it also has a large capture width at 6.3 eV resonance and the ratio of capture-to-neutron width is sufficiently large, the saturated yield method can be applicable. Then, the detection efficiency ϵ_{Sb} and the capture yield $Y_{Sb}(E)$ for Sb could be derived through Eqs.(6) to (9) as same as Au sample. In this measurement, the detection efficiency ϵ_{Sb} was determined to be 0.91.

4. Correction for Capture Yield

For the capture cross section measurement, capture yield is the primary quantity to be determined from the number of capture events occurring in the sample. The neutron capture yield is given as

$$Y_c(E) = (1 - e^{-N\sigma_t(E)t}) \frac{\sigma_c(E)}{\sigma_t(E)} f_c, \quad (10)$$

where N is the atomic density of sample material, σ_t the neutron total cross section, t the sample thickness, σ_c the neutron capture cross section, and f_c the correction factor for neutron scattering in the sample. When t is thin enough, Eq.(10) can be written as

$$Y_c(E) = N\sigma_c(E)t. \quad (11)$$

In the neutron capture cross section measurement, the effect of single and multiple neutron scattering in the sample is quite important in determining a capture cross section. This effect, which increases the effective thickness of the sample relative to geometrical thickness in the direction of the incident neutrons, must be considered in a capture cross section measurement in which the total number of capture events in a sample is measured. In the present work, we have made a Monte Carlo code to simulate the neutron capture and multiple scattering events in the sample and to carry out the corrections. The correction factor f_c was 0.975 to 0.985 for Au, and 0.965 to 0.971 for Sb. Then, the cross sections for the $^{197}\text{Au}(n, \gamma)$ and $\text{Sb}(n, \gamma)$ reactions were derived from the corrected yield data for the present measurements.

IV. RESULTS OF CAPTURE CROSS SECTIONS

The results of Au are given in Fig. 4. Table 1 also shows the comparison of mean cross sections in the present work with those in ENDF/B-VI and JENDL Dosimetry File. The statistical uncertainties are about 0.3% to 1.5%. Other uncertainties are due to detection efficiency of about 1.5% for the ^{10}B sample measurement and 1.8% for the Au sample measurement, sample thickness of about 0.5% and correction for capture yield of about 0.3%. The present result is in good agreement with the evaluated data in JENDL Dosimetry File and ENDF/B-VI. It could be considered that in the energy range below 10 eV the BGO detection system can be verified to be applicable to the absolute measurement of capture cross sections by detecting prompt capture

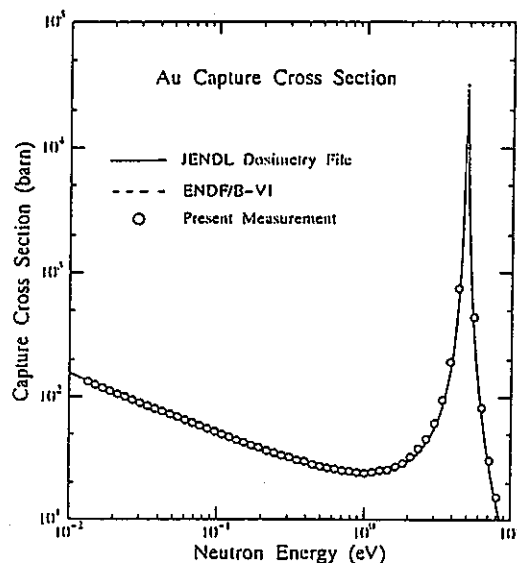


Fig. 4 Capture cross section for the $^{197}\text{Au}(n, \gamma)$ reaction.

Table 1 Comparison of mean values of the $^{197}\text{Au}(n, \gamma)$ cross section from the present work with those from ENDF/B-VI and JENDL Dosimetry File

Energy range (eV)	ENDF/B-VI (barn)	JENDL-DF (barn)	Present (barn)
0.0134-0.0213	119.7	117.7	117.7±2.9
0.0213-0.0338	95.4	95.8	94.1±2.3
0.0338-0.0538	76.1	76.2	75.7±1.8
0.0538-0.0855	60.9	61.0	61.2±1.5
0.0855-0.136	49.1	49.2	49.4±1.2
0.136-0.217	39.9	39.9	40.3±1.0
0.217-0.347	32.9	32.8	33.4±0.8
0.347-0.554	27.9	27.7	28.3±0.7
0.554-0.886	24.8	24.5	25.3±0.7
0.886-1.438	24.1	23.6	24.7±0.6

γ -rays using the linac TOF method.

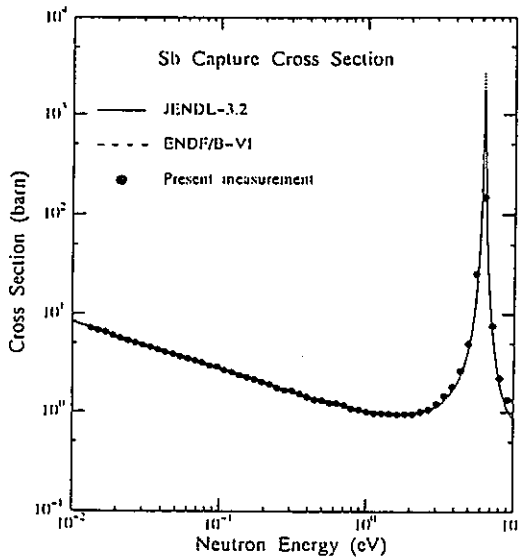
For the Sb measurement, statistical errors are about 1.0% to 4.5%, and the total uncertainties are from 2.6 to 5.1%, including the error of detection efficiencies, sample thickness and correction of capture yield. The measured result is shown in Fig. 5 and Table 2, and compared with the evaluated data in JENDL-3.2 and ENDF/B-VI. The present result shows good agreement with the data in JENDL-3.2 and ENDF/B-VI.

Since the resonance parameters have not been obtained in the present measurement, the capture cross sections in the resonance region are not compared in Tables 1 and 2.

V. CONCLUSION

The present study can be concluded as follows:

- (1) Making use of BGO scintillators, a total energy absorption γ -ray detection system was prepared for the absolute measurement of capture cross sections

Fig. 5 Capture cross section for the $\text{Sb}(n, \gamma)$ reaction.Table 2 Comparison of mean values of the $\text{Sb}(n, \gamma)$ cross section from the present work with those from ENDF/B-VI and JENDL-3.2

Energy range (eV)	ENDF/B-VI (barn)	JENDL-3.2 (barn)	Present (barn)
0.0134-0.0213	6.62	6.35	6.31 ± 0.18
0.0213-0.0338	5.26	5.05	5.00 ± 0.13
0.0338-0.0538	4.18	4.01	4.05 ± 0.10
0.0538-0.0855	3.33	3.20	3.30 ± 0.08
0.0855-0.136	2.66	2.55	2.64 ± 0.07
0.136-0.217	2.13	2.04	2.10 ± 0.06
0.217-0.347	1.71	1.65	1.67 ± 0.05
0.347-0.554	1.40	1.35	1.34 ± 0.05
0.554-0.886	1.17	1.13	1.14 ± 0.04
0.886-1.438	1.01	0.98	0.98 ± 0.03
1.438-2.344	0.96	0.94	0.95 ± 0.03

below 10 eV using the linac TOF method. It is necessary for this absolute measurement that samples have an appropriate resonance for the saturated yield method.

- (2) This detection system was firstly calibrated with a Sm sample for thermal neutrons. After that, the ^{10}B sample was employed to determine the absolute neutron flux from thermal to higher neutron energies by the $^{10}\text{B}(n, \alpha\gamma)$ reaction.
- (3) The detection system was applied to the absolute measurement of the $^{197}\text{Au}(n, \gamma)$ reaction cross section which was one of the well known cross sections as a standard. The measured result showed satisfactory agreement with the evaluated data in JENDL Dosimetry File and ENDF/B-VI.
- (4) To extend the application of the BGO detection system, Sb was selected as a sample, which has a

large scattering-to-capture cross section ratio. The measured result showed good agreement with the evaluated data in JENDL-3.2 and ENDF/B-VI.

- (5) From above results, it could be verified that the BGO detection system is applicable to the absolute measurement of capture cross sections below 10 eV except resonance energy region.

It can be expected in future that the BGO detection system is applicable to the absolute measurement of some other capture cross sections as a total energy absorption detector.

ACKNOWLEDGMENTS

The authors would like to express their sincere thanks to Prof. I. Kimura of Kyoto University for his continuous encouragement and invaluable suggestions throughout this study. The cooperation of Mr S. Kanazawa of Kyoto University is deeply appreciated throughout this work. This study was partially supported by the Special Project Research on Energy under a Grant in Aid for Scientific Research of the Ministry of Education, Science, Sports and Culture of Japan.

REFERENCES

- (1) Chrien, R.E. (Ed.): "Neutron Physics and Nuclear Data in Science and Technology", Neutron Radiative Capture, OECD/NEA, Pergamon Press, Vol.3, (1984).
- (2) Yamamoto, S., Fujita, Y., Shibata, T., Selvi, S.: *Nucl. Instrum. Methods*, A249, 484 (1986).
- (3) Wisshak, K., Guber, K., Käppeler, F., Krisch, J., Müller, H., Rupp, G., Voss, F.: *Proc. Int. Conf. on Nucl. Data for Sci. and Technol.*, at Mito, p.387 (1988).
- (4) Block, R.C., Marano, P.J., Drindak, N.J., Feiner, F., Seeman, K.W., Slovacek, R.E.: *ibid.*, p.383 (1988).
- (5) Muradyan, G.V., Shchepkin, Yu.G., Adamchuk, Yu.V., Ustroe, G.I.: *Preprint IAEA-2634*, (1976).
- (6) Knoll, G.F.: "Radiation Detection and Measurement", John Wiley & Sons, p.257 (1979).
- (7) Kobayashi, T., Kanda, K.: *KURRI-TR-198*, (1980).
- (8) Mughabghab, S.F., Divadeenam, M., Holden, N.E.: "Neutron Cross Sections", Academic Press, Vol.1, (1981).
- (9) Nakagawa, T., Shibata, K., Chiba, S., Fukahori, T., Nakajima, Y., Kikuchi, Y., Kawano, T., Kanda, Y., Ohsawa, T., Matsunobu, H., Kawai, M., Zukeran, A., Watanabe, T., Igarasi, S., Kosako, K., Asami, T.: *J. Nucl. Sci. Technol.*, 32[12], 1259 (1995).
- (10) Nakazawa, M., Kobayashi, K., Iwasaki, S., Iguchi, T., Sakurai, K., Ikeda, Y., Nakagawa, T.: JENDL Dosimetry File, JAERI 1325, (1992).
- (11) Rose, R.F. (Compiled and Edited): *BNL-NCS-17541*, (4th ed.) (ENDF/B-VI), (1991).
- (12) Kobayashi, K., Jin, G., Yamamoto, S., Takami, K., Kimura, Y., Kozuka, T., Fujita, Y.: *Annu. Rep. Res. Reactor Inst., Kyoto Univ.*, 22, 142 (1987).
- (13) Reactor Physics Constants, ANL-5800, (2nd ed.), USAEC, p.631 (1963).
- (14) IAEA Technical Series No.227, "Nuclear Data Standards for Nuclear Measurements", IAEA, Vienna, (1983).
- (15) Schmitt, H.W.: *ORNL-2883*, 1-28-60, (1960).